National River Conservation Directorate
Ministry of Jal Shakti,
Department of Water Resources,
River Development & Ganga Rejuvenation
Government of India

Flood Management Techniques

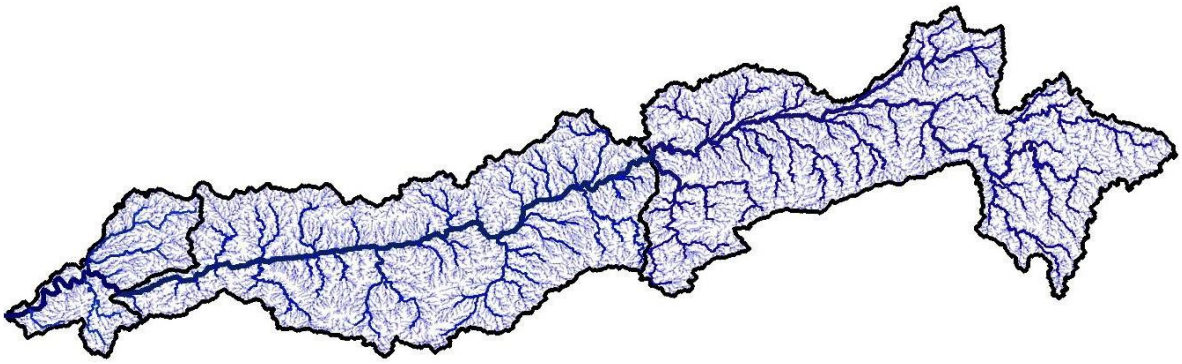

Narmada River Basin: Flood Management Techniques

National River Conservation Directorate (NRCD)

The National River Conservation Directorate, functioning under the Department of Water Resources, River Development & Ganga Rejuvenation, and Ministry of Jal Shakti providing financial assistance to the State Government for conservation of rivers under the Centrally Sponsored Schemes of 'National River Conservation Plan (NRCP)'. National River Conservation Plan to the State Governments/ local bodies to set up infrastructure for pollution abatement of rivers in identified polluted river stretches based on proposals received from the State Governments/ local bodies.
www.nrcd.nic.in

Centres for Narmada River Basin Management Studies (cNarmada)

The Center for Narmada River Basin Management Studies (cNarmada) is a Brain Trust dedicated to River Science and River Basin Management. Established in 2024 by IIT Gandhinagar and IIT Indore, under the supervision of cGanga at IIT Kanpur, the center serves as a knowledge wing of the National River Conservation Directorate (NRCD). cNarmada is committed to restoring and conserving the Narmada River and its resources through the collation of information and knowledge, research and development, planning, monitoring, education, advocacy, and stakeholder engagement.
www.cnarmada.org

Centre for Ganga River Basin Management and Studies (cGanga)

cGanga is a think tank formed under the aegis of NMCG, and one of its stated objectives is to make India a world leader in river and water science. The Centre is headquartered at IIT Kanpur and has representation from most leading science and technological institutes of the country. cGanga's mandate is to serve as think-tank in implementation and dynamic evolution of Ganga River Basin Management Plan (GRBMP) prepared by the Consortium of 7 IITs. In addition to this, it is also responsible for introducing new technologies, innovations, and solutions into India.
www.cganga.org

Acknowledgment

This report is a comprehensive outcome of the project jointly executed by IIT Gandhinagar (Lead Institute) and IIT Indore (Fellow Institute) under the supervision of cGanga at IIT Kanpur. It was submitted to the National River Conservation Directorate (NRCD) in 2024. We gratefully acknowledge the individuals who provided information and photographs for this report.

Team Members

Pranab Kumar Mohapatra, cNarmada, IIT Gandhinagar
Snehal Rathod, cNarmada, IIT Gandhinagar
Prabhat Kumar, cNarmada, IIT Gandhinagar

PREFACE

Floods are among the most devastating natural hazards, posing significant threats to human life, infrastructure, and environmental sustainability. In recent decades, the increasing frequency and intensity of flood events—driven by climate change, rapid urbanization, and anthropogenic interventions—have made flood management a critical area of study and practice. The complexity of flood dynamics necessitates an integrated and multidisciplinary approach combining hydrological understanding, engineering interventions, and modern technological advancements.

This report presents a comprehensive study on flood management techniques in the Narmada River Basin, one of India's most important and dynamic river systems. The basin, characterized by diverse physiographic features, multiple reservoirs, and significant socio-economic dependence, frequently experiences flood events, particularly during the monsoon season. These challenges highlight the need for effective planning, modelling, and mitigation strategies.

The work undertaken in this report focuses on both conventional and advanced flood management approaches, including structural and non-structural measures, as well as modern techniques such as remote sensing, Geographic Information Systems (GIS), machine learning, and Internet of Things (IoT)-based monitoring systems. In addition, the study emphasizes the application of hydrological and hydrodynamic modelling tools, particularly HEC-RAS and HEC-HMS, to simulate flood behaviour, assess inundation patterns, and evaluate flood risks under present and future climatic scenarios.

A significant component of this report is devoted to case-based analyses within the Narmada Basin, including flood dynamics of tributaries such as the Karjan River, climate change impact assessment, flood forecasting methodologies, and vulnerability mapping. The study also explores optimization of reservoir operations using fuzzy logic, demonstrating its effectiveness in reducing flood peaks and minimizing inundation impacts.

The objective of this report is to provide a holistic understanding of flood processes and management strategies, while also contributing to the development of sustainable and resilient solutions for flood mitigation. It is expected that the findings of this study will be useful for researchers, engineers, planners, and policymakers involved in water resources management and disaster risk reduction.

TABLE OF CONTENT **Page No.**

TABLE OF CONTENT **Page No.**

List of Figures

Figure 32: Flood hazard factors: a elevation, b percentage change in slope, c distance from the main river network, d drainage density, e average annual rainfall distribution, and f LULC characteristics of the study area.

Figure 33: Schematic representation of the proposed framework for flood risk mapping. The dataset consists of flood hazard and vulnerability factors as predictors and flood inundation map as predictand was given as input to the RF model for obtaining weightage of each factor to prepare flood risk maps.

Figure 34: The developed flood risk map of the study area by multiplying the flood hazard and vulnerability map. The lower urban area of the basin is prone to high flood risk, while the upper mountainous area is prone to low or no flood risk

Figure 35: Flood vulnerability map developed by National Flood Vulnerability Assessment System, Indian geo-platform of ISRO using multi-criteria evaluation technique. Source https:// bhuvan- app1. nrsc. gov. in/ nfvas/#

Figure 36: The methodology adopted for the development of Flood Vulnerability Index.

Figure 37: Flood Vulnerability Index (FVI) for various districts.

Figure 38: Spatial variation of flood vulnerability. Please refer to the online version of this paper to see this figure in colour: http://dx.doi.10.2166/wp.2021.063.

List of Tables

1. Introduction

Floods are among the most frequent, destructive, and complex natural disasters worldwide, significantly affecting human lives, infrastructure, ecosystems, and socio-economic systems (Mohapatra and Singh 2003; Teng et al. 2017; Khosravi et al. 2018; Yadav and Mangukiya 2021). Globally, floods constitute a major proportion of annual disasters, and their frequency has increased steadily over the past three decades (Teng et al. 2017). Scientific evidence suggests that extreme flood events are expected to become more frequent and intense in the future due to climate change, particularly as a result of increased precipitation extremes (Samarasinghe et al. 2010). Flood intensity has also been shown to be sensitive to temperature variations across different regions. Climate change has further contributed to erratic rainfall patterns characterized by prolonged dry spells followed by high-intensity precipitation events, leading to devastating flood events.

India is one of the most flood-prone countries in the world, ranking second after Bangladesh in terms of flood impacts, contributing to nearly one-fifth of global flood-related mortality (Agarwal and Narain 1991). Approximately 40 million hectares of land in India are flood-prone, with an average of 18.6 million hectares affected annually (National Flood Commission). Out of the total geographical area of 329 million hectares, about 12.16% is susceptible to flooding (National Disaster Management Authority 2008). Historical data indicate that between 1953 and 2017, floods caused over 107,535 fatalities and economic losses amounting to approximately USD 53.4 billion (Central Water Commission 2018). The monsoon-dominated climate, combined with diverse geographical conditions, makes India highly vulnerable to both floods and droughts (Chandole et al. 2024; Meena and Jha 2022; Mondal and Mujumdar 2012; Pal et al. 2022; Ramkar and Yadav 2018; Sharma et al. 2024). The interplay between these extremes poses significant threats to environmental sustainability and socio-economic stability.

Floods in India are primarily driven by factors such as high-intensity rainfall, riverbank erosion, encroachment of floodplains, rapid urbanization, industrialization, and deforestation (Rahman et al. 2010; Kumar et al. 2013; Ramkar and Yadav 2021). Additionally, anthropogenic activities and land-use changes have significantly altered hydrological processes, increasing flood frequency and magnitude, particularly in arid and semi-arid regions (Li et al. 2015; Papaioannou et al. 2016; Mangukiya and Yadav 2021; Yadav and Mangukiya 2021). Climate change has exacerbated flood risks, especially in drier regions of India, leading to more frequent and severe flood events (ASCE 2018; Padikkal et al. 2020; Joshy et al. 2022; Mangukiya and Andharia 2024; Mehta et al. 2023; Trivedi et al. 2023). From 1901 to 2020, heavy rainfall events in northern and central India have tripled, largely attributed to warming in the Arabian Sea.

Flood risk is typically defined as the product of flood hazard and vulnerability (Sayers et al. 2002; Winsemius et al. 2013). Flood hazard depends on geomorphological and environmental factors such as elevation, slope, drainage density, rainfall distribution, soil characteristics, and land use/land cover (Khosravi et al. 2016; Darabi et al. 2019). Vulnerability, on the other hand, is influenced by population density, socio-economic conditions, infrastructure, and exposure of economic assets (Jato-Espino et al. 2019; Deria et al. 2020). According to the IPCC (2014), vulnerability refers to the propensity to be adversely affected and includes sensitivity, susceptibility, and lack of adaptive capacity. Therefore, comprehensive flood risk assessment requires integration of physical, social, economic, and environmental dimensions (Grigg 2023).

The Narmada River Basin, one of the major river basins in India, frequently experiences flood events, particularly during the monsoon season (Fernandes et al. 2020). Historical records indicate that floods are a recurring phenomenon in the basin, with significant events reported in 1970, 1973, 1979, 1984, 1990, 1994, 2006, 2013, and 2014 (Rajaguru et al. 1995). The basin exhibits complex hydrological behavior due to the presence of multiple reservoirs, tributaries, and coastal interactions. Proposed hydraulic structures, such as the Bhadbhut barrage, are expected to influence flow dynamics and flood characteristics in the lower basin.

Flooding in tributaries such as the Karjan River is often influenced by backwater effects from the Narmada River, leading to waterlogging and inundation in low-lying areas. The lower Narmada basin includes several tributaries such as Ashvin, Kim, Heran, Karjan, and Orsang, extending to the Gulf of Cambay. These regions face significant challenges in flood management due to complex river dynamics and multiple inflow conditions.

Effective flood management begins with robust flood risk assessment, which supports decision-makers in implementing mitigation strategies and reducing adverse impacts. Such assessments should adopt a multi-scale approach, encompassing regional, local, and site-specific analyses. Key outputs of flood risk assessment include flood hazard maps, risk maps, and real-time flood forecasting and warning systems (Alsabhan and Dudin 2023). Modern flood risk analysis integrates meteorological, hydrological, hydraulic, ecological, and socio-economic approaches to provide a holistic understanding of flood dynamics.

Advancements in computational technologies and data availability have significantly improved flood modeling and risk assessment capabilities. Numerical models, remote sensing, Geographic Information Systems (GIS), and machine learning techniques are widely used for flood simulation and prediction (Wan et al. 2017; Pham et al. 2021; Liu et al. 2021). Satellite imagery has proven particularly effective in identifying flood-prone areas and assessing flood risks (Haq et al. 2012). Remote sensing and GIS-

based approaches have been successfully applied in India and globally for floodplain mapping, mitigation planning, and vulnerability assessment (Patel and Dholakia 2010; Mangukiya and Yadav 2021; Trambadia et al. 2022; Wang et al. 2002; Malik and Abdalla 2016). Wetlands, which play a crucial role in flood regulation, have also been studied using geospatial techniques (Deb and Talukdar 2010).

Hydrodynamic models, particularly one-dimensional (1D) and two-dimensional (2D) models, are extensively used for flood simulation. While 1D models are effective for river flow analysis, they are limited in representing floodplain dynamics (Timbadiya et al. 2014a; Kuiry et al. 2010; Hunter et al. 2007). In contrast, 2D models provide a more realistic representation of flood propagation and inundation (Connell et al. 2001; Carrivick 2006; Cook and Merwade 2009; Karim et al. 2015; Ticehurst et al. 2015). Models such as HEC-RAS, MIKE 21 FM, and FLOW-R2D have been widely applied for flood simulation and mapping (Brunner 2010; Nigussie and Altunkaynak 2019; Bellos et al. 2020; Wang et al. 2020). The HEC-RAS model, in particular, is widely used due to its simplicity, low data requirements, and capability to simulate both 1D and 2D flows (US Army Corps of Engineers 2010).

Flood frequency analysis (FFA) is another important tool used to estimate design flood magnitudes based on probability distributions (Tanaka et al. 2017). Common statistical methods include Gumbel distribution, Log-normal distribution, and Log-Pearson Type III distribution (Cunnane 1988; Yue et al. 1999; Hoshi et al. 1984; Phien and Ajirajah 1984). However, traditional FFA assumes stationarity, which may not hold under changing climatic and anthropogenic conditions, leading to uncertainties in flood prediction.

Machine learning techniques have gained popularity in flood risk assessment due to their ability to capture nonlinear relationships among variables (Ma et al. 2019; Costache 2019; Eini et al. 2020). Algorithms such as Random Forest (RF) have demonstrated high accuracy, robustness, and computational efficiency in flood risk mapping (Breiman 2001; Carvalho et al. 2018; Liu et al. 2021). These methods are particularly useful in handling heterogeneous datasets derived from multiple sources (Pollard et al. 2018; Towe et al. 2020).

This study addresses this gap by developing an integrated framework for flood risk and vulnerability assessment in the Narmada River Basin. It combines hydrological and hydraulic modeling, climate change scenarios, remote sensing, and data-driven approaches such as machine learning. The objective is to identify flood-prone areas, quantify vulnerability, and support decision-making for effective flood management. The outcomes of this study are expected to aid policymakers, planners, and disaster management authorities in developing sustainable and resilient flood management strategies for the region.

2. Flood Management Techniques

Flood management in the Narmada River Basin is a critical concern due to the basin's hydrological variability, monsoonal rainfall patterns, and increasing anthropogenic pressures. Effective flood mitigation requires an integrated approach that combines structural, non-structural, and modern technological interventions supported by robust modeling frameworks.

2.1 Structural Measures

Structural measures form the backbone of flood management in the Narmada basin and primarily include dams, reservoirs, barrages, levees, and embankments. These interventions aim to physically control, store, and regulate river flows during high discharge events. The Narmada basin has witnessed extensive development of large multipurpose projects under the Narmada Valley Development Plan. Major reservoirs such as Sardar Sarovar Dam**,** Indira Sagar**,** Omkareshwar**,** Tawa**,** and Bargi Dam play a significant role in flood moderation by attenuating peak flows (CWC 2020; NCA 2018). These reservoirs store excess monsoon runoff and release it in a regulated manner, thereby reducing downstream flood risks.

For instance, the Sardar Sarovar Dam has a substantial live storage capacity, which allows it to absorb flood peaks originating from upstream catchments (NCA 2018). Similarly, upstream reservoirs such as Indira Sagar contribute to flood cushioning by intercepting inflows before they propagate downstream (Jain et al. 2007).

Levees and embankments have also been constructed in vulnerable stretches, particularly in the lower Narmada basin near Bharuch and surrounding floodplains. These structures are designed to confine river flow within the channel and prevent lateral inundation during high discharge conditions (CWC 2015).

However, structural measures have limitations. Improper reservoir operation, sudden releases, or extreme rainfall events exceeding design capacity can still lead to severe flooding downstream (Mujumdar and Ghosh 2008). Additionally, sedimentation in reservoirs reduces their effective storage capacity over time, diminishing their flood control efficiency.

2.2 Non-Structural Measures

Non-structural measures complement structural interventions by focusing on planning, regulation, and community preparedness rather than physical infrastructure. Floodplain zoning is a key strategy in the Narmada basin, where land-use regulations restrict development in high-risk flood zones. Such policies

aim to minimize exposure of population and infrastructure to flood hazards (NDMA 2010). However, enforcement remains a challenge due to rapid urbanization and agricultural expansion in floodplains.

Early warning systems and flood forecasting play a vital role in reducing flood impacts. The Central Water Commission (CWC) operates real-time flood forecasting stations across the basin, providing advance warnings based on rainfall and upstream discharge data (CWC 2020). Public awareness programs and disaster preparedness initiatives are equally important. Community-based flood management strategies, including evacuation planning and awareness campaigns, help reduce vulnerability, especially in rural and flood-prone regions (NDMA 2010). Insurance mechanisms and risk financing are emerging as additional tools to mitigate economic losses due to floods, although their implementation in the basin remains limited.

2.3 Modern Techniques

Recent advancements in technology have significantly enhanced flood management capabilities in the Narmada basin.

2.3.1 Remote Sensing and GIS

Satellite-based data, such as SRTM DEM and MODIS land-use datasets, are widely used for flood mapping, inundation analysis, and watershed characterization (Ghosh et al. 2016). These tools enable large-scale spatial analysis and real-time monitoring of flood events.

2.3.2 Artificial Intelligence and Machine Learning

Machine learning techniques, such as Random Forest (RF), Artificial Neural Networks (ANN), and Support Vector Machines (SVM), are increasingly applied for flood prediction and risk mapping. These models can integrate heterogeneous datasets (rainfall, topography, land use) to improve prediction accuracy (Mosavi et al. 2018).

2.3.3 Internet of Things (IoT)

IoT-based sensor networks are emerging as powerful tools for real-time hydrological monitoring. Sensors deployed across the basin can measure rainfall, river stage, and flow parameters, enabling dynamic flood forecasting and early warning systems (Ray et al. 2019). These modern techniques offer significant advantages, including real-time data acquisition, improved prediction accuracy, and scalability. However, challenges remain in terms of data availability, infrastructure costs, and integration with existing systems.

2.4 Modeling Approaches

Hydrodynamic and hydrological modeling approaches are extensively used in the Narmada basin for flood simulation, forecasting, and risk assessment.

2.4.1 Hydrological Models

Models such as HEC-HMS are used to simulate rainfall–runoff processes and estimate inflows into reservoirs. These models help in understanding catchment response to rainfall and are essential for flood forecasting (Feldman 2000).

2.4.2 Hydrodynamic Models

Two-dimensional (2D) hydrodynamic models like HEC-RAS are widely used to simulate flood propagation and inundation patterns. These models incorporate terrain data, boundary conditions, and roughness parameters to predict flood depths and extents (Brunner 2016). Studies in the lower Narmada basin have successfully applied 2D models to generate flood inundation maps for different return periods (e.g., 10, 25, 50, and 100 years), aiding in risk assessment and planning.

2.4.3 Integrated Modeling Frameworks

Coupled hydrological–hydrodynamic models provide a comprehensive approach by linking rainfall-runoff processes with floodplain hydraulics. These integrated models improve prediction accuracy and support decision-making in flood management. Despite their effectiveness, modeling approaches are subject to uncertainties arising from input data quality, parameter estimation, and model assumptions (Beven 2001).

3. Flood Management Techniques in the Narmada River Basin

Following studies have been included in the report.

(i) Flood Dynamics of the Karjan River. Bhargav and Suresh (2025)

(ii)Assessing Future Flood Risk in the Narmada River Basin Using Climate Projections. Chowdhury and Choudhary (2024).

(iii) Hydrodynamic modeling for Narmada River flood prediction in coastal floodplain. Timbadiya and Krishnamraju (2023).

(iv) Flood forecasting in Narmada River basin using hierarchical clustering and hydrological modelling. Mehta et al. (2023).

(v) Flood frequency analysis and inundation mapping for lower Narmada basin. Mangukiya et al. (2022).

(vi) Flood hazard mapping in the lower Narmada Basin through hybrid machine learning and IoT-based approaches. Mangukiya and Sharma (2022)

(vii) Flood vulnerability assessment of Narmada River basin using data envelopment analysis. Pathak et al. (2021).

3.1 Flood Dynamics of the Karjan River

The Karjan River Basin is a major sub-basin of the Lower Narmada Basin, which forms the primary focus of this study. The Narmada Basin is subdivided into several sub-basins, including the Sukhi, Rami, and Karjan basins. The Karjan River, an important tributary of the Narmada River, originates in the Mandvi Hills near Bilwan within the Deccan Trappean highlands. It flows predominantly northward for approximately 90 km, traversing the hilly terrains of the Mosda–Sagbara and Dediyapada uplands. In its upper reaches, the river exhibits a highly sinuous course through structurally controlled valleys characterized by faults and fractures. The Tarav and Daman Khadi rivers join the Karjan River as major right-bank tributaries in this region, significantly contributing to its flow regime.

Further downstream, the river, along with its tributary Terav, forms a winding valley within the faulted ridges of the Deccan Trap terrain south of the Narmada. Originating near Bardipada, closer to the Tapi Basin than the Narmada, the Karjan River initially flows through fractured and structurally complex terrain before entering a well-defined valley and eventually emerging onto the alluvial plains near Jitnagar. It ultimately confluences with the Narmada River at Mota Bhilwada. The Karjan Dam, a key hydraulic structure within the basin, is located at approximately 22.504°N latitude and 73.405°E longitude. The present study focuses on the right bank region of the Karjan Reservoir (Fig. 1).

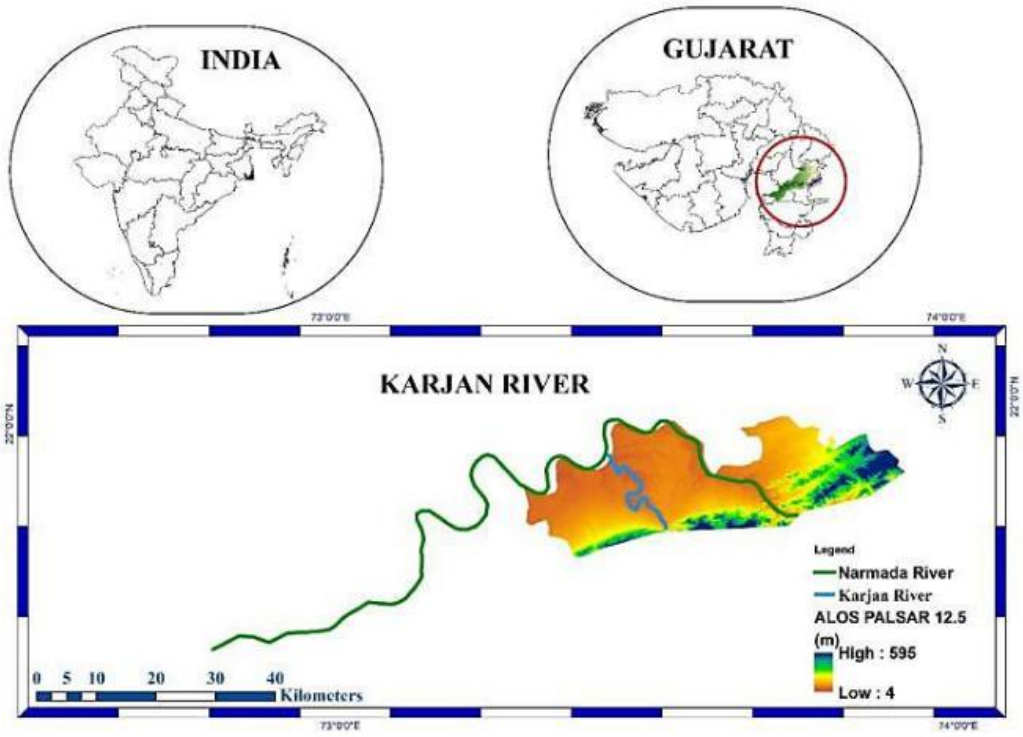

Figure 1: Study area of Karjan River Basin

Flooding in the Karjan River basin is a recurrent concern, particularly during periods of intense rainfall and high-flow conditions in the Narmada River. Backwater effects from the Narmada often induce flood-like conditions in the low-lying areas of the Karjan basin, exacerbating inundation risks. These events highlight the challenges faced by local communities in managing water levels and mitigating flood hazards. The present study addresses these challenges by analysing river dynamics under multiple inflow and single outflow conditions, with particular emphasis on flood propagation behaviour.

The Lower Narmada Basin comprises several rivers, including Ashvin, Kim, and Heran, along with smaller tributaries and major systems such as the Karjan and Orsang rivers, ultimately draining into the Gulf of Khambhat and covering parts of the Bharuch and Narmada districts. Flooding in the Karjan River is primarily driven by intense precipitation, which leads to overbank flow and waterlogging in adjacent floodplain areas.

Previous studies have contributed to understanding flood behaviour in the region. For instance, Bhargav and Suresh (2025) applied a one-dimensional hydrodynamic model using HEC-RAS integrated with GIS techniques to simulate flood dynamics and delineate inundation zones in the Karjan River basin. Their study demonstrated the application of HEC-RAS version 6.0, including the use of the RAS Mapper tool for extracting hydraulic geometry from ALOS PALSAR digital elevation data. The simulation outputs provided spatial distribution of flood depths, highlighting the utility of

geospatial approaches for flood forecasting and risk assessment. Such methodologies are valuable for supporting disaster management authorities in early warning and emergency planning.

In the present study, hydrodynamic model inputs were compiled from multiple open-access sources and institutional datasets. The ALOS PALSAR Digital Elevation Model (DEM), with a spatial resolution of 12.5 m, was obtained from the Alaska Satellite Facility. This DEM, based on L-band synthetic aperture radar, is particularly suitable for flood modelling in vegetated and topographically complex regions due to its ability to capture accurate ground elevations. Preliminary analysis of the study area, supported by satellite imagery, indicates significant flood susceptibility in the downstream reaches. A field survey is proposed to validate terrain characteristics and conduct bank discharge measurements. These observations are essential for calibrating and validating the one-dimensional hydraulic model, ensuring that simulated flow conditions adequately represent flood-generating scenarios within the basin.

The data acquisition process for the present modelling study integrates multiple sources to ensure an accurate representation of terrain and hydrological conditions. A Digital Elevation Model (DEM) derived from ALOS PALSAR, with a spatial resolution of 12.5 m and obtained from the Japan Aerospace Exploration Agency (JAXA), was used to develop the base terrain model for the study area. This dataset provides reliable elevation information, particularly suitable for regions with complex topography and vegetation cover.

Topographical maps at a scale of 1:50,000, sourced from the Survey of India, were utilized to support river reach delineation and to refine channel alignment and flow paths. Hydrological inputs were incorporated using streamflow data recorded at the Karjan Dam, obtained from Sardar Sarovar Narmada Nigam Limited (SSNNL). These data, available on a daily time scale, were used as upstream boundary conditions to capture temporal variations in discharge.

In addition, daily water surface level data from Rajpipla Bridge, also provided by SSNNL, were used for calibration and validation of the model. These observations were further employed to estimate Manning's roughness coefficient for the river reach. The integration of these datasets ensures a comprehensive characterization of both the physical terrain and flow dynamics, thereby enhancing the reliability of the modelling framework.

3.1.1 Method of analysis

A one-dimensional hydrodynamic model was developed using HEC-RAS to simulate flood behaviour and estimate spatial variations in water depth during flood events. The modelling framework consists

of two primary stages: (i) geospatial data processing and river geometry development, and (ii) hydraulic simulation using the HEC-RAS computational engine.

River geometry was generated using cross-sections extracted at an interval of 200 m along the river reach, with an average channel width of approximately 2000 m. Due to the unavailability of detailed ground-surveyed cross-sectional data, DEM-derived cross-sections were adopted for the analysis. The ALOS PALSAR DEM was imported into the RAS Mapper module of HEC-RAS, where it was processed to generate a Digital Terrain Model (DTM). Georeferenced spatial data were incorporated within the same framework to ensure consistency in projection and coordinate systems.

River centreline, bank lines, flow paths, and cross-sections were digitized within the RAS Mapper environment. Satellite imagery was overlaid on the terrain model to improve the accuracy of geometric representation. The downstream extent of the model includes the river confluence zone influenced by backwater effects from the Narmada River. Boundary conditions were defined using daily discharge data from Karjan Dam as the upstream input, while the downstream boundary at Rajpipla was represented using normal depth conditions. The model was configured to simulate overbank flow conditions and floodplain inundation along the study reach. Station-wise cross-sectional data (CS-11800, CS-7200, CS-5400, and CS-2400) used in the analysis are presented in Figs. 2a–d. Field observations from surveys conducted in 2020 indicate a maximum discharge of approximately 5437 m^3/s and a channel slope of 0.00195 for the study reach. A Manning's roughness coefficient of 0.03 was adopted, consistent with typical values for semi-arid river systems

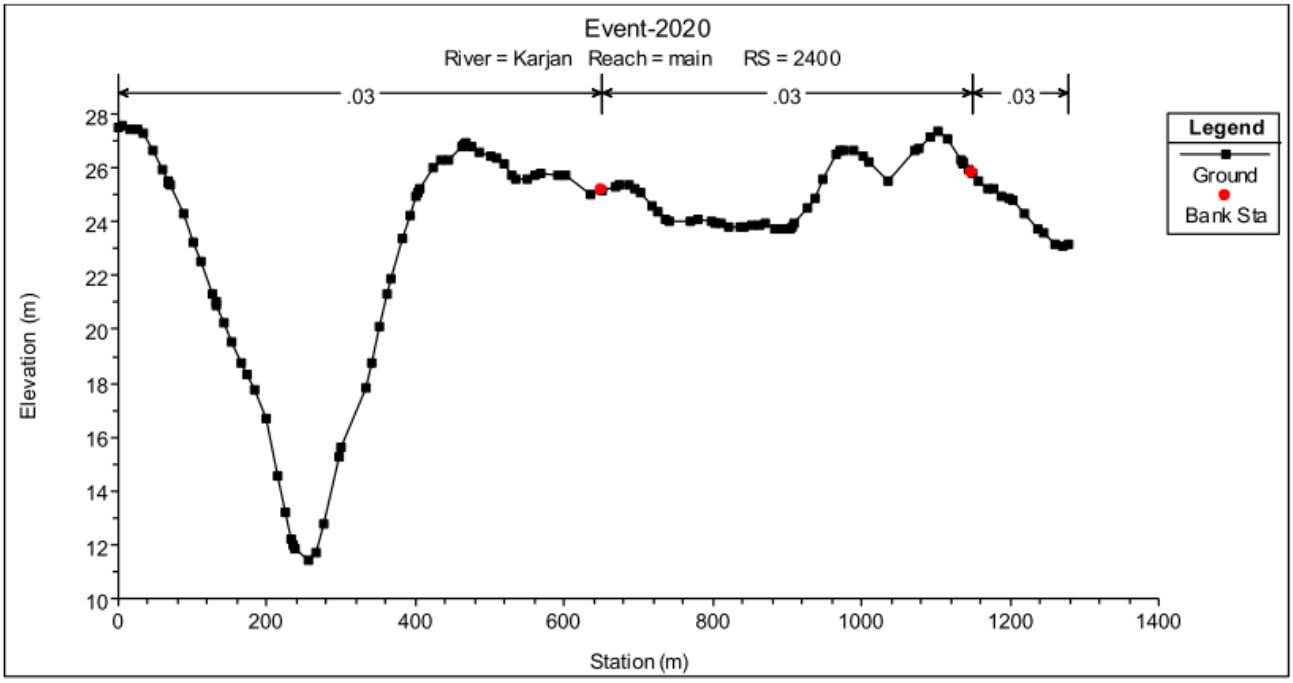

(a)

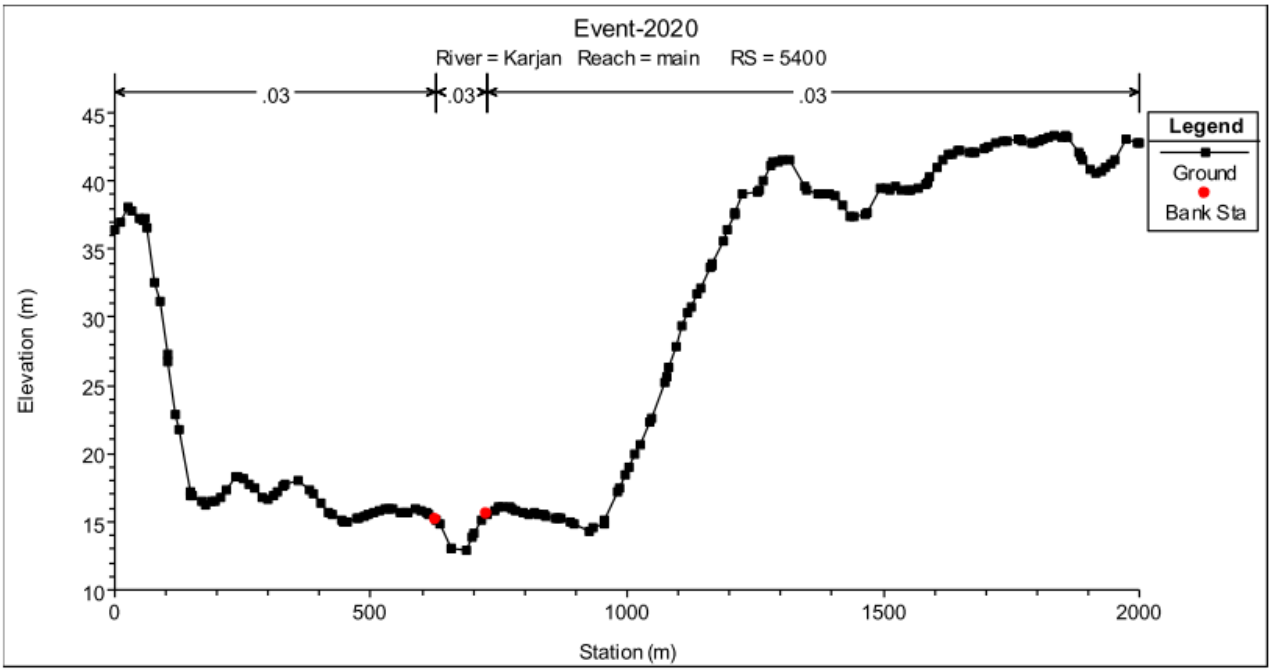
Event-2020
River = Karjan Reach = main RS = 5400
.03
.03
.03
Legend
Ground
Bank Sta
Elevation (m)
Station (m)
45
40
35
30
25
20
15
10
0
500
1000
1500
2000

(b)

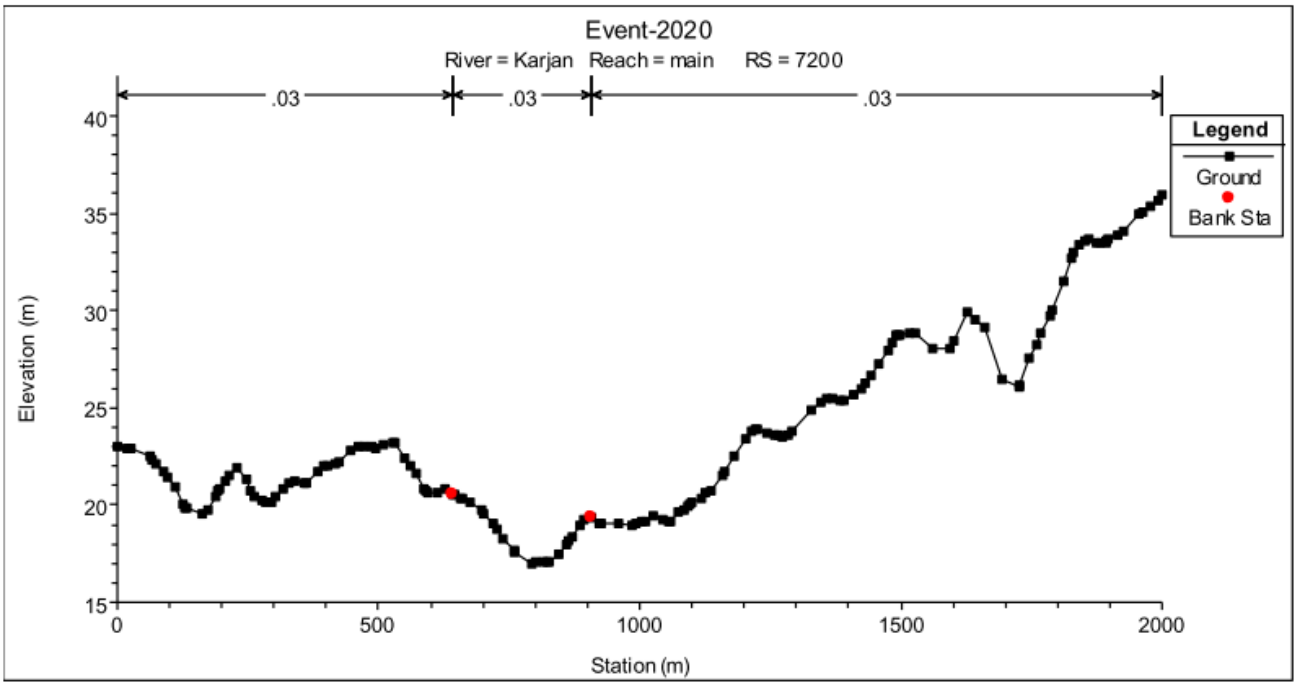
Event-2020
River = Karjan Reach = main RS = 7200
.03
.03
.03
Legend
Ground
Bank Sta
Elevation (m)
Station (m)
40
35
30
25
20
15
0
500
1000
1500
2000

(c)

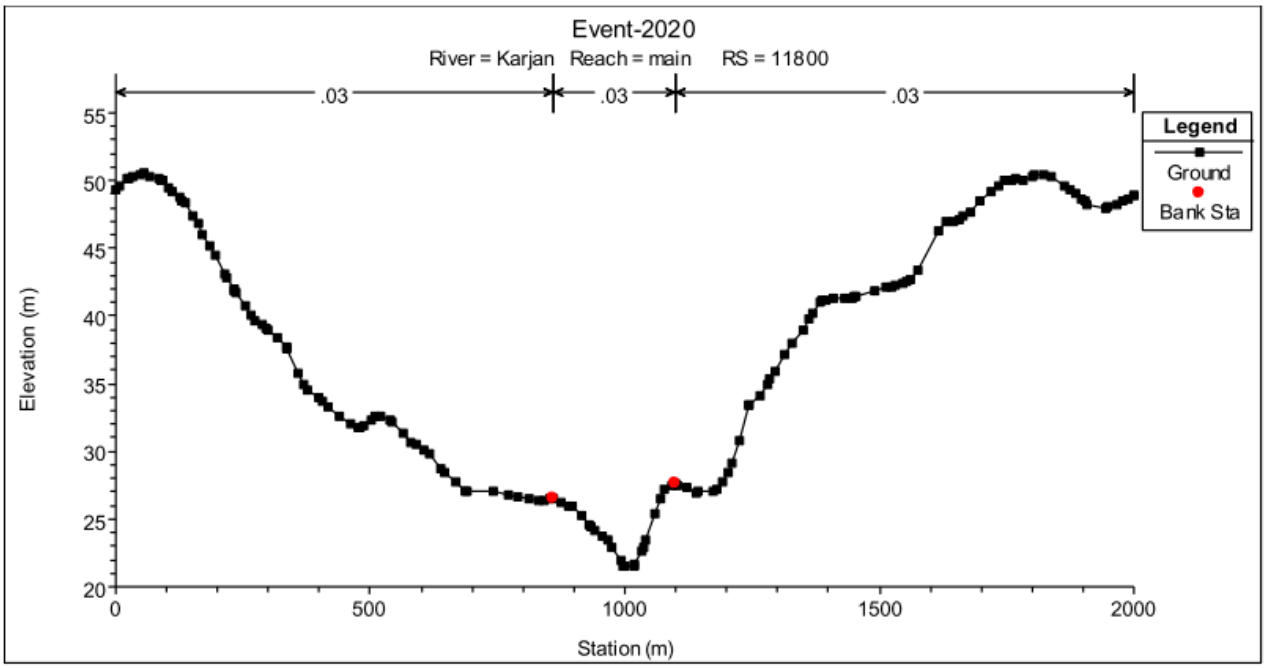

(d)

Figure 2(a, b, c & d): Station-elevation data of extracted cross-sections in HEC-RAS geometric data editor window.

3.1.2 Calibration

Calibration of the model was performed at the Rajpipla gauging station using the peak water depth recorded during a single flood event. Due to limited availability of observed data, a trial-and-error approach was adopted to achieve a close agreement between simulated and observed water depths. Stability analyses were also conducted to ensure the robustness of the simulation results. The calibrated model corresponds to a discharge of 31,844.50 m^3/s released from the Narmada Dam during the year 2020.The results indicate comparatively lower flood impact near cross-section 11400, which can be attributed to higher bed elevation and the presence of a bridge structure. In contrast, cross-sections 7200, 5400, and 2800—located near Dhamancha, Bhadam, and Juna Rundh at the confluence of the Karjan and Narmada rivers—exhibit higher flood susceptibility, as shown in Figs. 2(a–d). Variations in water depth at different locations along the river reach are presented in Figs. 3(a–d).

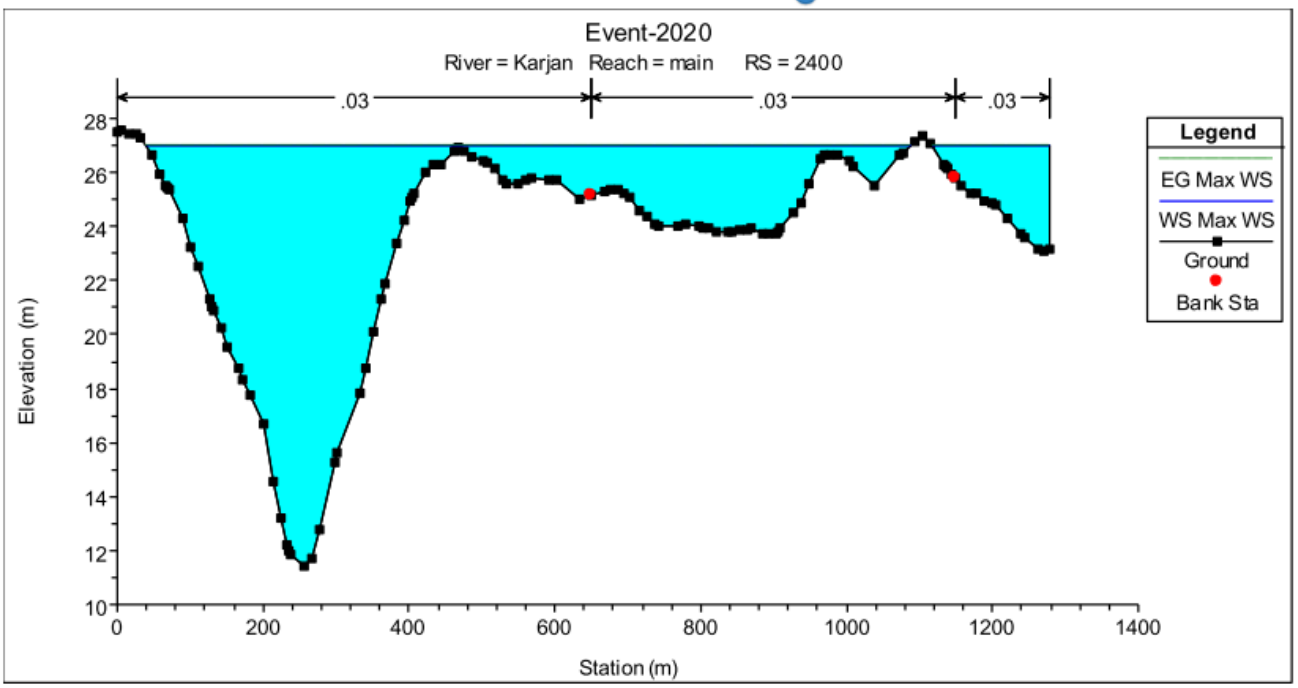
Event-2020
River = Karjan Reach = main RS = 2400
.03
.03
.03
Legend
EG Max WS
WS Max WS
Ground
Bank Sta
Elevation (m)
Station (m)
28
26
24
22
20
18
16
14
12
10
0
200
400
600
800
1000
1200
1400

(a)

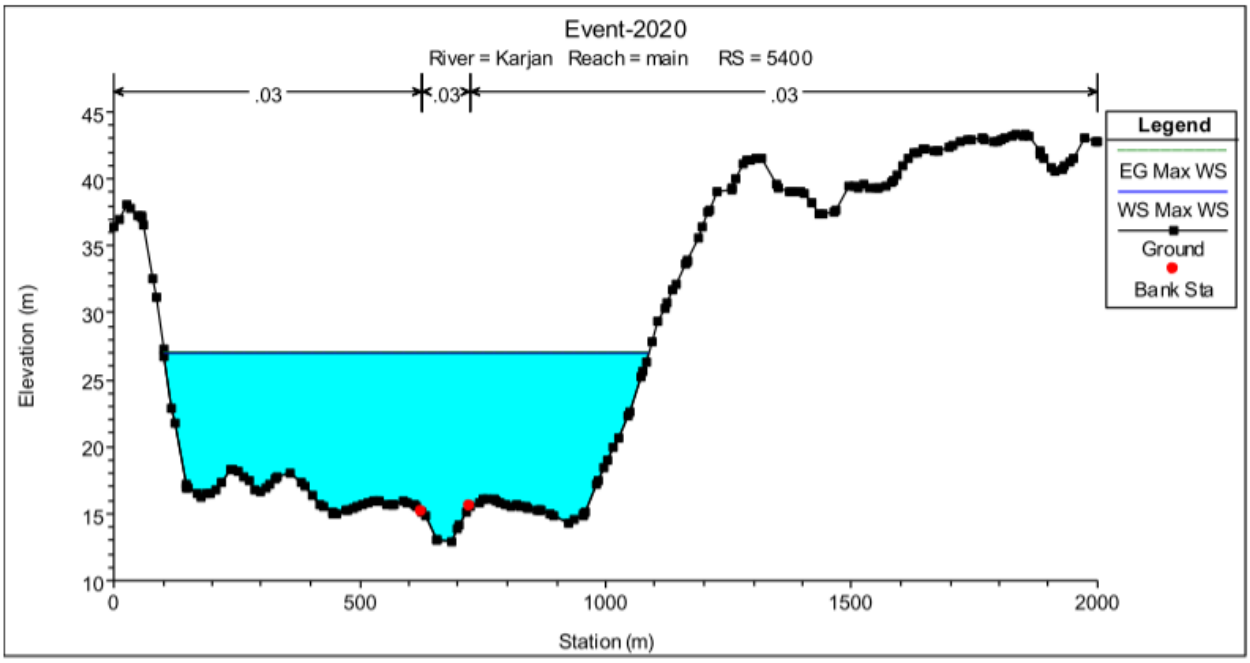
Event-2020
River = Karjan Reach = main RS = 5400
.03
.03
.03
Legend
EG Max WS
WS Max WS
Ground
Bank Sta
Elevation (m)
Station (m)
45
40
35
30
25
20
15
10
0
500
1000
1500
2000

(b)

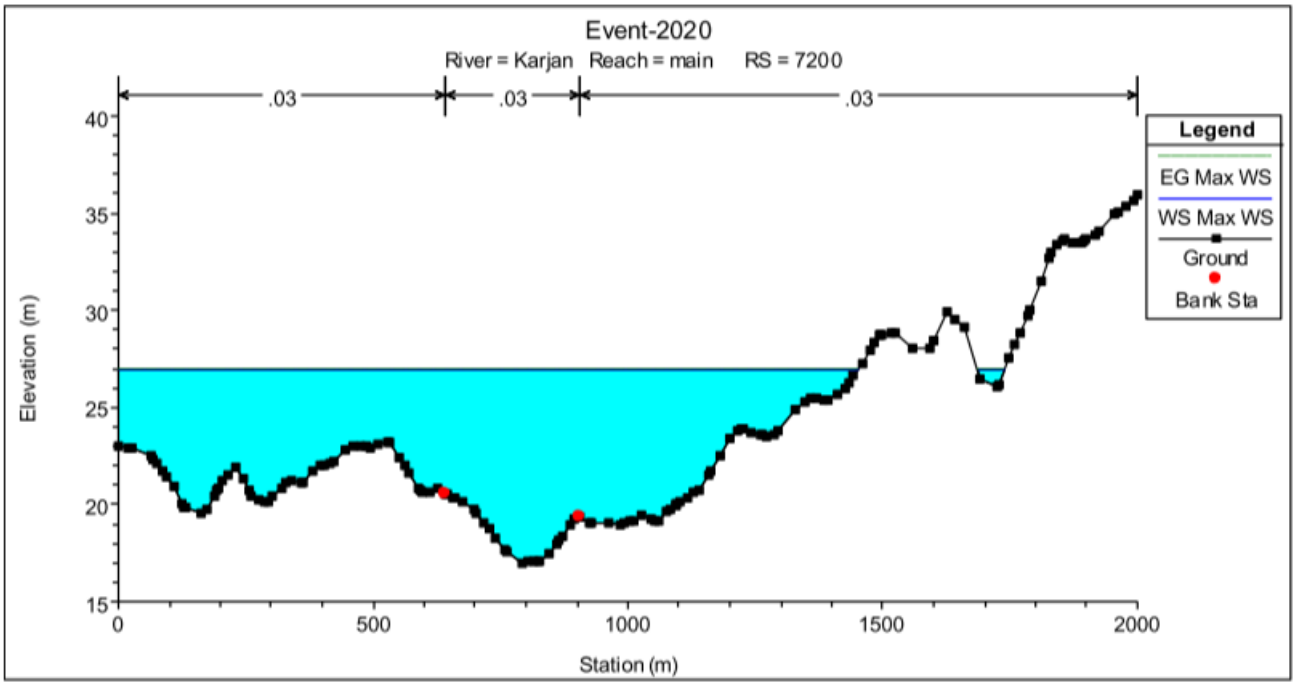

(c)

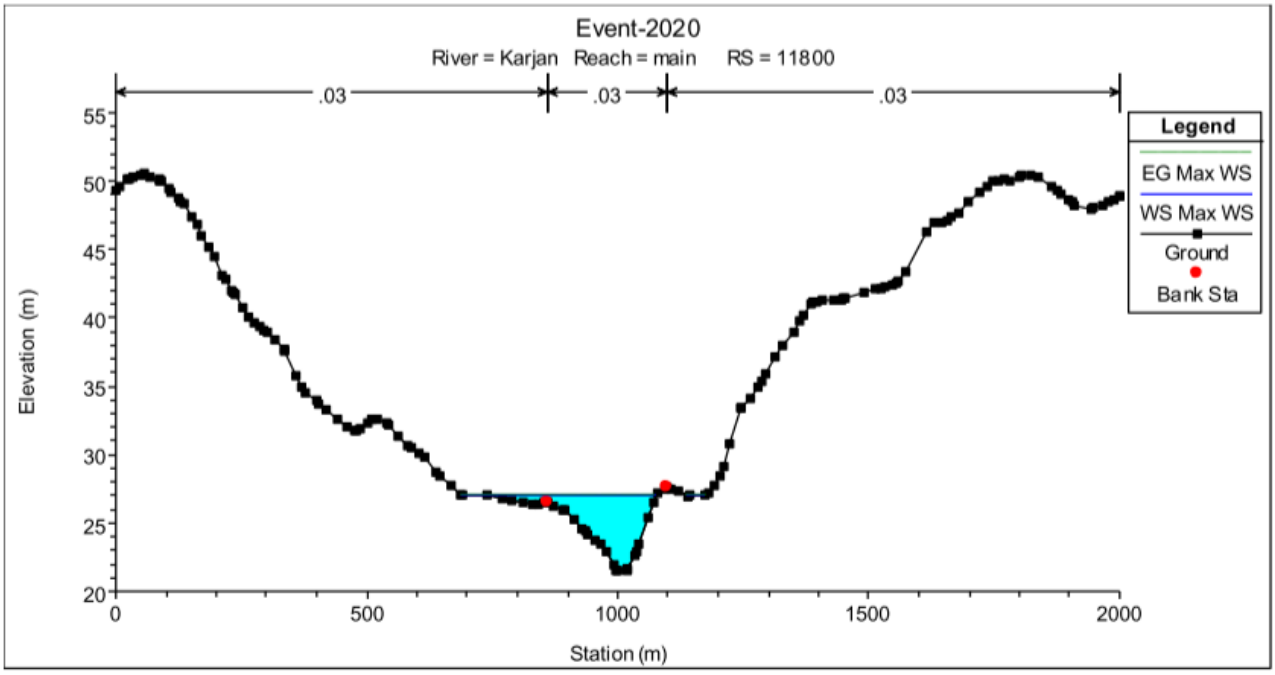

(d)

Figure. 3(a, b, c &d): Water Surface Profile at Various Locations

3.1.3 Validation

Model validation was carried out using observed water level data from the Rajpipla Bridge gauging station near Rajpipla town. Owing to the scarcity of field data, observations from this single station were used to evaluate the performance of the HEC-RAS model. The results suggest that the developed model is suitable for preliminary flood assessment and forecasting in data-scarce regions. However,

the present study is limited to one-dimensional channel flow modelling and considers only in-channel flow conditions, without incorporating lateral floodplain interactions. The inclusion of two-dimensional hydrodynamic modelling would provide a more comprehensive representation of floodplain inundation and enhance decision-making for flood management. Previous studies in the Karjan River region have demonstrated the advantages of two-dimensional and continuous simulation approaches. The analysis further indicates that low-lying areas such as Nandod, Bhadam, Juna Rundh, Dhanpor, and Dhamancha are particularly vulnerable to flooding. Therefore, the application of a coupled or fully two-dimensional HEC-RAS model is recommended, especially during extreme rainfall events and conditions influenced by backwater effects from the Narmada River.

3.1.4 Simulated Flood Map

The simulated flood inundation map for the 2020 event in the Karjan River basin is presented in Fig. 4, corresponding to a discharge of 31,844.5 m^3/s released from the Sardar Sarovar Dam. The map depicts spatial variations in water depth along the river channel using a color gradient, where darker blue shades indicate greater depths and lighter shades represent relatively shallow inundation. The results clearly show that the lower reaches of the Karjan River—particularly in the vicinity of Juna Rundh, Dhamancha, and Dhanpor—experienced severe flooding during the 2020 event. This is primarily due to the high discharge from the Narmada River, which significantly influences backwater conditions within the Karjan basin. The findings highlight that flooding in these low-lying areas is largely driven by elevated releases from the Narmada Dam, thereby increasing flood susceptibility in the downstream reaches of the Karjan River.

3.1.5 Discussion

This study highlights the enhanced capabilities of the latest version of HEC-RAS, which incorporates advanced mapping tools that significantly improve the efficiency of river geometry extraction and model development. Unlike earlier workflows that required integration with ARC-GIS and HEC-GeoRAS, the current approach utilizes the RAS Mapper environment, enabling a more streamlined and time-efficient modelling process. This integration facilitates improved accuracy in representing river geometry while reducing the complexity of initial data preparation.

Figure 4: Stimulated Flood Map

High-resolution ALOS PALSAR DEM data (12.5 m) were used to delineate the river geometry and floodplain characteristics. The model was applied to simulate flow conditions during the 2020 flood event, enabling detailed analysis of flood behaviour along the Karjan River. The results identified several low-lying areas prone to inundation, consistent with findings reported in previous studies. The flood depth distribution is illustrated in Fig. 4, while Fig. 3 presents a comparison between simulated and observed water depths, demonstrating satisfactory model performance.

Further analysis of water levels at different cross-sections, derived from the terrain data, indicates spatial variability in flood impacts along the river reach. Minor discrepancies between simulated and observed flood stages may be attributed to cumulative floodplain interactions and simultaneous inundation processes within the study area.

Some variations in depth predictions can also be linked to inherent limitations of DEM-based cross-sections, particularly in representing fine-scale topographic features. In addition, uncertainties in water level measurements may arise due to factors such as instrument precision, gauge positioning, and environmental disturbances (e.g., debris interference). To overcome these limitations, especially in relatively flat terrains, the use of higher-resolution elevation data—such as those derived from Unmanned Aerial Vehicle (UAV) surveys—can further enhance model accuracy and reliability.

3.2 Assessing Future Flood Risk in the Narmada River Basin Using Climate Projections

3.2.1 Study Area

This study focuses on assessing flood vulnerability in the Narmada River Basin under changing climatic conditions. The Narmada River, the largest westward-flowing river in India, traverses the states of Madhya Pradesh, Maharashtra, and Gujarat. Geographically, the basin extends between longitudes 72°32′E to 81°45′E and latitudes 21°20′N to 23°45′N. The river originates from the Amarkantak Plateau in the Anuppur district of Madhya Pradesh and flows westward for approximately 1,312 km before draining into the Gulf of Cambay (Arabian Sea). Flowing through the Deccan Trap region between the Vindhya and Satpura ranges, the river also historically demarcates northern and southern India. The total basin area is about 98,796 km², with nearly 87% lying in Madhya Pradesh, 1.5% in Maharashtra, and 11.5% in Gujarat.

The basin exhibits diverse land use and physiographic characteristics, with approximately 60% of the area under agriculture, 35% covered by forests, and the remaining 5% comprising grasslands and wastelands. Rainfall distribution is highly variable, with the upper catchment receiving between 1,000 and 1,850 mm annually, while the lower regions receive around 650 mm or less. Land use within the basin is dominated by agriculture (56.9%), followed by forest cover (32.8%), wetlands (6%), and built-up areas (1.13%). The upper and middle reaches are characterized by hilly terrain and dense forests, whereas the plains provide fertile land suitable for agriculture. The basin is predominantly covered by black soils, while the coastal regions in Gujarat consist of alluvial clays overlain by black soil.

For the present analysis, seven gauging stations—Dindori, Barmanghat, Sandia, Hoshangabad, Handia, Mandleshwar, and Garudeshwar—have been selected to represent the upper, middle, and lower reaches of the basin. These stations provide reliable precipitation and streamflow data required for assessing peak flows and flood risk under future climate scenarios. The basin is also characterized by the presence of several major hydraulic structures, including Bargi Dam, Indira Sagar Dam, Omkareshwar Dam, and Sardar Sarovar Dam on the main stem, along with important tributary dams such as Tawa, Kolar, and Barna. In addition, numerous minor and major water resource projects exist across the basin. In this study, the impacts of climate change on precipitation and streamflow at the selected gauging

stations are analyzed prior to conducting basin-scale flood modelling under projected climate scenarios.

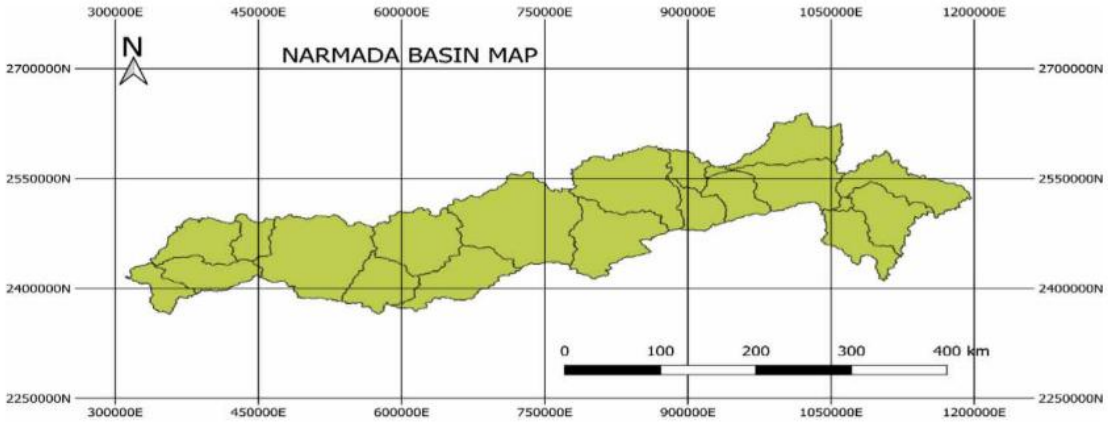

Figure 5: Map of the Narmada River Basin.

3.2.2 Data Preparation and Methodology

The present study aims to evaluate the impact of climate change on precipitation and streamflow within the Narmada River Basin through an integrated hydrological and hydraulic modelling framework. For this purpose, both observed and projected climate datasets were utilized along with streamflow records from seven Central Water Commission (CWC) gauging stations. Observed gridded precipitation data were obtained from the India Meteorological Department (IMD) at a spatial resolution of 0.25° × 0.25°, covering a period of 64 years (1951–2014). These data serve as key inputs for hydrological modelling and baseline assessment.

Future climate projections were derived from General Circulation Models (GCMs), namely ICHEC-EC EARTH and CCCma-CanESM2, under the CORDEX South Asia framework. Simulated historical and future daily precipitation datasets corresponding to Representative Concentration Pathways (RCP) 4.5 and 8.5 were considered for a 30-year period (2026–2055). The associated Regional Climate Models (RCMs), namely RCA4 and RegCM4-4, were used for downscaling, providing climate data at a spatial resolution of 0.44° × 0.44° (approximately 50 km). The ICHEC-EC EARTH model is associated with the Swedish Meteorological and Hydrological Institute (SMHI), while the CCCma-CanESM2 model has been adapted for the Indian region by the Indian Institute of Tropical Meteorology (IITM). The downscaled datasets were obtained in netCDF format and subsequently processed and bias-corrected using CM-Hyd software prior to their use in hydrological simulations.

Observed streamflow data required for model calibration and validation were sourced from the India Water Resources Information System (INDIA-WRIS). A Digital Elevation Model (DEM) with a spatial resolution of 90 m, obtained from the Shuttle Radar Topography Mission (SRTM) via the USGS Earth Explorer, was used for watershed delineation and terrain representation. Considering the large basin area (approximately 98,796 km²), the selected DEM resolution is suitable for basin-scale hydrological analysis.

Land use and land cover (LULC) data for the period 2006–2015 at a spatial resolution of 10 m were obtained from the National Remote Sensing Centre (NRSC). These data were incorporated into the HEC-RAS model along with corresponding Manning's roughness coefficients to represent surface characteristics. Additionally, data on dams and reservoirs were collected from the Narmada Control Authority, Indore, to support flood modelling using a dam-to-dam analysis approach. This integrated dataset forms the basis for simulating hydrological response and flood behaviour under present and future climate scenarios.

3.2.3 Objective of the Study

The primary objective of the present study is to assess the impact of climate change on precipitation and streamflow in the Narmada River Basin, and subsequently evaluate the associated flood hazards under future climate scenarios. In addition, the study aims to develop a mitigation strategy by optimizing peak flow releases from reservoirs to reduce flood risk within the basin.

3.2.4 Procedure and Methodology

Two General Circulation Models (GCMs), namely ICHEC-EC EARTH and CCCma-CanESM2, were selected based on their statistical performance and lower variability for the study region. These GCM outputs were dynamically downscaled using Regional Climate Models (RCMs), specifically RCA4 and RegCM4-4, at a spatial resolution of approximately 50 km.

Historical and future climate datasets generated from these models were processed and bias-corrected using CM-Hyd software, employing a linear scaling approach to reduce systematic errors. A 30-year period (2026–2055) of projected precipitation data was extracted and subjected to rainfall frequency analysis using Gumbel's extreme value distribution. Intensity–Duration–Frequency (IDF) curves were subsequently developed for both RCP 4.5 and RCP 8.5 scenarios across multiple return periods, providing estimates of extreme rainfall intensities and daily precipitation maxima.

Hydrological modelling was performed using the HEC-HMS model, with calibration and validation carried out at selected gauging stations within the basin. The calibrated model was then used to estimate peak discharges for various return periods and climate scenarios. These peak discharge values served

as inputs for hydraulic modelling using the HEC-RAS 2D framework, enabling the generation of flood inundation maps, depth profiles, and risk assessments. Model calibration and validation were also conducted for the HEC-RAS 2D simulations to ensure reliability in predicting parameters such as flow velocity and water surface elevation (WSE). Flood risk analysis was carried out along different river stretches between major dams in the basin.

The hydraulic modelling process involves the use of upstream and downstream boundary conditions in the form of hydrographs and normal depth, along with tributary inflows derived from HEC-HMS simulations. The HEC-RAS 2D model solves the continuity and momentum equations based on the Saint-Venant formulation. In this study, the diffusive wave approximation was adopted, assuming gravity and friction as dominant forces, which improves computational efficiency and reduces model instability. The model outputs provide spatial information on flood extent, inundation depth, velocity, and water surface elevation across the floodplain.

Calibration of the HEC-RAS model was performed using observed water level data and real-time dam release data obtained from the Narmada Control Authority, particularly for estimating Manning's roughness coefficients. Following flood inundation mapping, reservoir operation was optimized using a fuzzy logic-based approach implemented in MATLAB (R2023b). A fuzzy inference system (FIS) was developed with reservoir storage and inflow as input variables and release as the output. Five triangular membership functions—very low, low, medium, high, and very high—were defined based on historical data and reservoir capacity. The optimized reservoir release rules were then applied to re-run the hydraulic model, enabling assessment of flood mitigation effectiveness. A comparative analysis was carried out to evaluate changes in inundation extent, depth, and other hydraulic parameters under optimized and non-optimized scenarios across different return periods. This integrated approach facilitates improved flood management and decision-making under climate change conditions.

3.2.5 Results and Discussion

The HEC-RAS 2D model was developed and subsequently applied to perform unsteady flow simulations for analysing flood inundation and mapping across different river reaches between successive dams. Flood modelling was carried out considering peak discharges released from individual reservoirs under varying climatic scenarios. The results of the flood simulations are presented in tabular form for distinct dam-to-dam river segments, enabling a comparative assessment of hydraulic behaviour along the basin.

Flood Inundation Modelling for Peak Flows

Prior to conducting flood simulations using peak discharge scenarios, the HEC-RAS 2D model was first applied using observed real-time flow data from each reservoir. This step was essential for calibration and validation of the model, particularly for estimating Manning's roughness coefficients (n values) in conjunction with land use and land cover data. Calibration and validation were performed for each dam-to-dam river reach using observed water level data available at corresponding gauging stations. Once the model performance was found to be satisfactory, it was employed to simulate flood conditions using peak flow inputs derived from hydrological modelling. The outputs of the hydraulic simulations include key parameters such as inundation area, maximum water depth, flow velocity, and water surface elevation (WSE). These results are summarized in tabular form for different river segments, providing a comprehensive understanding of flood characteristics under extreme flow conditions.

(i) Dindori Dam-to-Bargi Dam segment

Fig. 6 shows the flood simulation of the Dindori-to-Bargi Dam segment. Also, Table 1 shows the parameters of 2D flood modelling for Dindori-to-Bargi Dam segment.

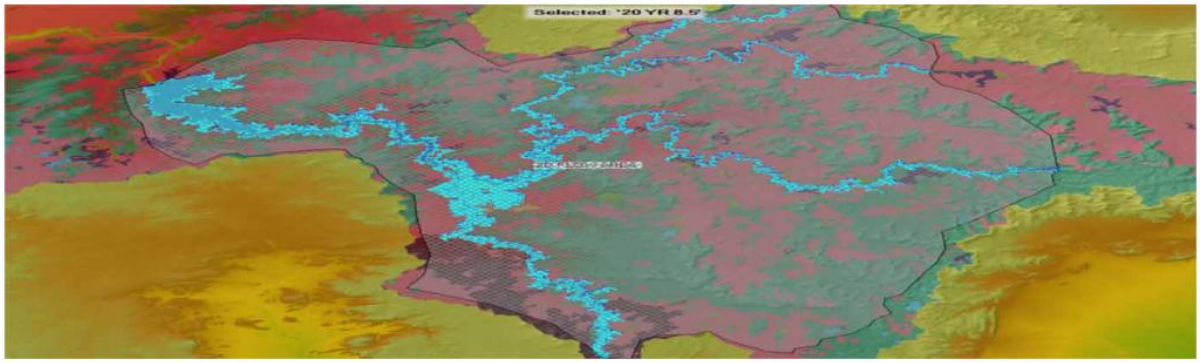

Figure 6: Flood simulation of the Dindori-to-Bargi Dam segment.

Table 1. Parameters of 2D flood modelling for the Dindori Dam–to–Bargi Dam segment

Parameters	**RCP 4.5 (20 yr)**	**RCP 4.5 (50 yr)**	**RCP 4.5 (100 yr)**	**RCP 8.5 (20 yr)**	**RCP 8.5 (50 yr)**	**RCP 8.5 (100 yr)**
Inundation area (km^2)	492.87	558.24	610.48	601.96	669.32	724.14
Max. depth (m)	31.46	32.86	33.57	33.16	35.14	37.47
Max. velocity (m/s)	2.18	3.45	6.44	2.92	8.16	9.23
Max. WSE (m)	418.53	419.78	420.74	420.59	421.89	422.91

(ii) Bargi Dam-to-ISP Dam segment

Fig. 7 shows the flood simulation of the Bargi Dam-to-ISP Dam segment. Also, Table 2 shows the parameters of 2D flood modelling for the Bargi Dam-to-ISP Dam segment.

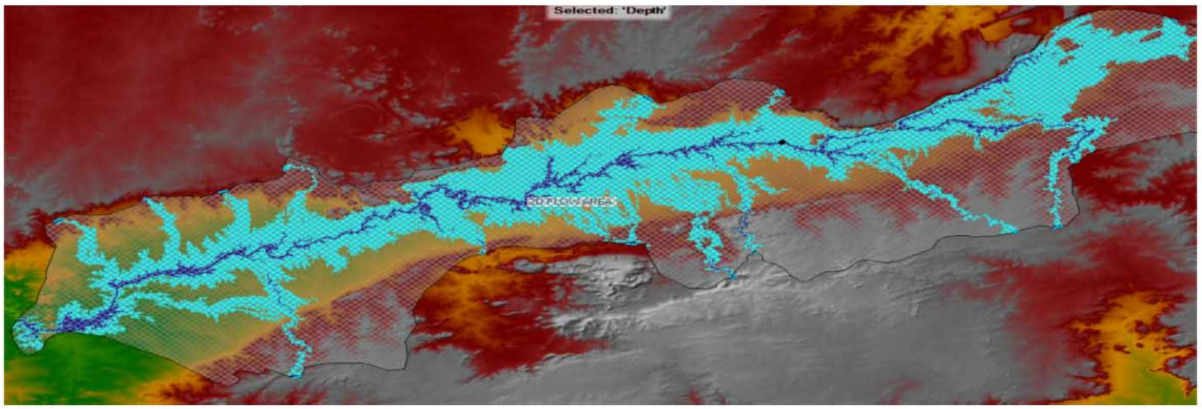

Figure 7: Flood simulation of the Bargi-to-ISP Dam segment.

Table 2. Parameters of 2D flood modelling for the Bargi Dam–to–Indira Sagar Project Dam segment

Parameters	**RCP 4.5 (20 yr)**	**RCP 4.5 (50 yr)**	**RCP 4.5 (100 yr)**	**RCP 8.5 (20 yr)**	**RCP 8.5 (50 yr)**	**RCP 8.5 (100 yr)**
Inundation area (km²)	6,333.03	7,239.47	7,928.13	7,428.48	8,534.89	9,377.86
Max. depth (m)	68.72	73.41	77.62	77.40	80.91	87.42
Max. velocity (m/s)	5.37	6.04	7.12	6.19	7.34	8.05
Max. WSE (m)	236.04	240.24	243.83	242.93	249.22	254.23

(iii) ISP Dam-to-OSP Dam segment

Fig. 8 shows the flood simulation of the ISP Dam-to-OSP Dam segment. Also, Table 3 shows the parameters of 2D flood modelling for the ISP Dam-to-OSP Dam segment.

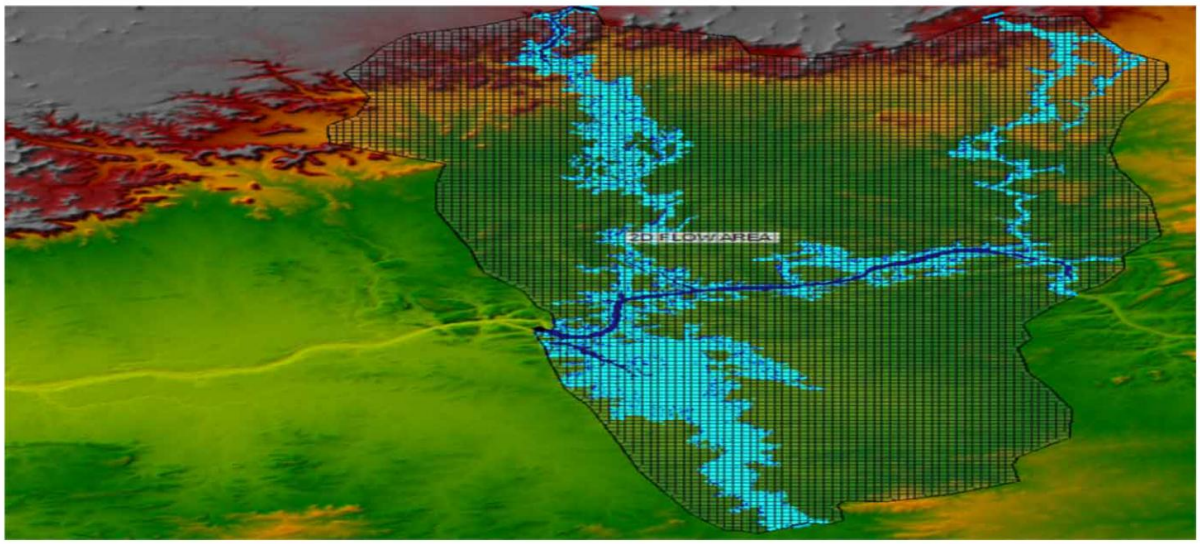

Figure 8: Flood simulation of the ISP-to-OSP Dam segment.

Table 3. Parameters of 2D flood modelling for the Indira Sagar Project Dam–to–Omkareshwar Sagar Project Dam segment

Parameters	**RCP 4.5 (20 yr)**	**RCP 4.5 (50 yr)**	**RCP 4.5 (100 yr)**	**RCP 8.5 (20 yr)**	**RCP 8.5 (50 yr)**	**RCP 8.5 (100 yr)**
Inundation area (km^2)	140.33	172.22	200.81	180.27	225.46	266.58
Max. depth (m)	48.71	52.39	54.99	54.82	59.21	62.31
Max. velocity (m/s)	4.68	5.05	5.34	5.67	6.41	7.21
Max. WSE (m)	194.75	198.82	202.21	201.94	204.52	208.91

(iv) OSP Dam–to–SSP Dam Segment

The results presented in the preceding sections provide a comprehensive representation of flood behaviour and inundation patterns across the river reaches between successive dams (Fig. 9). Table 4 summarizes key hydraulic parameters, including inundation area, maximum water depth, flow velocity, and water surface elevation (WSE), derived from the 2D flood modelling carried out using the HEC-RAS model.

Analysis of these results indicates that both inundation area and maximum depth increase significantly with increasing return periods, from 20 years to 100 years. Furthermore, under the RCP 8.5 scenario, higher values of inundation extent and depth are observed compared to the RCP 4.5 scenario, reflecting the intensified impact of extreme climatic conditions. Similarly, other hydraulic parameters such as maximum velocity and WSE also show a consistent increasing trend with higher return periods. These

findings highlight the growing flood risk in the downstream reaches under future climate scenarios, particularly under high-emission conditions.

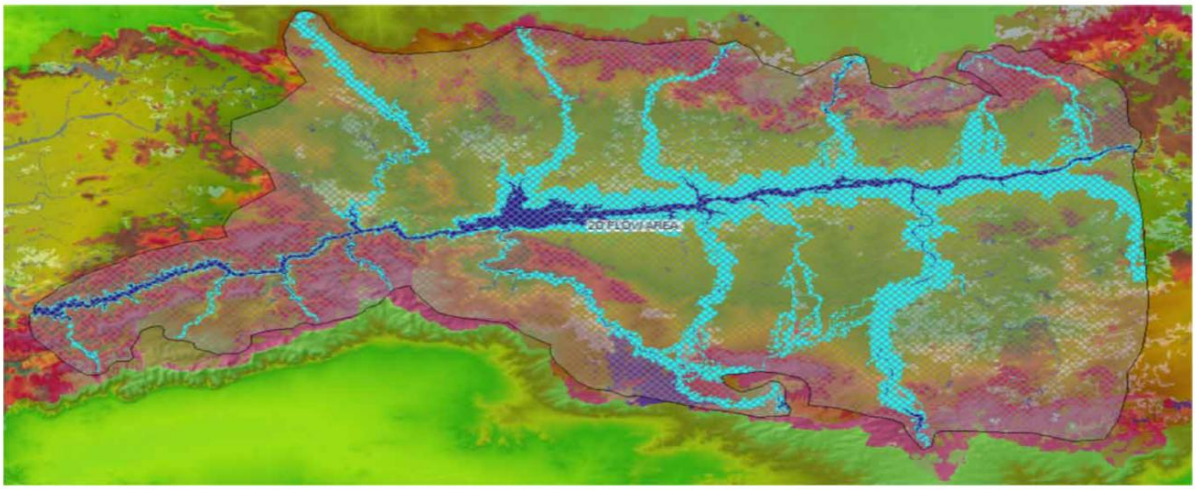

Figure 9: Flood simulation of the OSP-to-SSP Dam segment.

Table 4. Parameters of 2D flood modelling for the Omkareshwar Sagar Project Dam–to–Sardar Sarovar Project Dam segment

Parameters	**RCP 4.5 (20 yr)**	**RCP 4.5 (50 yr)**	**RCP 4.5 (100 yr)**	**RCP 8.5 (20 yr)**	**RCP 8.5 (50 yr)**	**RCP 8.5 (100 yr)**
Inundation area (km^2)	1,585.19	1,914.29	2,128.50	2,049.10	2,385.34	2,639.20
Max. depth (m)	64.75	68.51	72.23	71.84	76.75	77.51
Max. velocity (m/s)	6.78	7.49	8.77	8.06	9.73	10.49
Max. WSE (m)	108.24	112.19	115.10	113.91	118.90	122.54

Flood Modelling for Optimized Reservoir Releases

Following the completion of 2D flood modelling in HEC-RAS for peak discharges from reservoirs, optimal release values for each reservoir were determined using a fuzzy optimization approach. These optimized discharges were subsequently used as inputs for further flood simulations along different river segments. Table 5 presents a comparison of peak flow releases and optimized releases from individual reservoirs under various climate change scenarios. The results indicate that reservoir releases are substantially reduced through the application of fuzzy optimization under both RCP 4.5 and RCP 8.5 scenarios, thereby contributing to effective flood mitigation. Flood modelling was then performed using these optimized release values to evaluate their impact on inundation characteristics. The corresponding inundation area and maximum water depth obtained from optimized releases are compared with those from peak discharge conditions, highlighting a noticeable reduction in both parameters. This comparison demonstrates the effectiveness of optimized reservoir operations in minimizing flood extent and severity.

Table 5. Releases from the reservoir during peak flow and optimum flow (in Mm^3)

Bargi dam → ISP dam segment						
Scenario	**Max Release (Peak Flow)**			**Optimum Release**		
	20 yrs	50 yrs	100 yrs	20 yrs	50 yrs	100 yrs
RCP 4.5	2,056	2,649	3,176	887	1,320	1,590
RCP 8.5	2,309	3,068	3,775	995	1,470	1,780
ISP → OSP dam segment						
Scenario	**Max Release (Peak Flow)**			**Optimum Release**		
	20 yrs	50 yrs	100 yrs	20 yrs	50 yrs	100 yrs
RCP 4.5	816	1,146	1,484.19	240.98	343	444
RCP 8.5	1,069.15	1,547.03	2,054.03	314	457	613
OSP dam → SSP dam segment						
Scenario	**Max Release (Peak Flow)**			**Optimum Release**		
	20 yrs	50 yrs	100 yrs	20 yrs	50 yrs	100 yrs
RCP 4.5	1,363.728	1,873	2,346.304	185	204	225
RCP 8.5	1,875.191	2,631.731	3,362.419	240	256	269

Table 6. Parameters for peak and optimized flows for various segments

Bargi → ISP (RCP 4.5)						
Parameter	**Original Peak Flow**			**Optimized Release**		
	20 yrs	50 yrs	100 yrs	20 yrs	50 yrs	100 yrs
Max. inundation area (sq. km)	6,333.034	7,239.47	7,928.13	5,740.618	6,493.956	7,081.853

Maximum depth (m)	68.722	73.405	77.617	67.788	74.115	76.943

Bargi → ISP (RCP 8.5)

Parameter	**Original Peak Flow**			**Optimized Release**		
	20 yrs	50 yrs	100 yrs	20 yrs	50 yrs	100 yrs
Max. inundation area (sq. km)	7,428.481	8,534.888	9,377.86	6,810.516	7,654.64	8,506.062
Maximum depth (m)	77.396	80.913	87.421	77.4	80.737	87.16

ISP → OSP (RCP 4.5)

Parameter	**Original Peak Flow**			**Optimized Release**		
	20 yrs	50 yrs	100 yrs	20 yrs	50 yrs	100 yrs
Max. inundation area (sq. km)	140.328	172.223	200.807	109.365	135.989	153.949
Maximum depth (m)	48.706	52.387	54.992	47.233	52.64	55.345

ISP → OSP (RCP 8.5)

Parameter	**Original Peak Flow**			**Optimized Release**		
	20 yrs	50 yrs	100 yrs	20 yrs	50 yrs	100 yrs
Max. inundation area (sq. km)	180.272	225.458	266.576	145.739	177.381	203.743
Maximum depth (m)	54.818	59.207	62.307	55.164	59.662	62.672

OSP → SSP (RCP 4.5)

Parameter	**Original Peak Flow**			**Optimized Release**		
	20 yrs	50 yrs	100 yrs	20 yrs	50 yrs	100 yrs
Max. inundation area (sq. km)	1,585.194	1,914.285	2,128.497	1,300.658	1,571.612	1,767.576

Maximum depth (m)	64.751	68.514	72.226	64.756	68.5	72.213
OSP → SSP (RCP 8.5)						
Parameter	**Original Peak Flow**			**Optimized Release**		
	20 yrs	50 yrs	100 yrs	20 yrs	50 yrs	100 yrs
Max. inundation area (sq. km)	2,049.098	2,385.338	2,639.198	1,755.381	2,082.014	2,312.986
Maximum depth (m)	71.835	76.753	77.506	71.83	76.737	77.496

Comparison of Maximum Inundation Area and Depth for Peak and Optimized Flows

Following the completion of flood modelling using optimized reservoir releases, a comparative assessment was conducted between peak flow conditions and optimized flow scenarios, as summarized in Table 6.

The results presented in the preceding sections highlight the spatial extent of inundation in terms of area and depth, along with associated hydraulic parameters such as maximum velocity and maximum water surface elevation (WSE), under different climate change scenarios. This analysis examines variations in potential inundation characteristics after implementing optimized reservoir releases derived through fuzzy optimization for multiple return periods.

A comparison between optimized releases and original peak flows indicates a substantial reduction in reservoir outflows. In the Bargi-to-ISP segment, releases decrease by approximately 57% and 56% for the 20-year return period under RCP 4.5 and RCP 8.5 scenarios, respectively. For the 50- and 100-year return periods, the reduction ranges between 50% and 52%. This decrease in discharge leads to a corresponding reduction in inundation area of about 10%.

In the ISP-to-OSP segment, optimized releases are reduced to nearly 70% of peak flow values across all return periods and climate scenarios. This reduction results in a more pronounced decline in inundation area, ranging from approximately 20% to 23%.

For the OSP-to-SSP segment under the RCP 4.5 scenario, optimized releases decrease significantly to about 86%, 89%, and 90% of peak flow values for the 20-, 50-, and 100-year return periods, respectively. This reduction leads to a decrease in inundation area of around 17–18% under RCP 4.5 and 12–14% under RCP 8.5.

Despite these notable reductions in inundation extent, the maximum water depth remains largely unchanged across all scenarios and return periods for both peak and optimized flow conditions. Additionally, inundation areas are consistently higher under the RCP 8.5 scenario compared to RCP 4.5.

Overall, the comparison across the three river segments demonstrates that the Bargi-to-ISP stretch experiences a relatively modest reduction in inundation area (approximately 10%), whereas the ISP-to-OSP segment shows the highest reduction (exceeding 20%). The OSP-to-SSP segment exhibits a moderate reduction of less than 20%. Across all segments, maximum water depth remains nearly constant for a given return period.

These findings suggest that optimizing reservoir releases is an effective strategy for flood mitigation. Furthermore, the results indicate that inundation area increases with higher return periods under both RCP 4.5 and RCP 8.5 scenarios, emphasizing the growing flood risk under more extreme hydrological conditions.

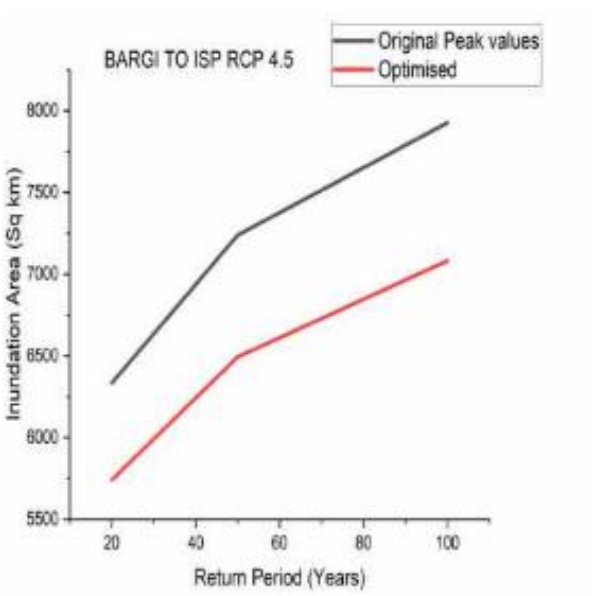

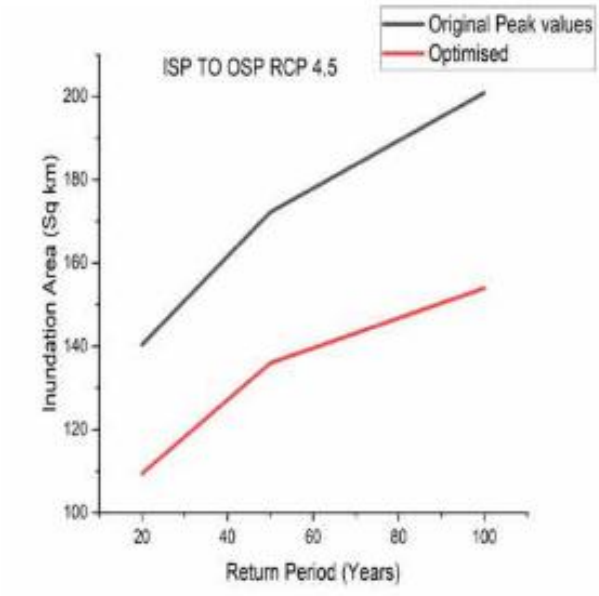

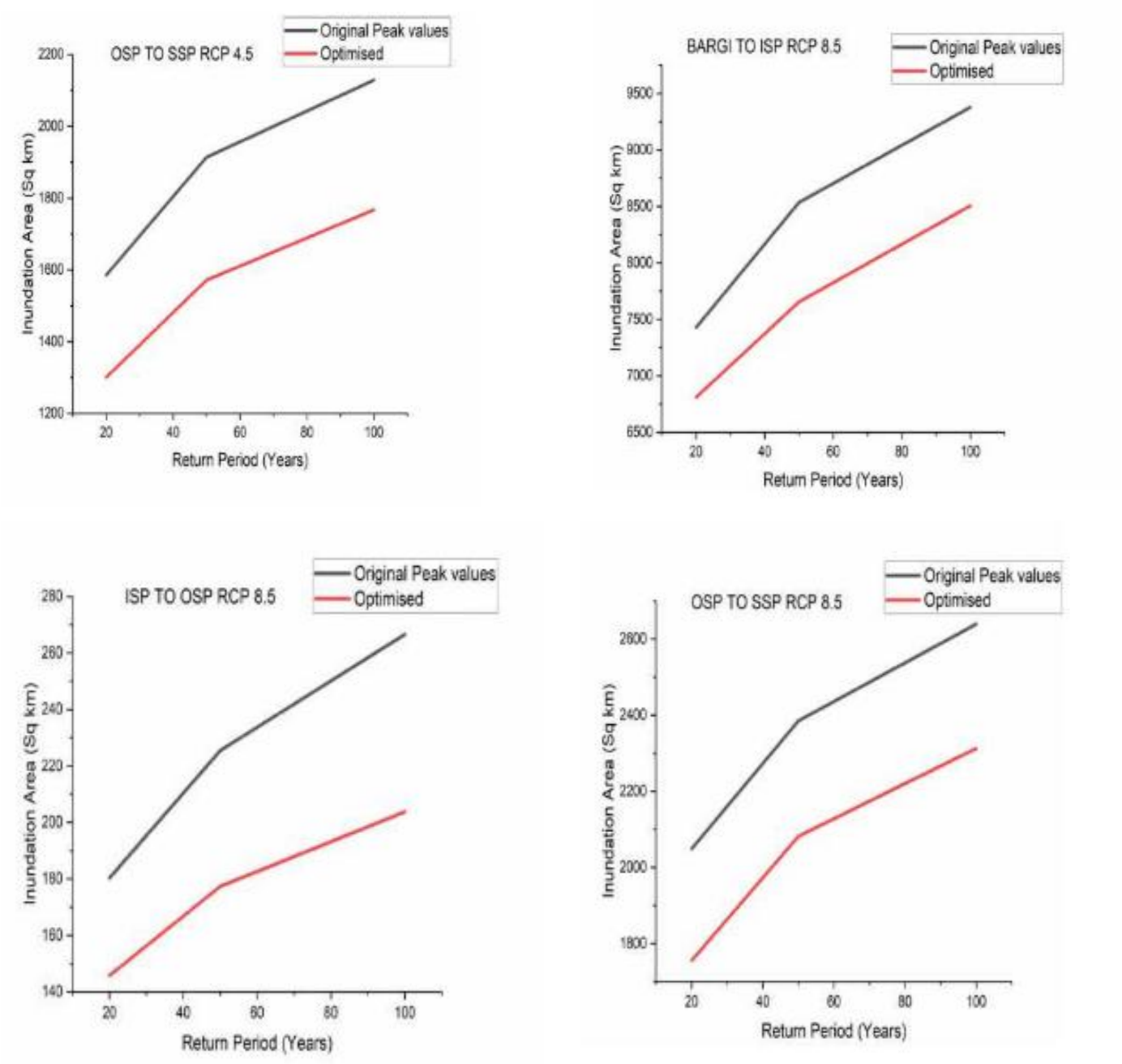

Figure 10: Graphs of inundation area vs. return periods for different stretches.

3.3 Hydrodynamic modeling for Narmada River flood prediction in coastal floodplain

3.3.1 Data and Methods

This study focuses on a 63 km stretch of the lower Narmada River, extending from Shuklatirth to the Arabian Sea. The study area covers approximately 885 km² and includes a key gauging station at Golden Bridge, Bharuch, where hourly water level data are recorded. The station has a warning level of 6.70 m, a danger level of 7.31 m, and a recorded highest flood level of 12.65 m on September 6, 1970. As no major tributaries join the river within this reach, lateral inflow was neglected in the analysis. In the absence of a gauging station at Shuklatirth, river discharge was routed over a 100 km upstream stretch from Garudeshwar (the nearest upstream gauging station) to Shuklatirth, which was

taken as the starting point (chainage 0) of the 2D hydraulic model. The study reach includes four major bridge structures: a railway bridge at Bharuch with a span of 1407 m (located at approximately 15 km downstream of Shuklatirth), the Golden Road Bridge with a span of 1429 m situated just upstream of the railway bridge, and two additional road bridges near Zadeshwar at a chainage of about 10 km.

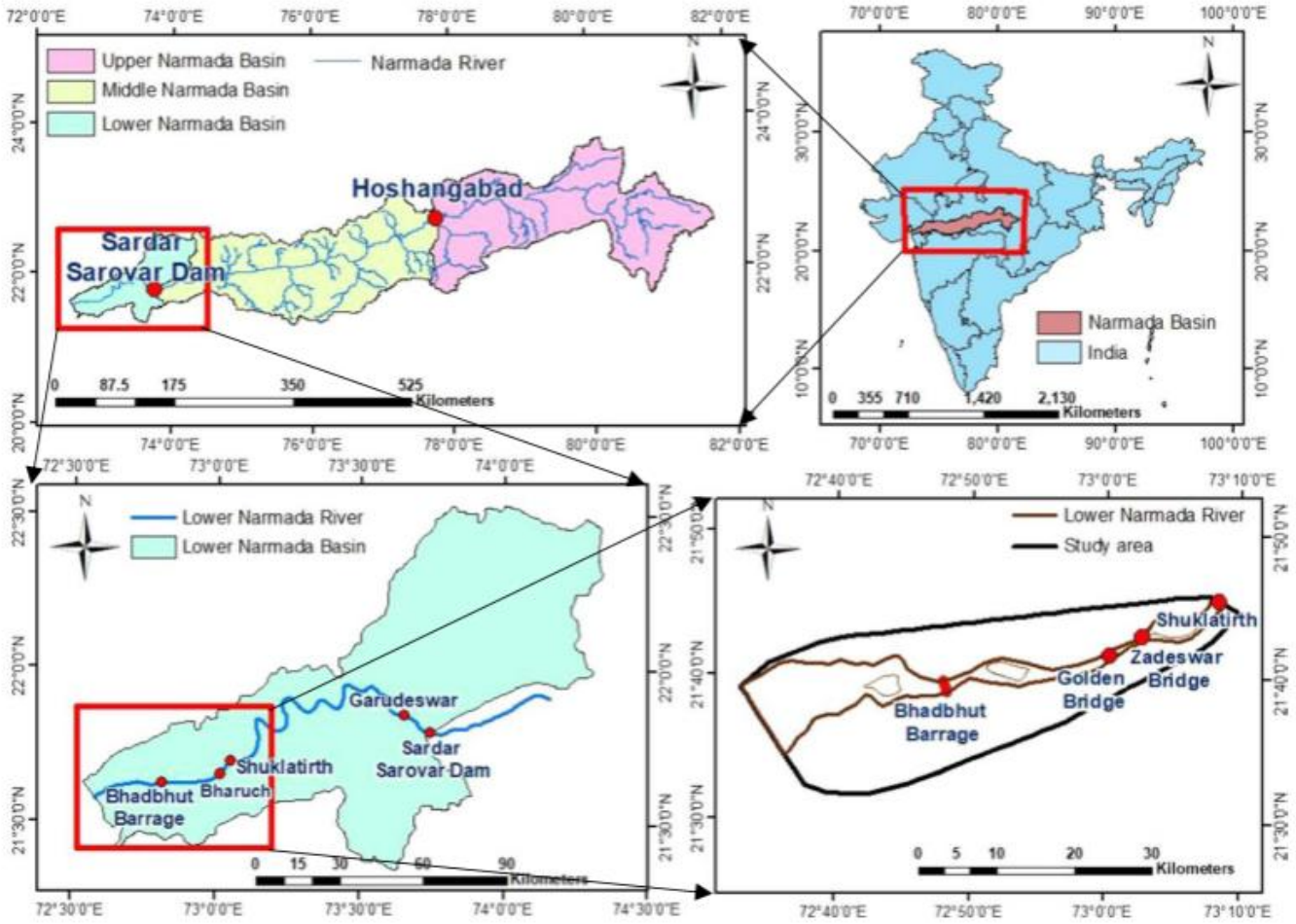

Figure 11: Index map of Narmada basin along with study reach

3.3.2 Data Collection

Hydrographic and topographic surveys for the study area were conducted by the relevant authorities. The required datasets, including hydrographic information and topographic details in the form of contour maps, were obtained from the office of the Executive Engineer, PIU-1 (Project Implementation Unit-1), Gujarat Engineering Research Institute (GERI), Vadodara, India, in AutoCAD format.

Hydrological data comprising hourly water levels at Golden Bridge (chainage 15 km) and Garudeshwar, along with hourly discharge data at Garudeshwar, were sourced from the office of the Executive Engineer, Central Water Commission (CWC), Tapi Division, Surat, India. Additionally,

observed hourly tidal level data for the period from July 28, 2006, to September 18, 2006, were collected from PIU-1, GERI, Vadodara.

The observed tidal data were adjusted based on the lunar cycle, and tidal levels corresponding to the simulation period were used as downstream boundary conditions. The routed flood hydrograph at Shuklatirth for the 2013 flood event, along with the corresponding hourly tidal levels at the Arabian Sea boundary (chainage 63 km), were utilized in the modelling framework.

Flood frequency analysis for the lower Narmada River was carried out by the Kalpasar Department, Government of Gujarat, using historical flood records. Key design parameters, including the 100-year return period flood, standard project flood, and observed maximum flood values, were obtained from this source.

Information regarding the proposed Bhadbhut barrage was also collected; however, it was not incorporated into the present study, as the project is still in the final tendering stage.

3.3.3 Methodology

The two-dimensional hydraulic model for the study was developed using the MIKE 21 FM module within the MIKE Zero platform. This modelling framework allows the integration of hydraulic structures such as gates, dikes, and turbines, enabling a realistic representation of river flow dynamics. The overall methodology adopted for modelling the lower Narmada River is illustrated in Fig. 12 and consists of three key stages. First, a two-dimensional model was developed, followed by its calibration and validation using observed data. Second, hydraulic structures such as gates and embankments were incorporated into the calibrated model. Finally, simulations were carried out to estimate water levels under varying conditions of gate operation and embankment configurations for different flood discharges.To evaluate the impact of structural interventions, multiple scenarios were considered in the analysis. These include: (1) a baseline condition without the Bhadbhut barrage, (2) a scenario with the barrage gates closed and no upstream embankments, (3) a scenario with the barrage gates open and embankments extending up to Zadeshwar Bridge along both riverbanks, and (4) a scenario with the barrage gates open and embankments provided along both banks up to Shuklatirth.

3.3.4 Hydrologic Channel Routing

The discharge observed at the Garudeshwar gauging station was routed to Shuklatirth using the Muskingum channel routing method. The routing parameters, K and X, were estimated based on empirical relationships proposed by Tewolde and Smithers (2006). In this study, the values of K and X were taken as 6 hours and 0.251, respectively. A time step of 1 hour was used for the routing

computations. Simulations were carried out for a range of Manning's roughness coefficients (n), and the corresponding results are summarized in Table 7.

Table 7. Muskingum parameter values

Sl. No.	Manning's *n*	K (hr)	X
1	0.015	6	0.251
2	0.020	7	0.204
3	0.025	8	0.162
4	0.030	9	0.123
5	0.035	10	0.086

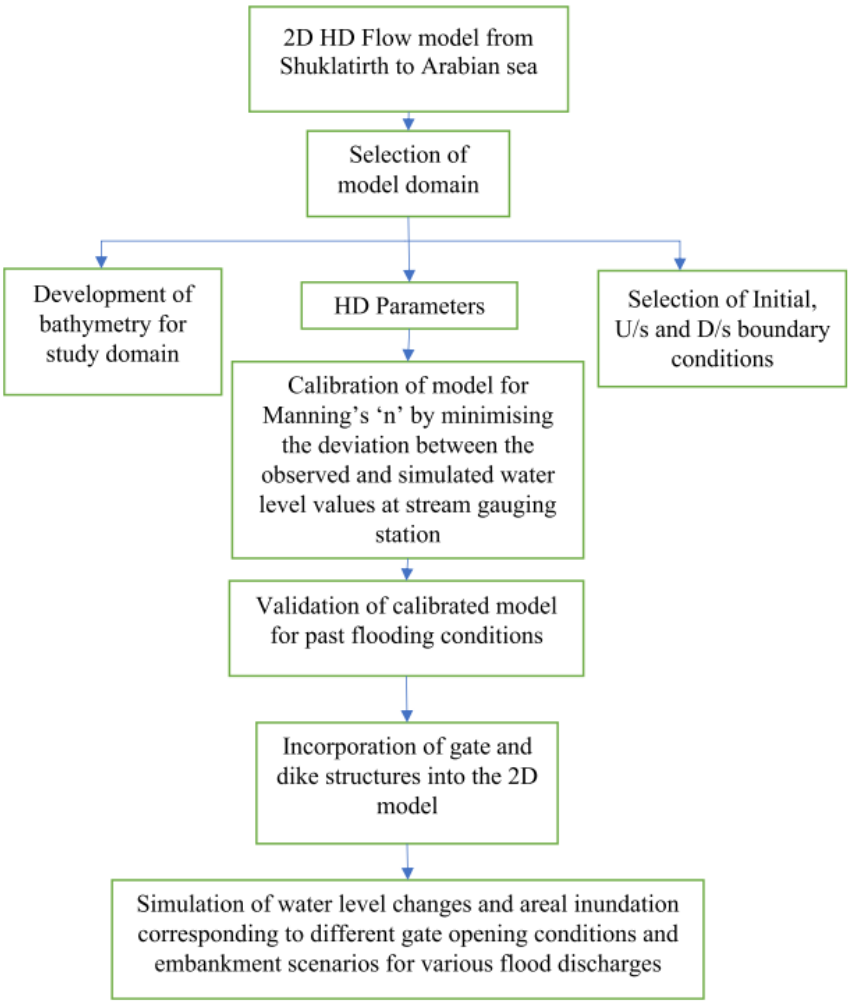

Figure 12: Methodology used for the development of two-dimensional hydrodynamic model

3.3.5 Model Calibration

The calibration of the model's roughness parameter was performed using a trial-and-error approach to minimize the discrepancy between simulated and observed flow variables. The flood event of 2006, with a peak discharge of 19,433 m^3/s, was simulated over a period of 120 hours, from August 6, 2006 (00:00:00) to August 10, 2006 (23:00:00). Multiple simulations were conducted by varying Manning's *n* values for both the river channel and the adjoining land surface.

Model performance was evaluated using two statistical indicators: the Nash–Sutcliffe Efficiency (NSE) and the Root Mean Square Error (RMSE), following Timbadiya et al. (2014b). These metrics were computed by comparing observed and simulated water levels at the Golden Bridge gauging station in Bharuch.

The results (Table 8) indicate that the simulated water levels closely match the observed data when Manning's *n* values are set to 0.015 for the river channel and 0.03 for the land surface.

Table 8. Calibration of 2D Model for Manning's *n*

Trial	Manning's *n* (River Stretch)	Manning's *n* (Land Surface)	RMSE in Water Levels (m)	NSE
1	0.03	Distributed (LULC-based)	2.11	-0.51
2	0.02	Distributed (LULC-based)	1.89	-0.21
3	0.015	Distributed (LULC-based)	1.78	-0.08
4	0.03	0.06	2.10	-0.50
5	0.03	0.04	1.72	-0.007
6	0.02	0.06	1.90	-0.23
7	0.02	0.04	1.52	0.209
8	0.015	0.06	1.18	0.22
9	0.015	0.04	1.03	0.46
10	0.015	0.03	0.84	0.79

Note: "Distributed (LULC-based)" indicates Manning's *n* values assigned spatially based on land-use/land-cover classification.

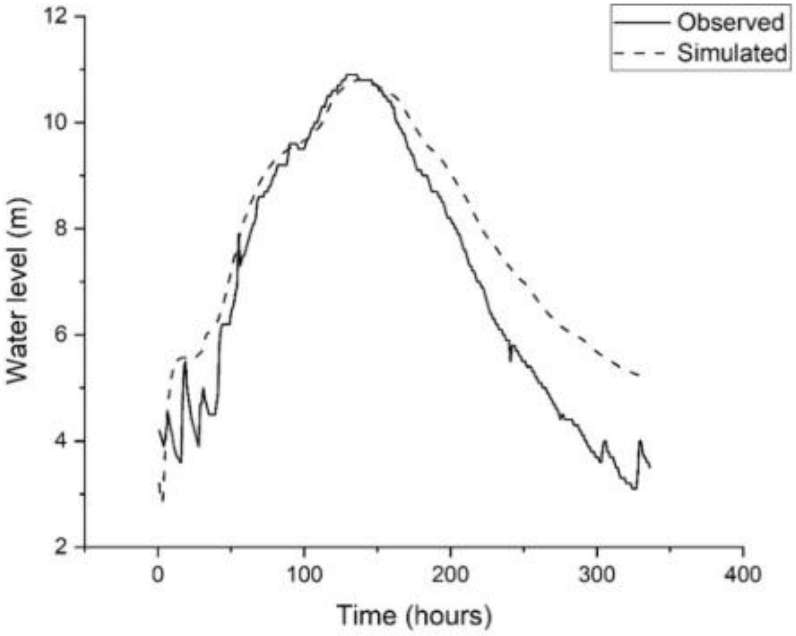

Figure 13: Observed and simulated flood water levels at Golden Bridge, Bharuch, for August 2013 flood

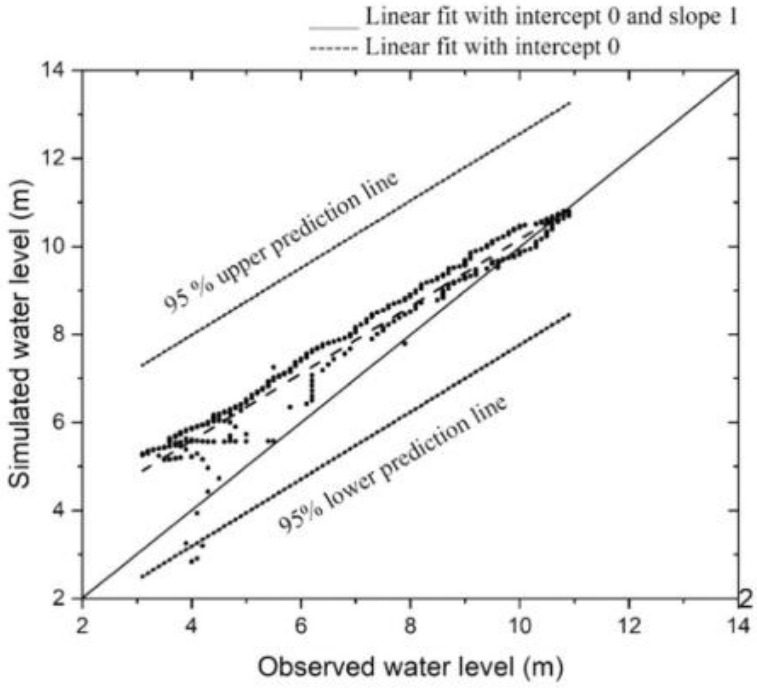

Figure 14: Simulated water levels versus observed water levels at the Golden Bridge, Bharuch

3.3.6 Model Validation

The calibrated model was validated using the 2013 flood event, which had a peak discharge of 32,220 m^3/s. The simulation covered a duration of 336 hours, from August 20, 2013 (00:00:00) to September 2, 2013 (23:00:00).

Model performance was assessed by comparing observed and simulated water levels at the Golden Bridge gauging station in Bharuch (Figs. 13 and 14). In addition, the performance indicators—Root

Mean Square Error (RMSE) and Nash–Sutcliffe Efficiency (NSE)—were computed for the same location.

The validation results yielded an RMSE of 1.1 m and an NSE of 0.79, indicating satisfactory model performance in accordance with established criteria (Moriasi et al., 2007). Therefore, the calibrated Manning's *n* values of 0.015 for the river channel and 0.03 for the land surface were deemed appropriate for subsequent simulations.

3.3.7 2D Flood Simulations

The simulation period was selected from August 20, 2013 (00:00:00) to September 2, 2013 (23:00:00), covering a total duration of 336 hours, including the peak flood event. The simulations were performed using the GPU-based parallel computing capability of MIKE 21 (FM). The computational domain was partitioned into four subdomains, each consisting of 3,415 mesh elements, resulting in a total of 13,660 elements.

Model outputs were recorded at one-hour intervals. Water-level hydrographs were extracted at key locations, including Zadeshwar Bridge, Golden Bridge, and the proposed Bhadbhut barrage. These simulations were conducted for a range of flood discharges and embankment scenarios, as described earlier.

3.3.8 Results and Discussion

The developed 2D model was used to simulate key hydraulic parameters, including flow velocity, water surface slope, and discharge fluxes in both the river channel and floodplain for the 2006 and 2013 flood events.

Prediction of Water Levels

The observed and simulated water levels at the Golden Bridge gauging station in Bharuch are compared in Figs. 13 and 14. The comparison indicates a close agreement between simulated and observed flood levels, demonstrating the reliability of the model.

The 2013 Flood Event

The simulated flood extents on August 26, 2013 (12:00:00) for different embankment scenarios are overlaid on Google Earth imagery and presented in Fig. 15(a–d). As the flood wave propagates, overtopping of the left bank occurs, resulting in significant inundation on the left floodplain, as shown

in Fig. 15a. This inundation further increases under scenario 2 due to gate closure at the barrage (Fig. 15b).

In scenario 3, the construction of embankments up to Zadeshwar Bridge reduces the inundation extent (Fig. 15c). However, some floodwater still escapes the channel due to the constriction in river width near the bridge. This issue can be mitigated either by widening the river section at this location or by extending the embankments further upstream, as illustrated in Fig. 15d.

The highest water levels at Zadeshwar Bridge are observed in scenario 4, where embankments extend up to Shuklatirth. This occurs because upstream overbank flow is prevented, leading to increased confinement of flow within the channel. At Golden Bridge, the peak water levels for scenarios 1 (9.9 m) and 2 (9.97 m) are nearly identical, indicating that backwater effects due to gate closure at the Bhadbhut barrage result in overtopping upstream before reaching Zadeshwar Bridge.

The difference in water levels between scenarios 1 and 3 (Fig. 16) represents the volume of water retained within the river channel due to embankment construction up to Zadeshwar Bridge. Similarly, the variation between scenarios 3 and 4 reflects the reduction in upstream spill when embankments are extended to Shuklatirth.

The gated structure was operated under multiple gate-opening conditions, and the corresponding maximum water-level variations for embankment scenario 3 are presented in Fig. 17.

Significant variations in water levels were observed at Zadeshwar Bridge and Golden Bridge for the initial gate-opening conditions, while the changes became negligible for higher openings. At Zadeshwar Bridge, the maximum water levels for all gate operations remain below the soffit levels of both bridges, indicating structural safety under these conditions when embankments extend up to Zadeshwar.

However, at Golden Bridge, the maximum water level under the first gate-opening condition exceeds the soffit level of the railway bridge, indicating potential risk. The most pronounced effects of gate operation are observed at the Bhadbhut barrage site, where water levels exceed the full reservoir level (7.5 m) for the first three gate-opening conditions.

These elevated water levels could be mitigated in the future by incorporating the proposed canal system to divert excess flow to the Kalpasar reservoir or by providing a side-channel spillway along the left embankment. Simulation of these mitigation measures is identified as a scope for future work.

Fig. 18 present water-level variations for different gate operations under embankment scenario 4 (extended up to Shuklatirth). The maximum water levels at Zadeshwar Bridge in this scenario are approximately 4 m higher than those in scenario 3. This increase is attributed to the confinement of backwater flow, which, in scenario 3, would otherwise spill upstream of Zadeshwar. In contrast, the peak water levels at Golden Bridge and the Bhadbhut barrage remain nearly unchanged between scenarios 3 and 4.

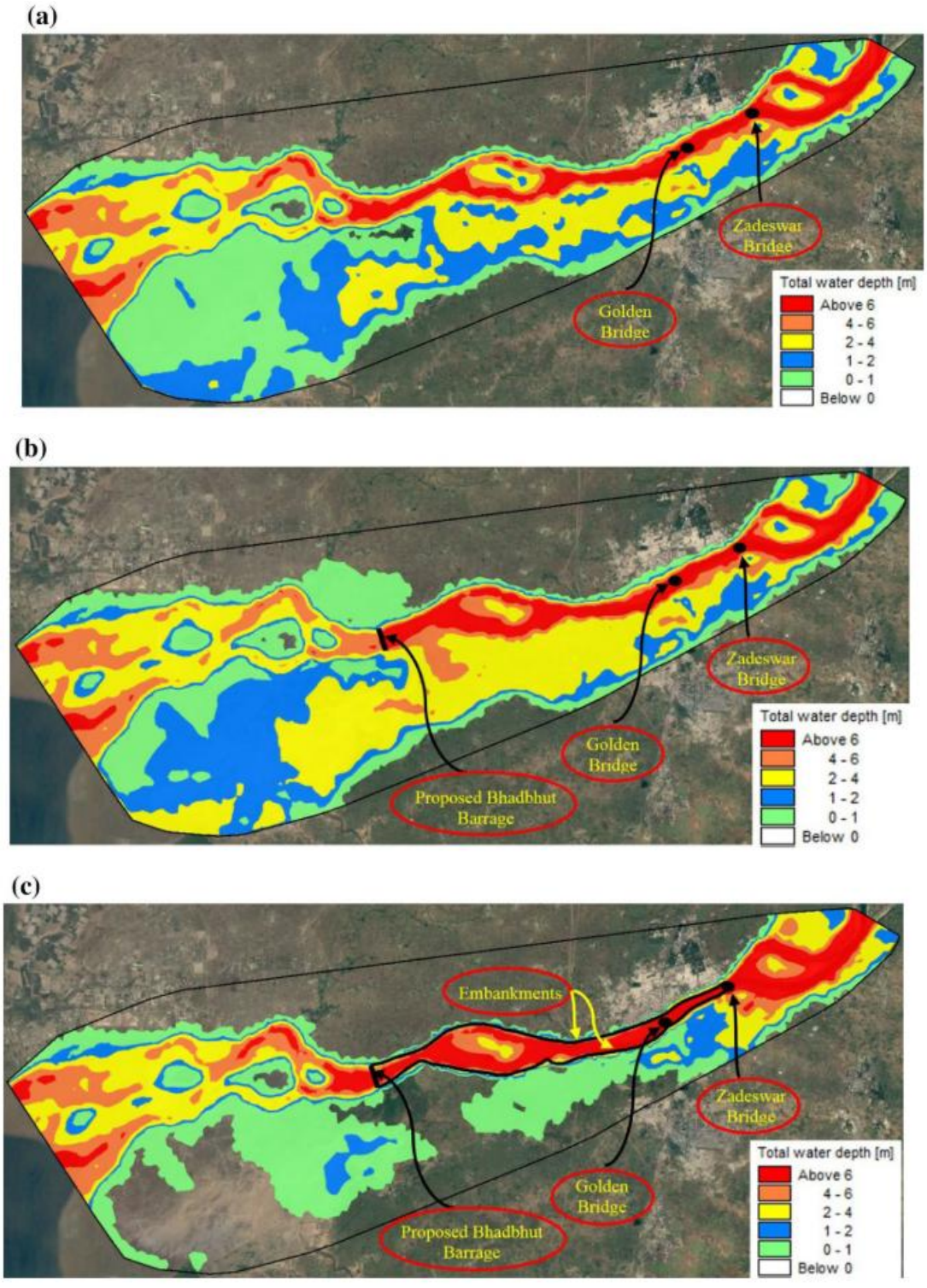

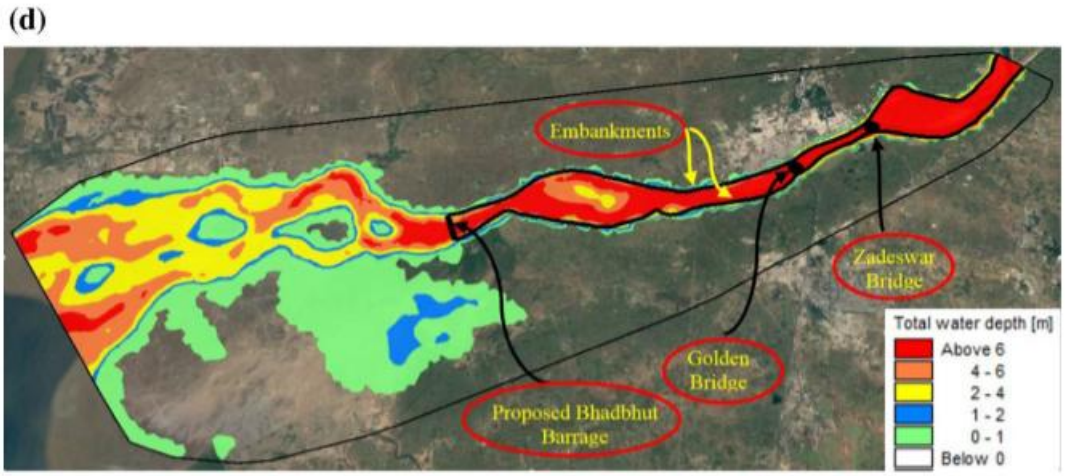

Figure 15: (a) Flooding condition in lower Narmada River for embankment scenario 1 (without barrage) on 26-08-2013 at time 12:00:00. (b) Flooding condition in lower Narmada River for embankment scenario 2 (with barrage gate closed and no embankment) on 26-08-2013 at time 12:00:00. (c) Flooding condition in lower Narmada River for embankment scenario 3 (barrage gate opened and embankment up to Zadeshwar Bridge) on 26-08-2013 at time 12:00:00. (d) Flooding condition in lower Narmada River for embankment scenario 4 (barrage gate opened and embankment up to Shuklatirth) on 26-08-2013 at time 12:00:00

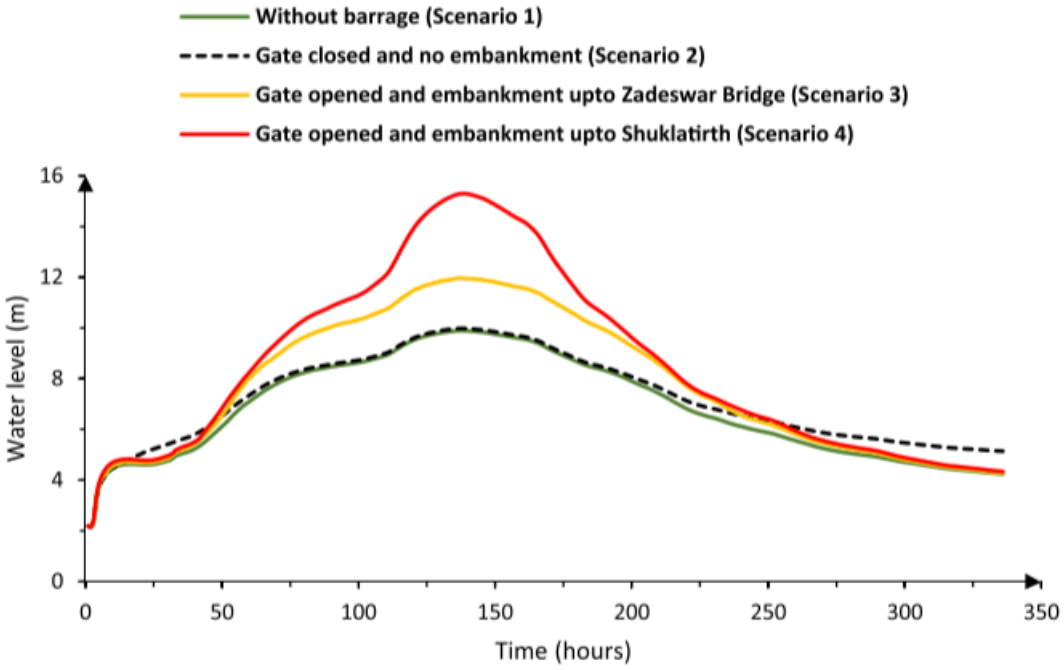

Figure 16: Water-level variations at Zadeshwar Bridge for different embankment scenarios of 2013 flood event

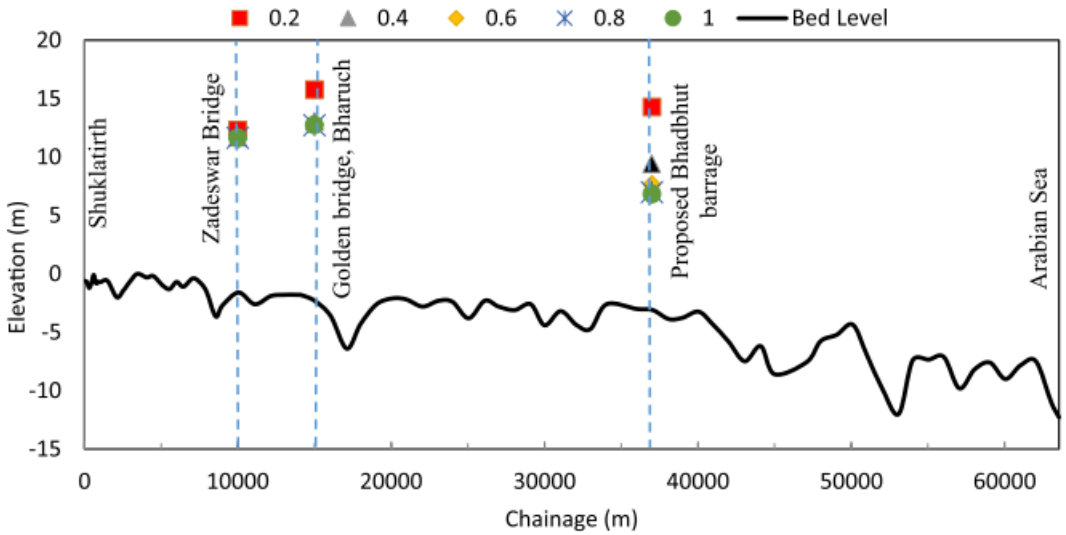

Figure 17: Maximum water-level variations for different gate-opening conditions when the embankments are provided up to Zadeshwar Bridge (scenario 3) and considering 2013 flood event

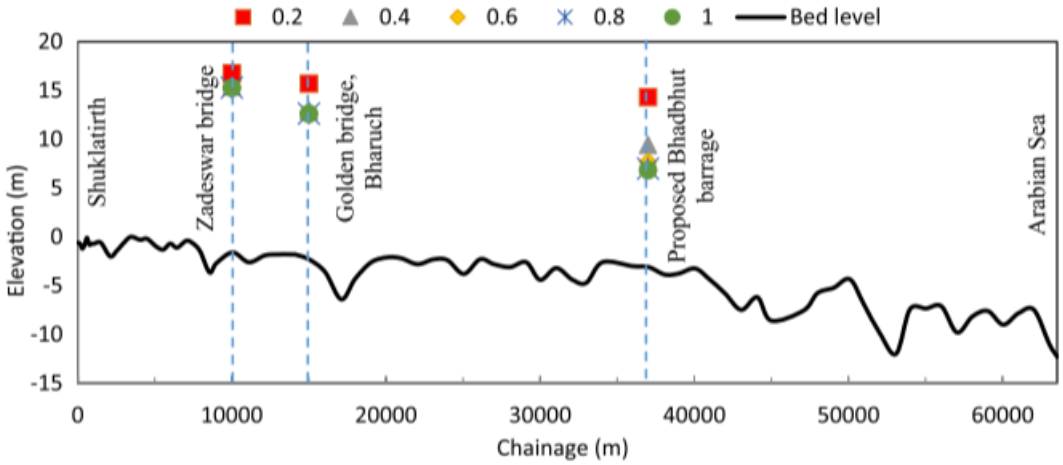

Figure 18: Maximum water-level variations for different gate-opening conditions when the embankments are provided up to Shuklatirth (scenario 4) considering 2013 flood event

3.4 flood forecasting in Narmada River basin using hierarchical clustering and hydrological modelling

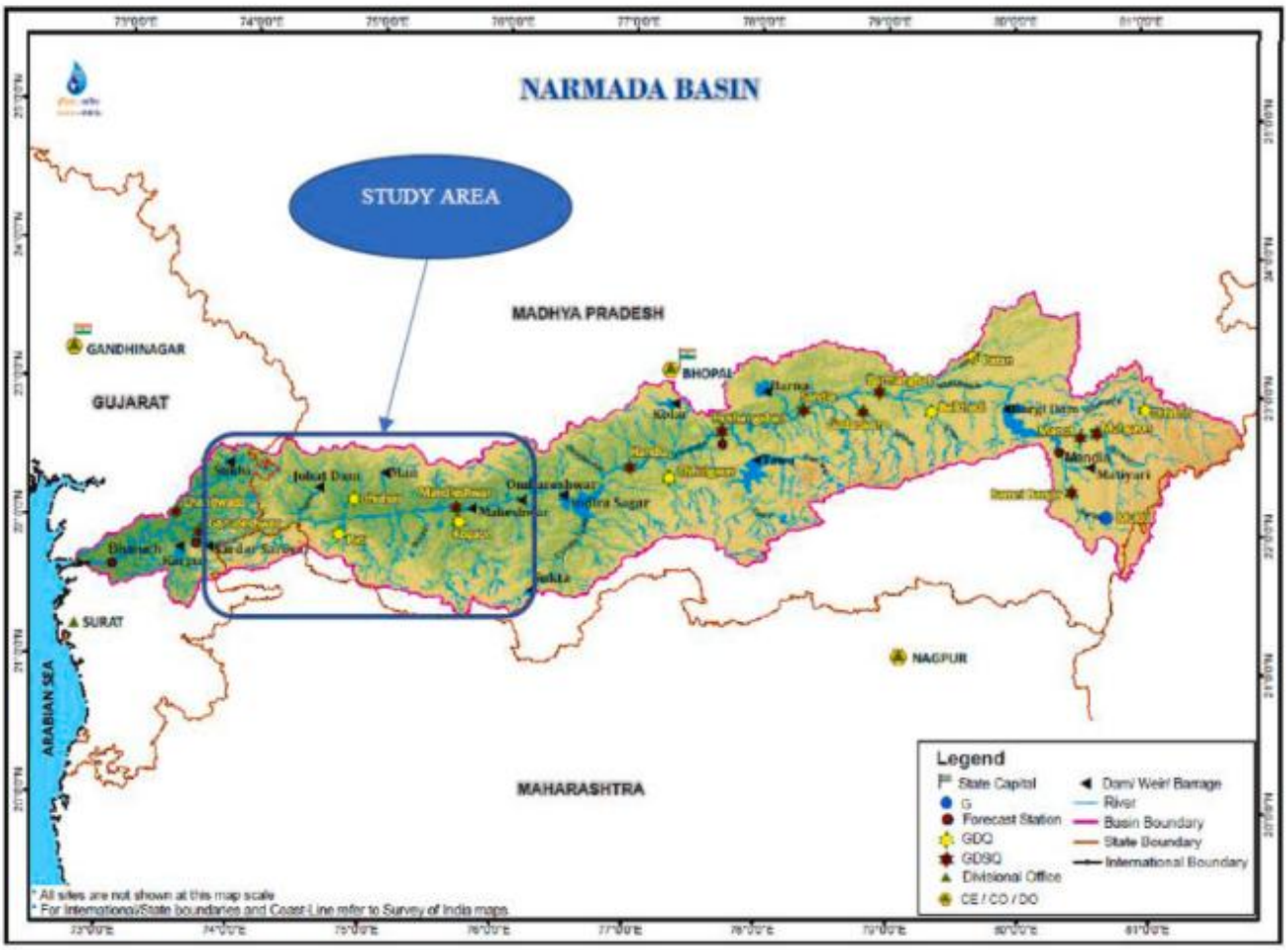

Figure 19: Location of study area in Narmada Basin (Source: indiawris.gov.in).

3.4.1 Study Area and Data Collection

The study focuses on a 270 km reach of the Narmada River. Digital Elevation Model (DEM) data were obtained from the Bhuvan portal (bhuvan-app3.nrsc.gov.in). Discharge data were sourced from the Central Water Commission (CWC), Bhopal, while rainfall data for the period 2010–2018 were provided by the Narmada Control Authority. Inflow data for the Sardar Sarovar Dam were obtained from Narmada Bhavan, Kevadiya Colony, Gujarat.

To support flood forecasting and improve the analysis of the rain gauge network, rainfall data from multiple gauge stations distributed across the Narmada basin were collected. The spatial distribution

of these stations ensures adequate coverage of the basin. Table 9 lists the locations of the rain gauge stations along with their corresponding basin IDs and geographic coordinates. The stations include OSP, Dhadgaon, Kogaon, Khargone, Dharmpuri, Man, Maheshwar, Rajpur, Sendhwa, Barwani, Dhuusar, Jobat, Alirajpur, Pati, Toranmal, Molgi, and SSP.

Table 9. Location of Rain Gauge Stations with Basin IDs

Basin ID	Location	Latitude	Longitude
W1400	OSP	22° 14′ 37.26″	76° 09′ 46.83″
W820	Dhadgaon	22° 05′ 24″	76° 07′ 12″
W1014	Kogaon	22° 09′ 38.9″	75° 39′ 21.7″
W1220	Khargone	21° 49′ 48″	75° 36′ 36″
W890	Dharmpuri	22° 10′ 12″	75° 21′ 00″
W640	Man	22° 25′ 11.7″	75° 06′ 28.8″
W650	Maheshwar	22° 10′ 48″	75° 10′ 48″
W930	Rajpur	21° 55′ 48″	75° 07′ 48″
W1000	Sendhwa	21° 40′ 48″	75° 05′ 24″
W700	Barwani	22° 02′ 24″	74° 54′ 00″
W1140	Dhuusar	22° 12′ 00″	74° 52′ 12″
W710	Jobat	22° 25′ 12″	74° 34′ 12″
W670	Alirajpur	22° 18′ 19″	74° 21′ 09″
W1120	Pati	21° 56′ 24″	74° 45′ 00″
W1150	Toranmal	21° 52′ 48″	74° 27′ 36″
W1100	Molgi	21° 45′ 53.3″	74° 00′ 24.8″
W1130	SSP	21° 49′ 49″	73° 45′ 09″

3.4.3 Methodology

The overall methodology adopted in this study is illustrated in Fig. 20. The first step involves identifying representative rain gauge stations using the Hierarchical Clustering (HC) technique, based on the rainfall characteristics of individual gauge locations.

The Narmada River basin is then delineated using the Thiessen polygon method, and the resulting spatial distribution of rainfall influence areas is generated in ArcGIS (version 10.1).

Subsequently, rainfall–runoff modeling is performed using the Hydrologic Engineering Center's Hydrologic Modeling System (HEC-HMS, version 4.3). The simulated runoff from the hydrological model is validated by comparing it with observed discharge data at gauging stations and the recorded inflow to the Sardar Sarovar Dam.

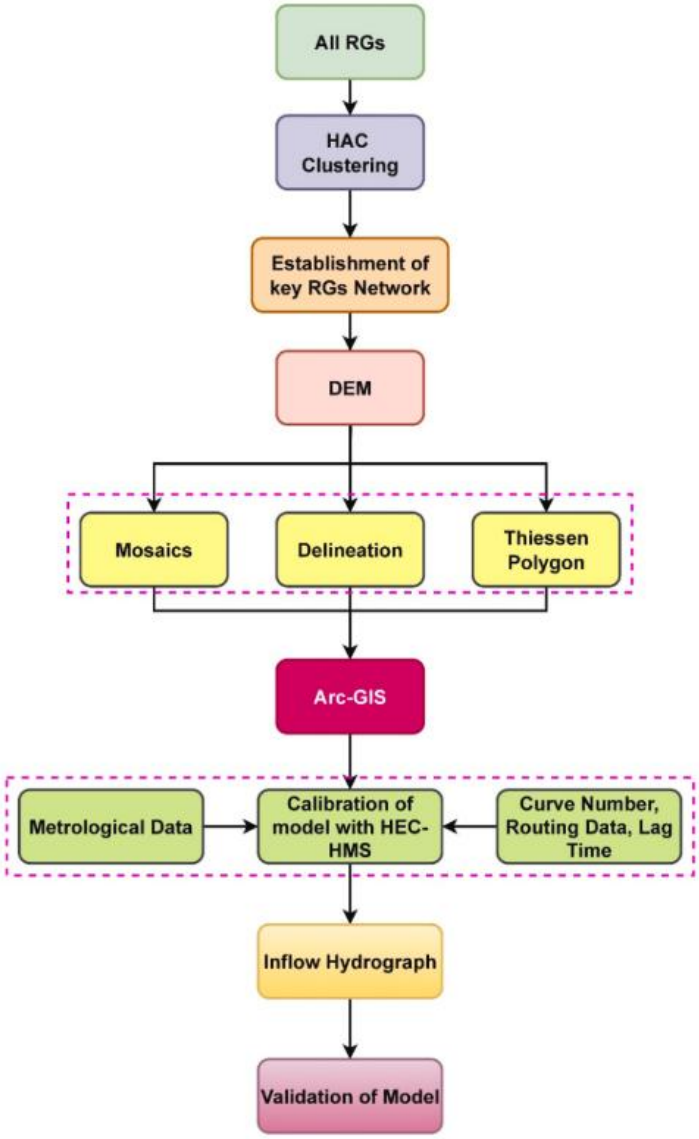

Figure 20: Flowchart of methodology.

3.4.4 Results and Discussion

Hierarchical Clustering

Hierarchical clustering (HC) is a statistical technique used to group objects based on similarity, with the results typically represented using a dendrogram that illustrates the nested structure of clusters. In this study, an agglomerative (bottom-up) approach was adopted, wherein individual rain gauge stations were initially treated as separate clusters and progressively merged based on similarity in rainfall characteristics until a unified cluster structure was obtained.

The dendrogram (Fig. 21) reveals that the rain gauge stations can be broadly classified into two major groups. The first group comprises five stations—Kogaon, Khargone, Pati, Dhulsar, and Jobat—which

exhibit similar rainfall patterns. Within this group, Pati shows strong similarity with Dhulsar and Jobat, while this sub-cluster further aligns with Khargone, followed by Kogaon.

The second group includes Udaynagar, Kannod, Khandwa, Sendhwa, Dhonchiya, Barwani, Dhadgaon, New Harsud, and Maheshwar. The rainfall characteristics of Udaynagar are found to be comparable with those of Dhonchiya, Kannod, Khandwa, and Sendhwa, as well as with New Harsud and Maheshwar. Additionally, Dhadgaon and Barwani form a closely related sub-group within this cluster.

Thiessen Polygon Method

The Thiessen polygon method, developed by A.H. Thiessen, is widely used to estimate mean areal precipitation over a catchment using point rainfall data from gauge stations. The method assumes that the rainfall measured at a station is uniformly distributed over its area of influence, extending up to the midpoint between neighboring stations. Thiessen polygons are constructed by drawing perpendicular bisectors between adjacent rain gauge stations, thereby defining zones of influence for each station. The area of each polygon determines the weight assigned to the corresponding gauge in computing areal rainfall. In cases where data from a station are missing, the associated polygon must be adjusted accordingly. However, the method does not explicitly account for spatial variability in rainfall due to topographic effects.In the present study, seventeen Thiessen polygons were delineated to represent the spatial distribution of rainfall across the study area, as shown in Fig. 22.

Hydrological Modelling

Rainfall–runoff modeling was carried out using observed rainfall data. Data from the years 2012, 2015, and 2016 were used for model calibration, while data from 2017 and 2018 were used for model validation.

Comparison of Observed and Simulated Flow

Model calibration involves adjusting model parameters to obtain the best possible agreement between simulated and observed discharge. In this study, calibration was performed using data from 2012, 2015, and 2016 at two key locations. Initially, calibration was conducted at the upstream gauging station at Mandleshwar. Subsequently, calibration was extended to the Sardar Sarovar Dam site.

Model Calibration and Validation at Mandleshwar Gauging Site

Model calibration at the Mandleshwar gauging station was carried out using rainfall data from the Dhadgaon, Kogaon, Khargone, and Omkareshwar stations. The comparison between observed and simulated discharge for the year 2012 is presented in Fig. 23a. The observed peak discharge was 25,442

m^3/s, whereas the model simulated a peak discharge of 26,949.4 m^3/s, slightly overestimating the observed value. The peak occurred on August 7, 2012.

Similarly, comparisons for the years 2015 and 2016 are shown in Fig. 23b and Fig. 23c, respectively. For 2015, the observed peak discharge was 11,326.5 m^3/s, while the simulated peak was 12,640.2 m^3/s, indicating an overestimation. The peak occurred on August 6, 2015. In 2016, the observed peak discharge was 9,000 m^3/s, whereas the simulated peak was 8,373.3 m^3/s, indicating a slight underestimation. The peak occurred on August 7, 2016.

Model validation was performed using independent datasets from 2017 and 2018 to assess the predictive capability of the model. The comparisons between observed and simulated hydrographs are shown in Fig. 23d and Fig. 23e. For 2017, the observed peak discharge was 2,590 m^3/s, while the simulated peak was 2,775.2 m^3/s, indicating an overestimation. The peak occurred on August 13, 2017. Similarly, for 2018, the observed peak discharge was 2,590 m^3/s, and the simulated peak was 2,675.2 m^3/s, again slightly overestimating the observed value. The peak occurred on August 18, 2018.

Model Calibration and Validation at Sardar Sarovar Dam

Calibration at the Sardar Sarovar Dam site was performed using rainfall data from multiple stations, including Maheshwar, Dharampuri, Man, Barwani, Rajpur, Sendhwa, Alirajpur, Dhulsar, Pati, Jobat, Toranmal, Dhadgaon, Molgi, and the Sardar Sarovar Dam station.

The comparison between observed and simulated discharge for 2012 is shown in Fig. 24a. The observed peak discharge was 25,751.3 m^3/s, while the simulated peak was 26,254 m^3/s, indicating a slight overestimation. The peak occurred on August 8, 2012.

For 2015 (Fig. 24b), the observed peak discharge was 11,326.7 m^3/s, whereas the simulated peak was 11,141.6 m^3/s, indicating a slight underestimation. The peak occurred on August 8, 2015. For 2016 (Fig. 24c), the observed peak discharge was 9,464.6 m^3/s, while the simulated peak was 9,510.9 m^3/s, showing good agreement with a marginal overestimation. The peak occurred on August 5, 2016.

Model validation was conducted using data from 2017 and 2018, with results shown in Fig. 24d and Fig. 24e. For 2017, the observed peak discharge was 2,590.9 m^3/s, while the simulated peak was 2,775.2 m^3/s, indicating an overestimation. The peak occurred on August 13, 2017. For 2018, the observed peak discharge was 2,741.4 m^3/s, whereas the simulated peak was 2,446.9 m^3/s, indicating an underestimation. The peak occurred on August 18, 2018.

Overall, the model demonstrates reasonable agreement with observed discharge across both calibration and validation periods, with minor over- and under-estimations of peak flows.

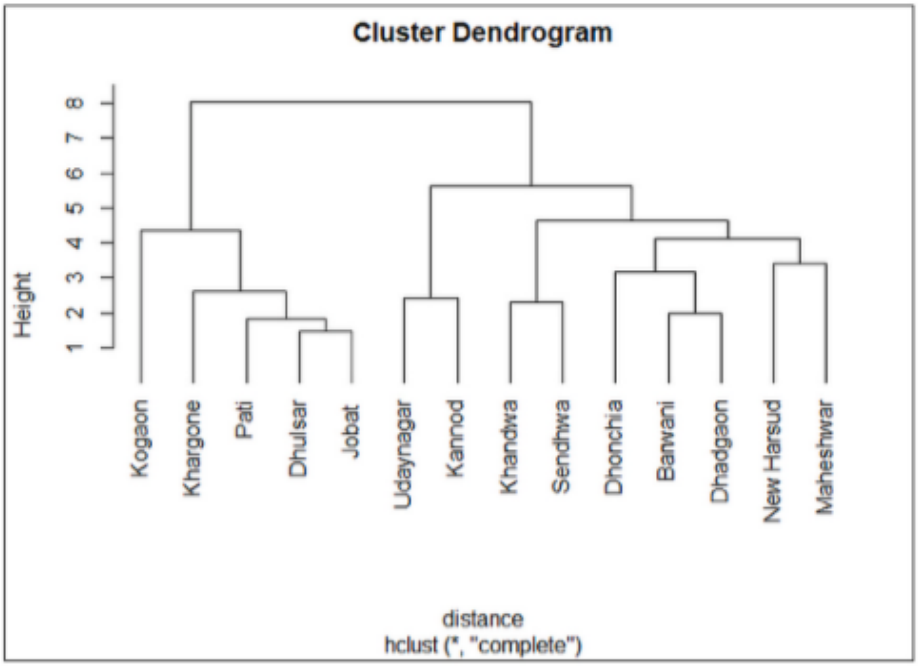

Figure 21: Cluster Dendrogram using complete linkage distance.

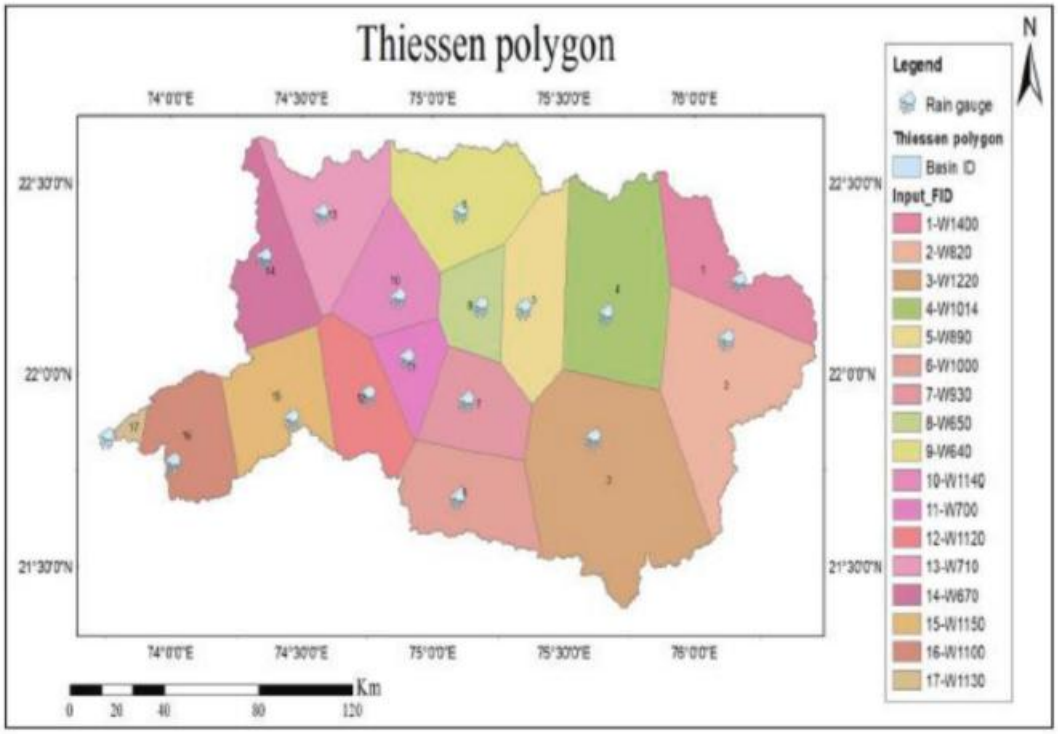

Figure 22: Rain gauge stations in the Thiessen polygon.

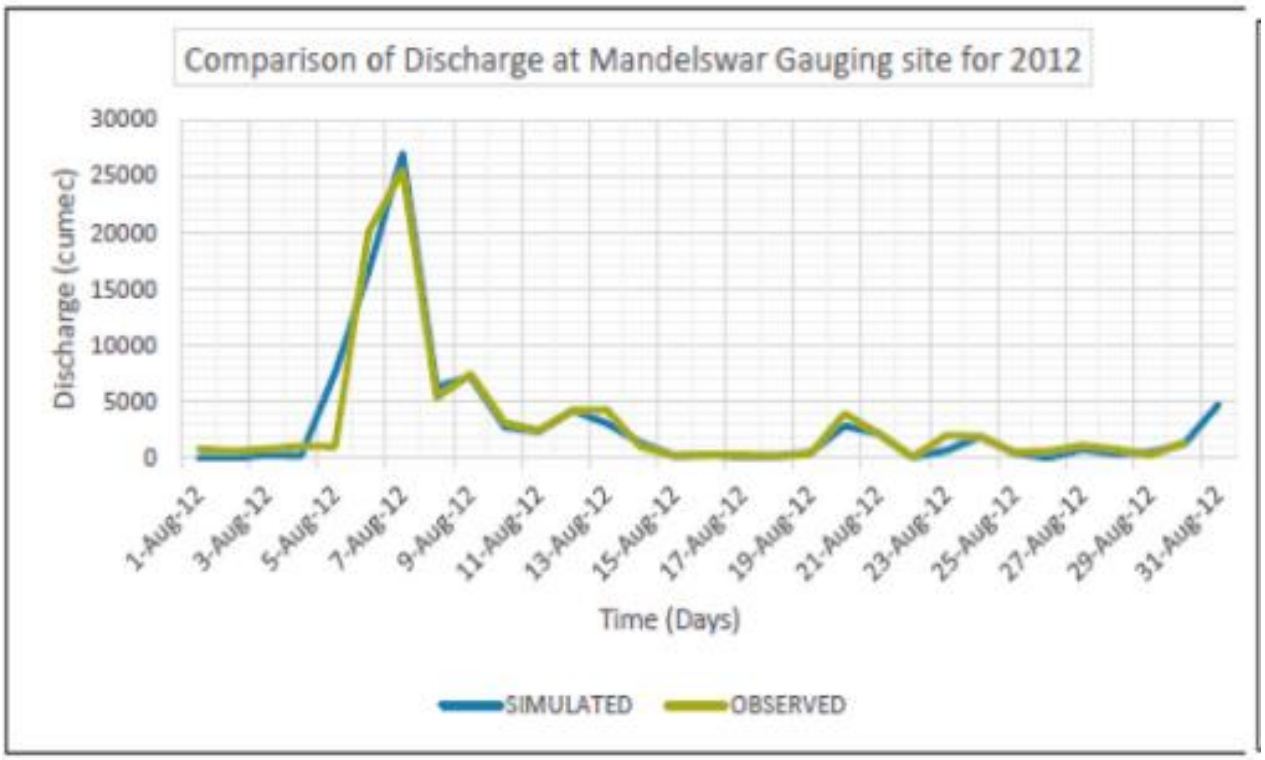
Comparison of Discharge at Mandelswar Gauging site for 2012
Discharge (cumec)
30000
25000
20000
15000
10000
5000
0
1-Aug-12
3-Aug-12
5-Aug-12
7-Aug-12
9-Aug-12
11-Aug-12
13-Aug-12
15-Aug-12
17-Aug-12
19-Aug-12
21-Aug-12
23-Aug-12
25-Aug-12
27-Aug-12
29-Aug-12
31-Aug-12
Time (Days)
SIMULATED
OBSERVED

(a)

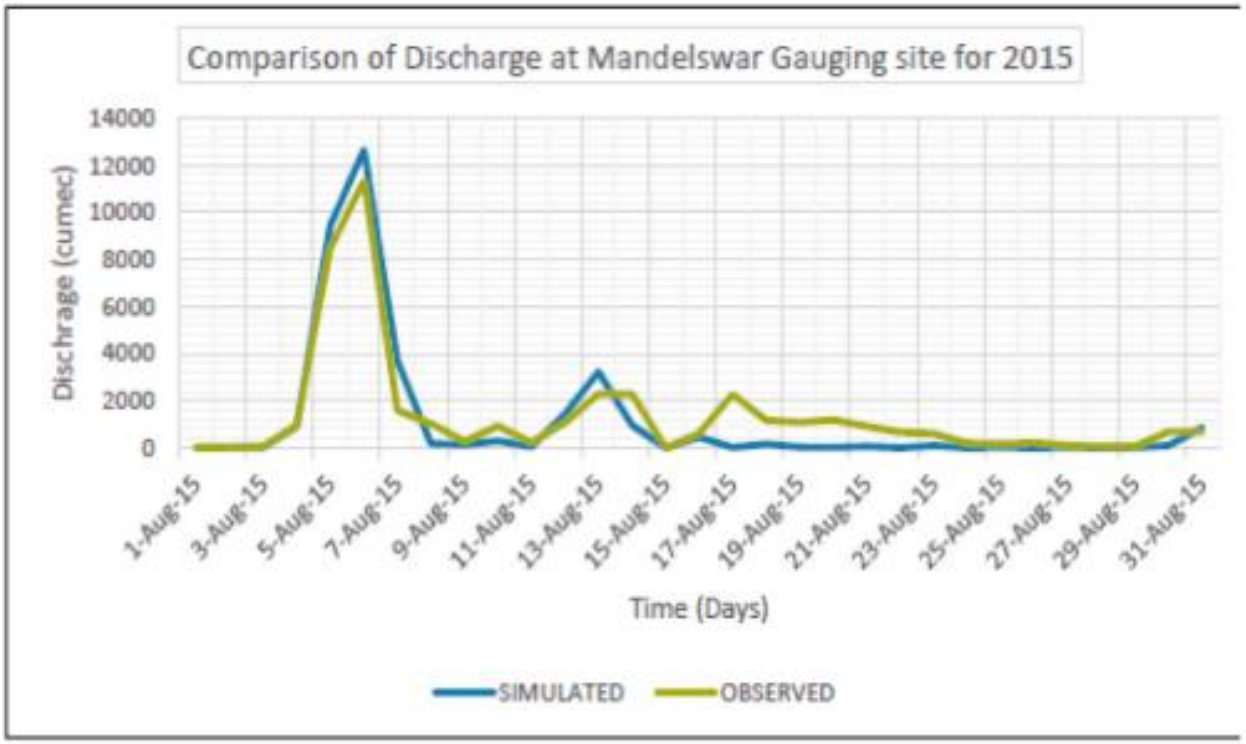
Comparison of Discharge at Mandelswar Gauging site for 2015
Discharge (cumec)
14000
12000
10000
8000
6000
4000
2000
0
1-Aug-15
3-Aug-15
5-Aug-15
7-Aug-15
9-Aug-15
11-Aug-15
13-Aug-15
15-Aug-15
17-Aug-15
19-Aug-15
21-Aug-15
23-Aug-15
25-Aug-15
27-Aug-15
29-Aug-15
31-Aug-15
Time (Days)
SIMULATED
OBSERVED

(b)

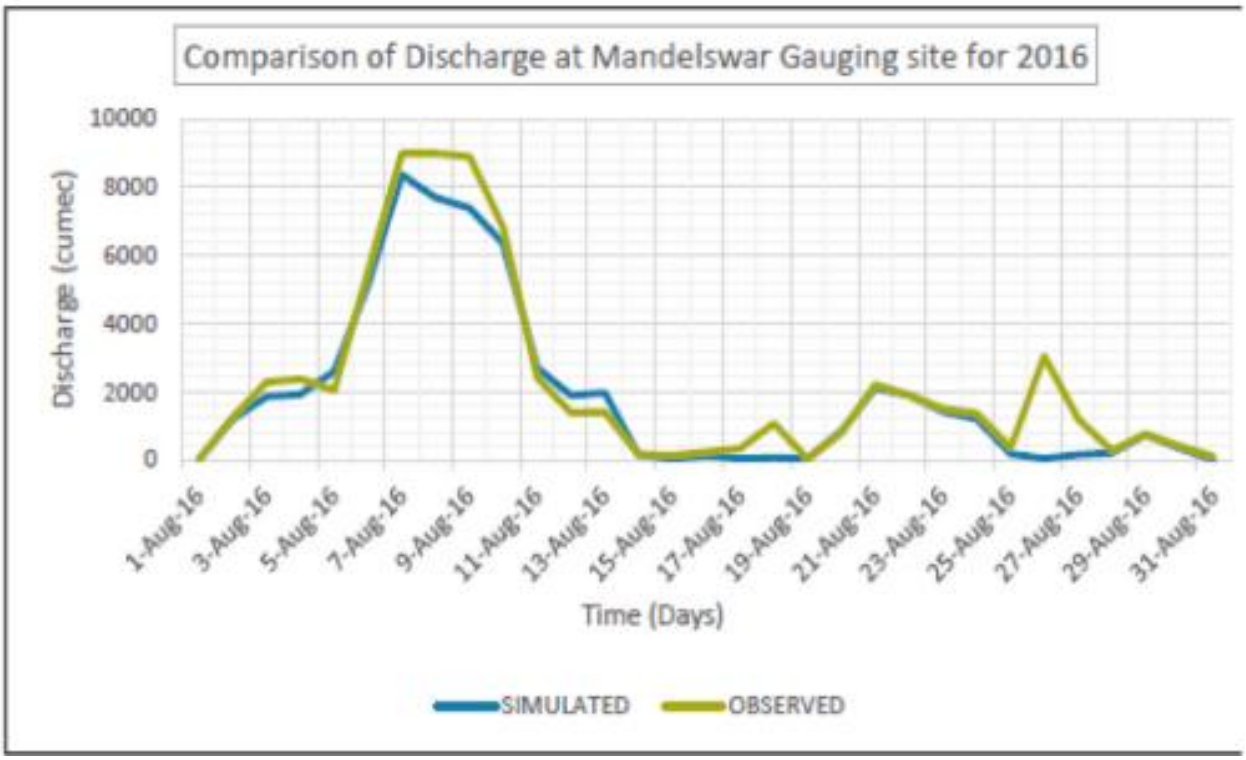
Comparison of Discharge at Mandelswar Gauging site for 2016
Discharge (cumec)
10000
8000
6000
4000
2000
0
1-Aug-16
3-Aug-16
5-Aug-16
7-Aug-16
9-Aug-16
11-Aug-16
13-Aug-16
15-Aug-16
17-Aug-16
19-Aug-16
21-Aug-16
23-Aug-16
25-Aug-16
27-Aug-16
29-Aug-16
31-Aug-16
Time (Days)
SIMULATED
OBSERVED

(c)

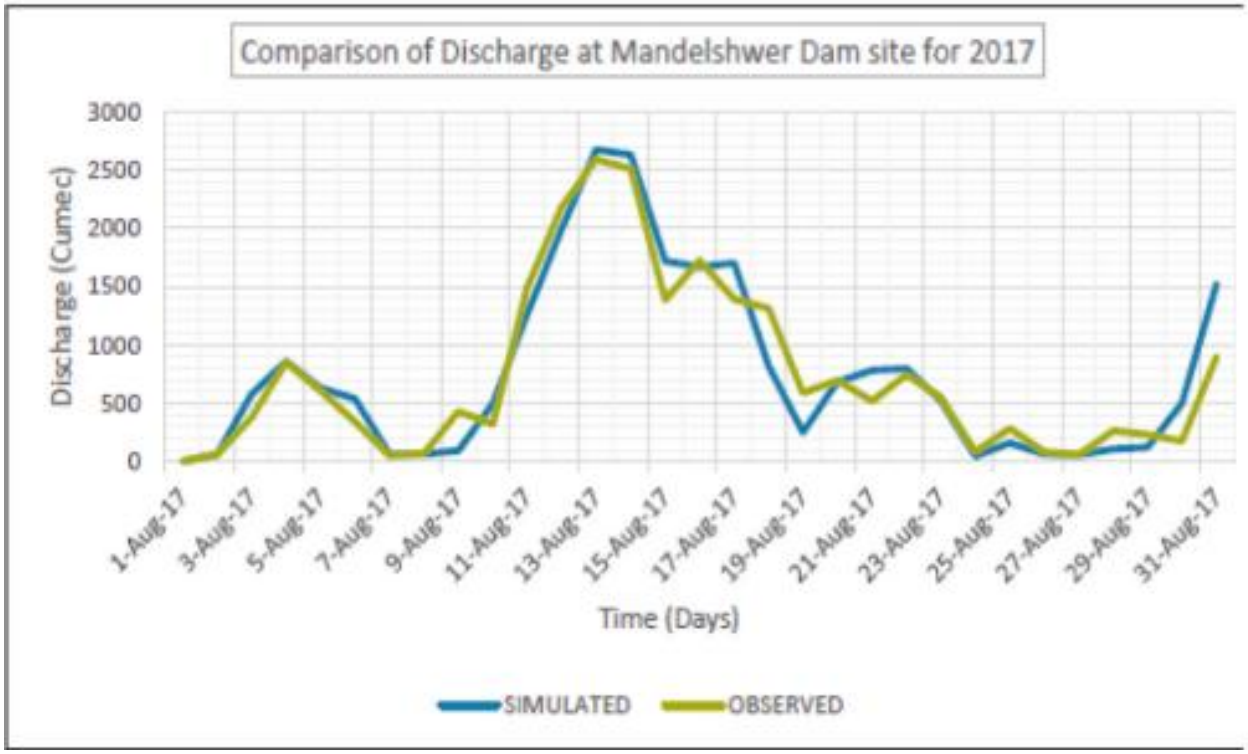
Comparison of Discharge at Mandelshwer Dam site for 2017
Discharge (Cumec)
3000
2500
2000
1500
1000
500
0
1-Aug-17
3-Aug-17
5-Aug-17
7-Aug-17
9-Aug-17
11-Aug-17
13-Aug-17
15-Aug-17
17-Aug-17
19-Aug-17
21-Aug-17
23-Aug-17
25-Aug-17
27-Aug-17
29-Aug-17
31-Aug-17
Time (Days)
SIMULATED
OBSERVED

(d)

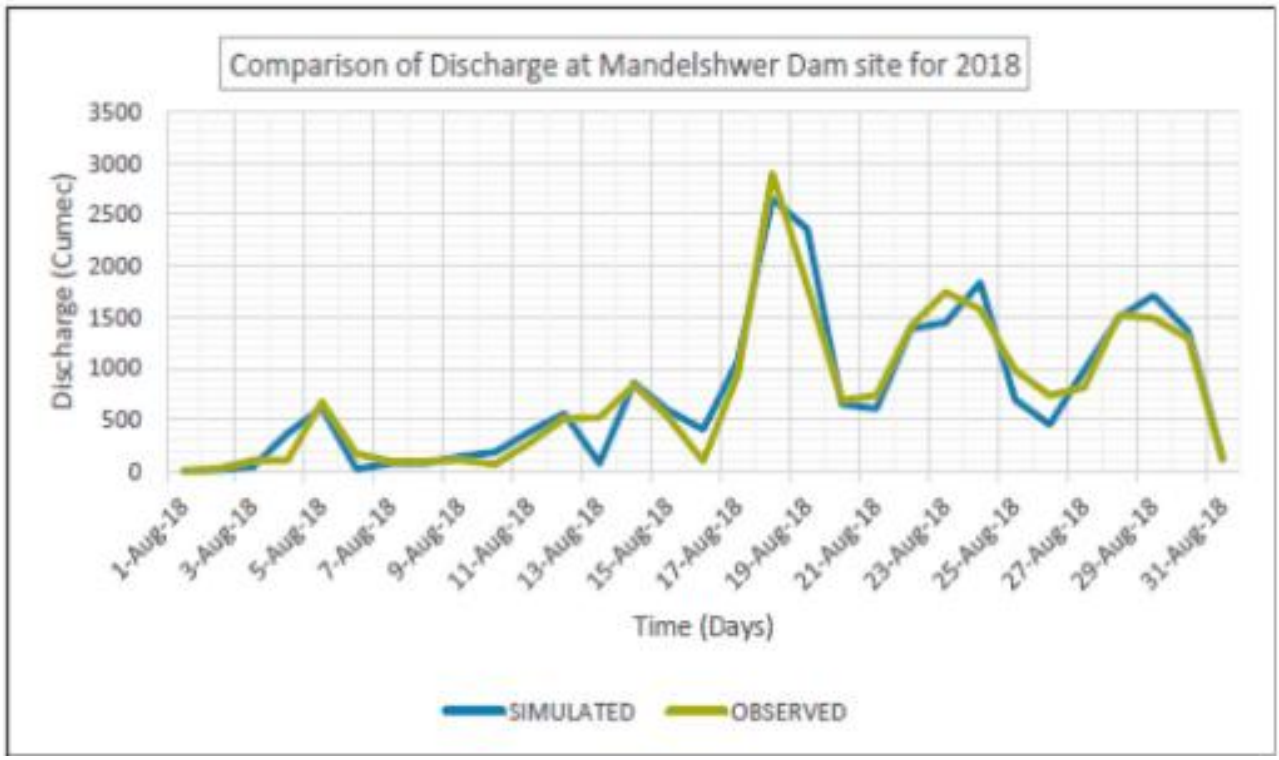

(e)

Figure 23: (a) Observed flow vs Simulated Flow 2012. (b) Observed flow vs Simulated Flow 2015. (c) Observed flow vs Simulated Flow 2016. (d) Observed flow vs Simulated Flow 2017. (e) Observed flow vs Simulated Flow 2018.

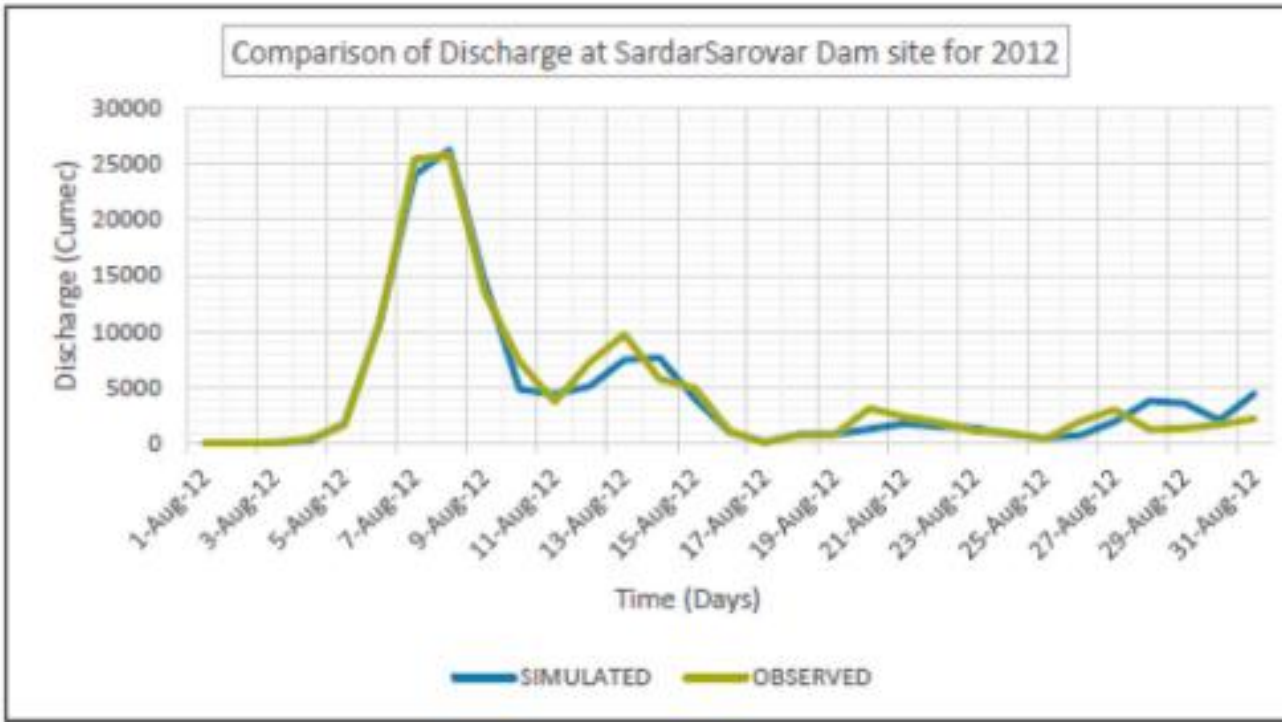
Comparison of Discharge at SardarSarovar Dam site for 2012
Discharge (Cumec)
30000
25000
20000
15000
10000
5000
0
1-Aug-12
3-Aug-12
5-Aug-12
7-Aug-12
9-Aug-12
11-Aug-12
13-Aug-12
15-Aug-12
17-Aug-12
19-Aug-12
21-Aug-12
23-Aug-12
25-Aug-12
27-Aug-12
29-Aug-12
31-Aug-12
Time (Days)
SIMULATED
OBSERVED

(a)

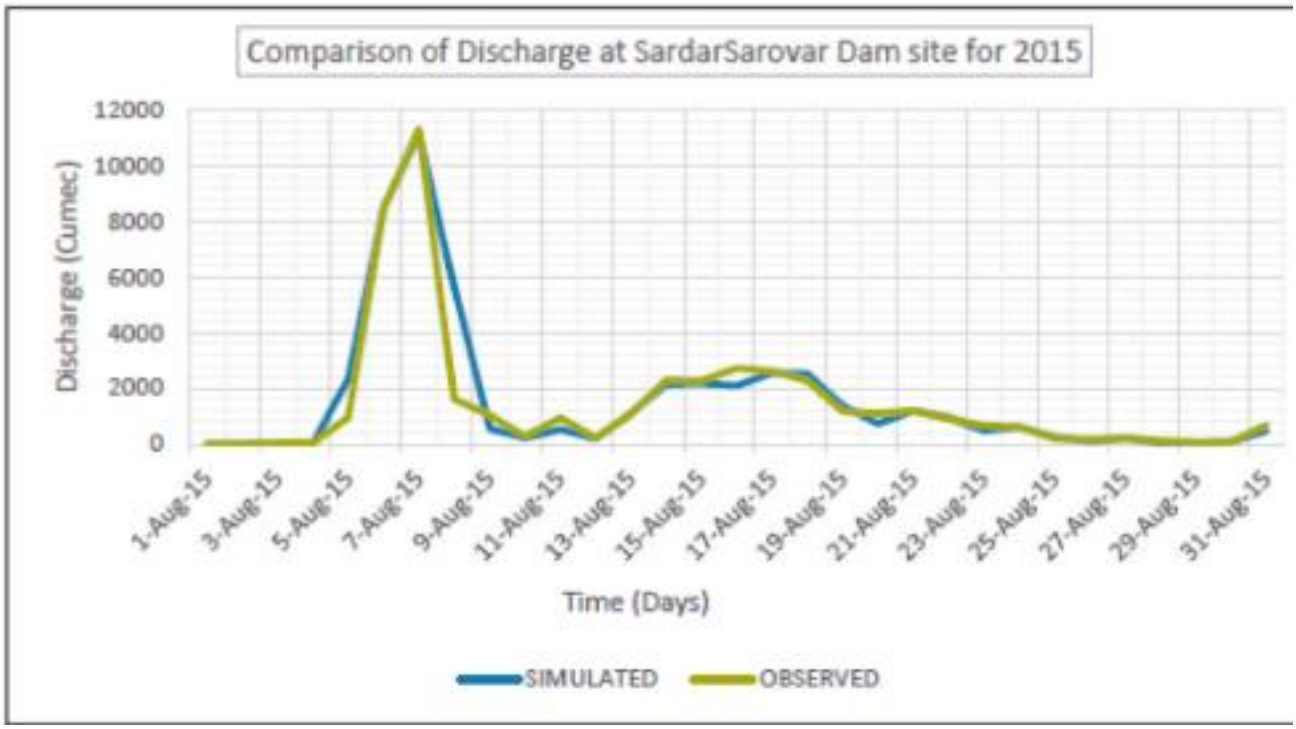
Comparison of Discharge at SardarSarovar Dam site for 2015
Discharge (Cumec)
12000
10000
8000
6000
4000
2000
0
1-Aug-15
3-Aug-15
5-Aug-15
7-Aug-15
9-Aug-15
11-Aug-15
13-Aug-15
15-Aug-15
17-Aug-15
19-Aug-15
21-Aug-15
23-Aug-15
25-Aug-15
27-Aug-15
29-Aug-15
31-Aug-15
Time (Days)
SIMULATED
OBSERVED

(b)

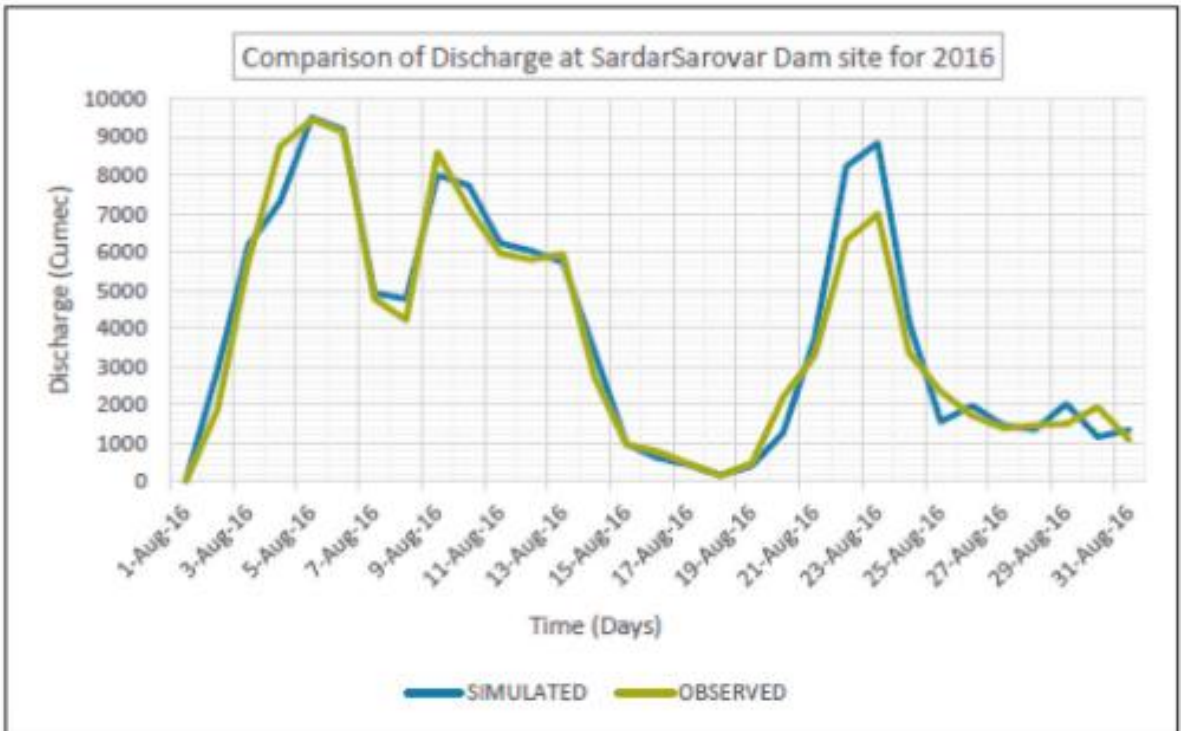
Comparison of Discharge at SardarSarovar Dam site for 2016
Discharge (Cumec)
10000
9000
8000
7000
6000
5000
4000
3000
2000
1000
0
1-Aug-16
3-Aug-16
5-Aug-16
7-Aug-16
9-Aug-16
11-Aug-16
13-Aug-16
15-Aug-16
17-Aug-16
19-Aug-16
21-Aug-16
23-Aug-16
25-Aug-16
27-Aug-16
29-Aug-16
31-Aug-16
Time (Days)
SIMULATED
OBSERVED

(c)

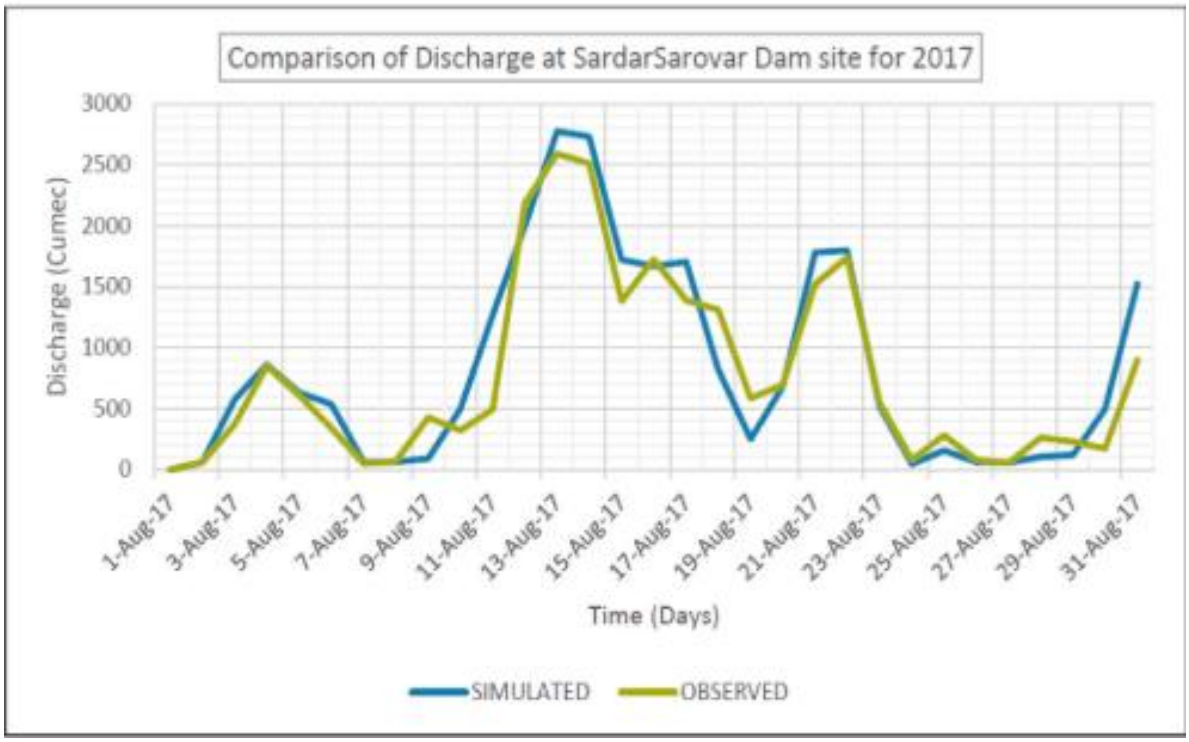
Comparison of Discharge at SardarSarovar Dam site for 2017
Discharge (Cumec)
3000
2500
2000
1500
1000
500
0
1-Aug-17
3-Aug-17
5-Aug-17
7-Aug-17
9-Aug-17
11-Aug-17
13-Aug-17
15-Aug-17
17-Aug-17
19-Aug-17
21-Aug-17
23-Aug-17
25-Aug-17
27-Aug-17
29-Aug-17
31-Aug-17
Time (Days)
SIMULATED
OBSERVED

(d)

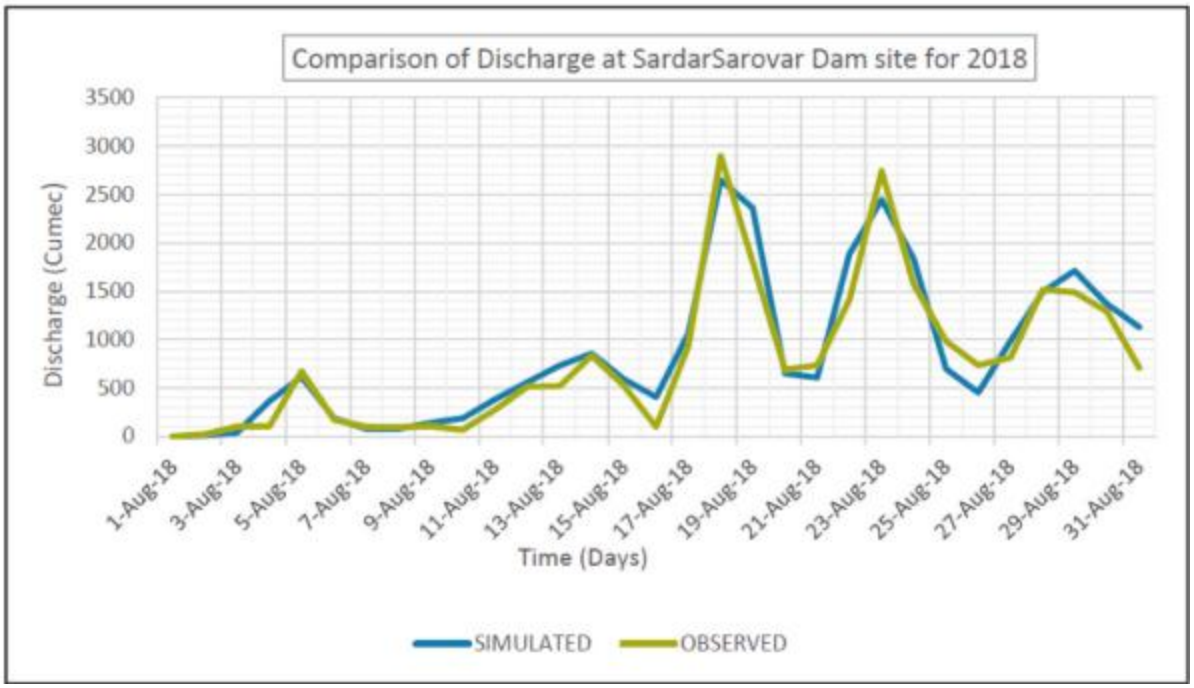

(e)

Figure 24: (a) Observed flow vs Simulated Flow 2012. (b) Observed flow vs Simulated Flow 2015. (c) Observed flow vs Simulated Flow 2016. (d) Observed flow vs Simulated Flow 2017. (e) Observed flow vs Simulated Flow 2018.

3.5 Flood frequency analysis and inundation mapping for lower Narmada basin

3.5.1 Study Area and Data Collection

This study focuses on the lower coastal plain region of the basin (Fig. 25).

The lower Narmada basin has historically experienced several significant flood events, notably in 1970, 1973, 1984, 1990, 1994, 2006, and 2013. The upper hilly regions receive relatively high annual rainfall (1,400–1,650 mm), which contributes to downstream flooding despite the semi-arid conditions in the lower basin. The climate in the lower basin is moderated by proximity to the Arabian Sea, with temperatures typically ranging from 10°C to 40°C. The dominant land-use/land-cover classes in the basin include agricultural land (approximately 60%), barren land (12%), and urban areas (3%).

The data required for this study were obtained from a combination of open-source platforms and government agencies. Digital Elevation Model (DEM) data at 1-arc second resolution were acquired from the Shuttle Radar Topography Mission (SRTM) via the United States Geological Survey (USGS) Earth Explorer portal. Land-use/land-cover data were obtained from the Moderate Resolution Imaging Spectroradiometer (MODIS) database. Stage–discharge data at the Garudeshwar station were collected from the Sardar Sarovar Narmada Nigam Limited (SSNL). Historical flood records were compiled from reports published by the Central Water Commission (CWC), SSNL, and the South Asia Network on Dams, Rivers and People (SANDRP).

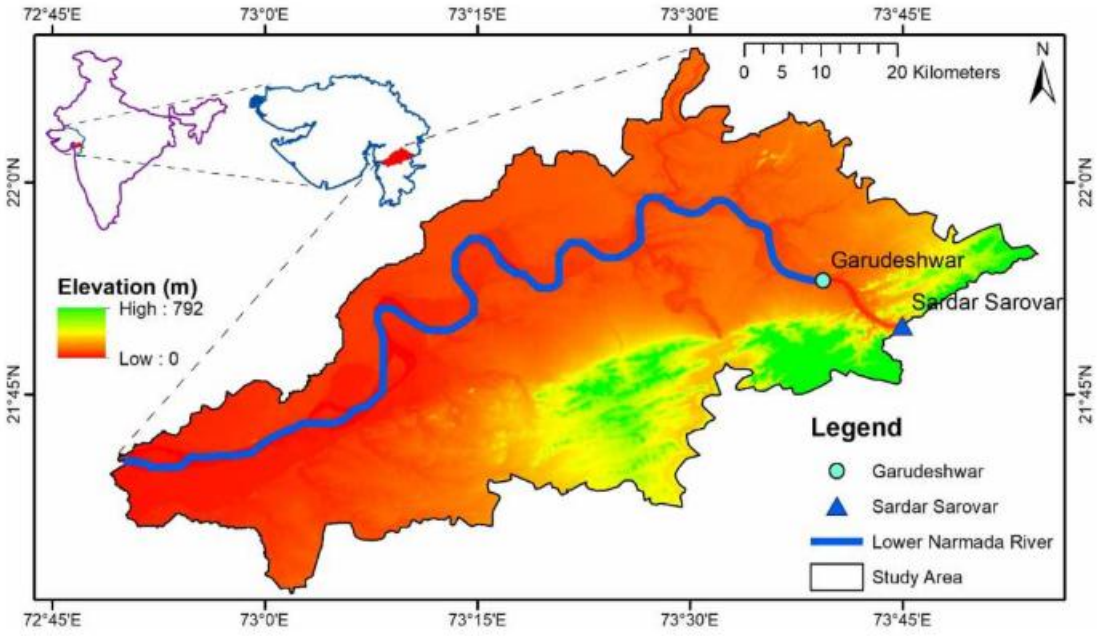

Figure 25: Study area map representing the location of the Garudeshwar weir and river reach, and elevation of the region.

3.5.2 Methodology

The methodology adopted in this study comprises data collection and preprocessing, flood frequency analysis at the Garudeshwar weir, and the development of a hydraulic model for the downstream reach to assess flood-prone areas. A schematic representation of the overall approach is presented in Fig. 26.

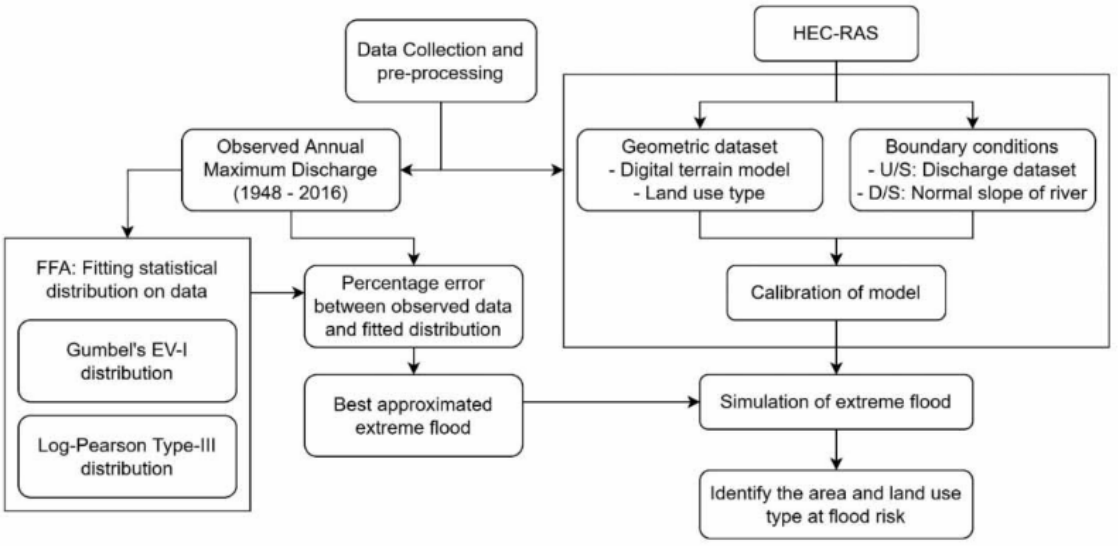

Figure 26: Schematic representation of the adopted methodology.

3.5.3 Flood Frequency Analysis

Flood frequency analysis (FFA) is a statistical approach used to estimate flood magnitudes corresponding to specific return periods or exceedance probabilities. It involves deriving key statistical parameters, such as the mean, standard deviation, and skewness, from long-term annual peak discharge data, which are then used to develop frequency distributions.

In this study, FFA was performed using the Gumbel Extreme Value Type-I (EV-I) and Log-Pearson Type-III distributions. Flood magnitudes were estimated for return periods of 10, 25, 50, and 100 years. Annual peak discharge data for the period 1948–2016 were used for the analysis.

3.5.4 Development of Two-Dimensional (2D) Hydrodynamic (HD) Model

A two-dimensional hydrodynamic (2D HD) model was developed using HEC-RAS (version 6.0) to simulate extreme flood events in the lower Narmada basin. In the absence of detailed surveyed terrain

data, a 1-arc second resolution Shuttle Radar Topography Mission (SRTM) Digital Elevation Model (DEM) was used to represent the topography of the study area.

Preprocessing of the DEM was performed in QGIS (version 3.20), including sink filling and peak removal to eliminate spurious depressions and elevations arising from data resolution limitations. The processed DEM was then imported into HEC-RAS Mapper to define the computational terrain for both the river channel and adjoining floodplain.

A 2D computational mesh with a uniform grid size of 50 m × 50 m was generated to simulate the hydraulic behavior of the floodplain. The observed discharge hydrograph for the 2013 flood event at the Garudeshwar weir was specified as the upstream boundary condition, while a normal depth condition based on channel slope was applied at the downstream boundary.

The Manning's roughness coefficient (*n*), a critical parameter governing flow resistance, was assigned using land-use/land-cover data derived from MODIS for the floodplain. For the river channel, roughness values were obtained through calibration of a one-dimensional hydrodynamic model by comparing simulated and observed water levels at the downstream gauging station at Bharuch.

The calibrated and validated model was subsequently used to simulate flood events corresponding to return periods of 10, 25, 50, and 100 years. The resulting inundation maps were exported and integrated with land-use and high-resolution imagery (e.g., Google Earth) in QGIS to delineate and quantify flood-prone areas.

The developed model also has potential applications in flood early warning systems, where real-time or forecasted upstream discharge can be used as input to predict downstream flood conditions.

3.5.5 Results and Discussion

A total of 69 years (1948–2016) of observed annual maximum discharge data were used to fit the Gumbel Extreme Value Type-I (EV-I) and Log-Pearson Type-III distributions. The estimated flood magnitudes for return periods of 10, 25, 50, and 100 years were subsequently simulated using HEC-RAS to delineate potential flood-prone areas. The results of the flood frequency analysis and the corresponding inundation mapping are presented in Sections 4.1 and 4.2, respectively.

Results of Flood Frequency Analysis

The statistical parameters of the annual peak discharge series, including the mean and standard deviation, were first computed. For the Gumbel EV-I distribution, the reduced variate corresponding to return periods of 10, 25, 50, and 100 years was determined, and the associated reduced mean and

standard deviation values were obtained from standard tables based on the sample size. Flood magnitudes for the selected return periods were then estimated using the Gumbel formulation.

For the Log-Pearson Type-III distribution, the annual peak discharge data were transformed into logarithmic (base 10) form. The coefficient of skewness was calculated, and the frequency factor was obtained from standard tables based on the skewness and return period. The flood magnitudes were then computed and subsequently transformed back to the original scale using antilogarithmic conversion.

A flood frequency curve was developed using a logarithmic relationship based on the results from both methods (Fig. 27), indicating that both distributions provide a good fit to the data.

To further evaluate model performance, the estimated flood magnitudes from both methods were compared with the fitted curve of the observed annual peak discharge series, and percentage deviations were computed (Fig. 28). The analysis indicates that the Log-Pearson Type-III distribution provides more reliable estimates for lower return periods (T < 60 years), whereas the Gumbel EV-I distribution performs better for higher return periods (T > 60 years).

Based on these findings, the flood magnitudes derived from the Log-Pearson Type-III method were adopted for return periods of 10, 25, and 50 years, while the Gumbel EV-I estimate was used for the 100-year return period. These selected values were subsequently used for flood inundation mapping.

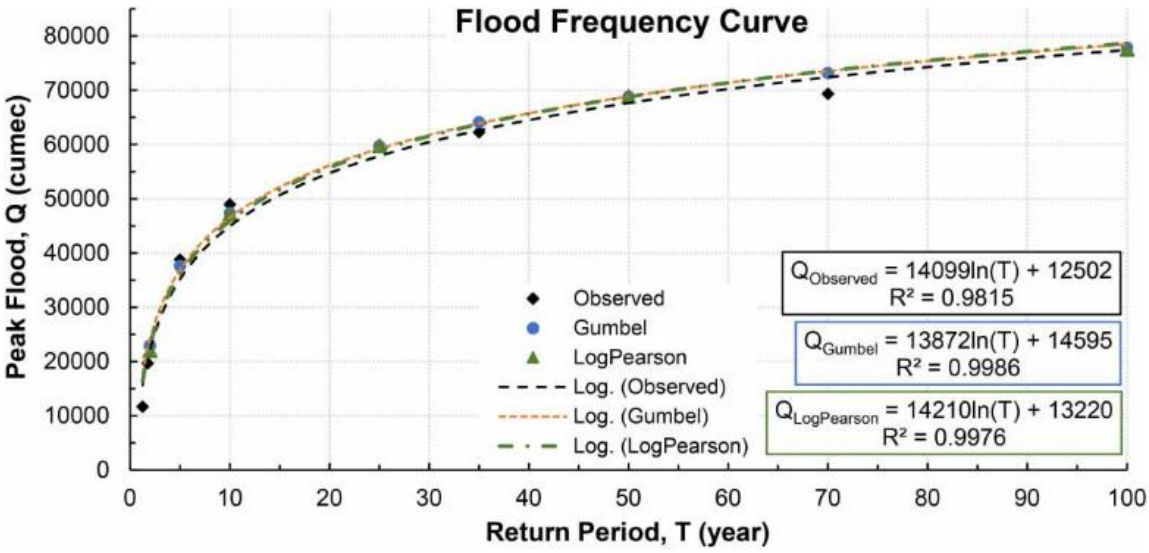

Figure 27: Fitted flood frequency curve using observed data, Gumbel's EV-I distribution, and Log Pearson Type-III distribution.

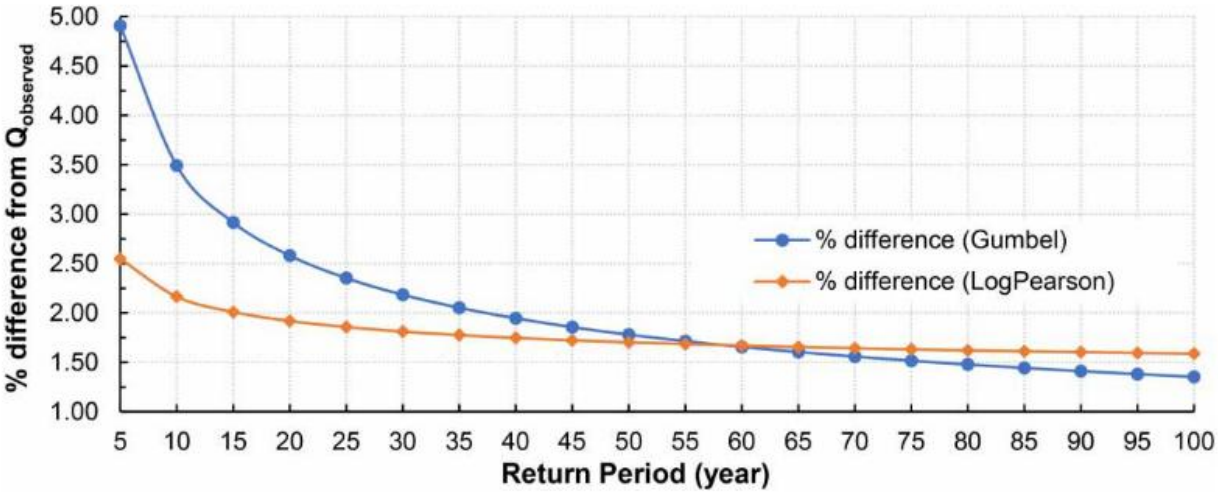

Figure 28: Percentage difference between observed peak flood and fitted distribution.

Results of Hydrodynamic (HD) Model

The 2D hydrodynamic (HD) model was developed in HEC-RAS (version 6.0) using SRTM DEM, MODIS-based land-use/land-cover data, and observed discharge at the Garudeshwar weir. The observed hydrograph for the 2013 flood event (peak discharge of 32,056 m^3/s) was applied as the upstream boundary condition, while a normal depth condition based on channel slope was specified at the downstream boundary.

The riverbed roughness coefficient (Manning's n) was determined through calibration of a 1D HD model by varying n within the range of 0.02–0.03 (Chow, 1959) and comparing simulated and observed water levels at the Bharuch gauging station. An optimal value of $n = 0.022$ was selected, corresponding to a minimum absolute error of 0.3 m in peak water level. Model validation was performed using the independent flood event of 2006, demonstrating satisfactory agreement between observed and simulated water levels.

The calibrated and validated model was subsequently used to simulate flood scenarios corresponding to return periods of 10, 25, 50, and 100 years, and the resulting inundation maps are presented in Fig. 29. The results indicate a significant increase in inundation extent and flood depth with increasing return period.

A depth-wise analysis of inundation reveals that areas with water depth less than 1 m remain nearly constant (approximately 50 km^2) across all return periods. In contrast, areas with depths between 1–3 m decrease with increasing return period, while those with depths between 3–6 m initially increase and

then decline. Notably, areas with water depth greater than 6 m show a substantial increase as the return period increases.

Further analysis of inundation across different land-use classes indicates a marked increase in the extent of flooded cropland and urban areas with increasing return period, highlighting the growing flood vulnerability of the region.

Based on the inundation maps, flood-prone villages were identified (Fig. 30). Risk levels were categorized based on flood depth and associated return periods, with high-risk zones defined by greater flood depths occurring at lower return periods, and low-risk zones associated with shallow flooding at higher return periods. The identified risk levels for individual villages provide valuable inputs for planning flood mitigation strategies and informing policy decisions.

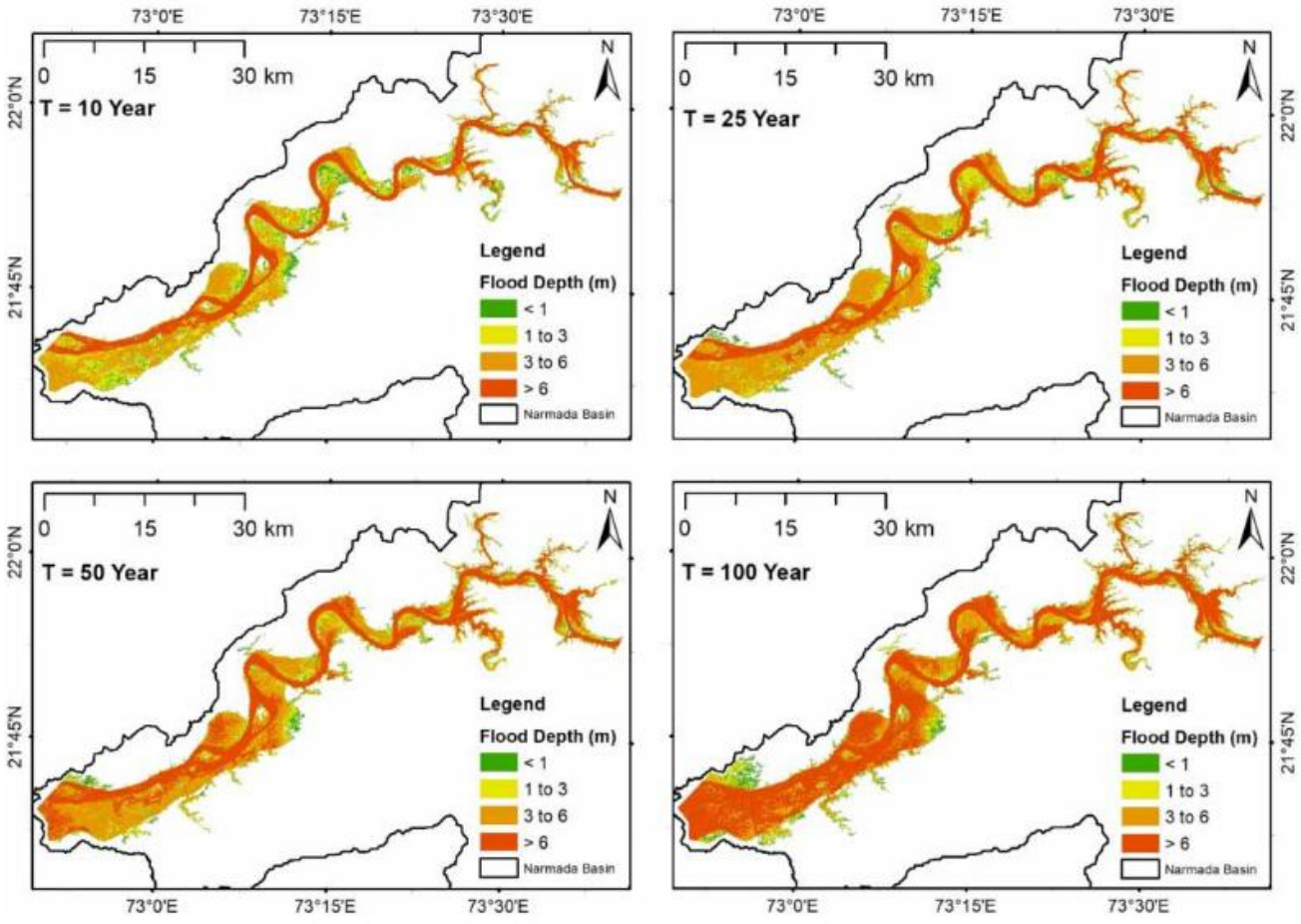

Figure 29: Flood inundation map corresponding to 10-, 25-, 50-, and 100-year return period.

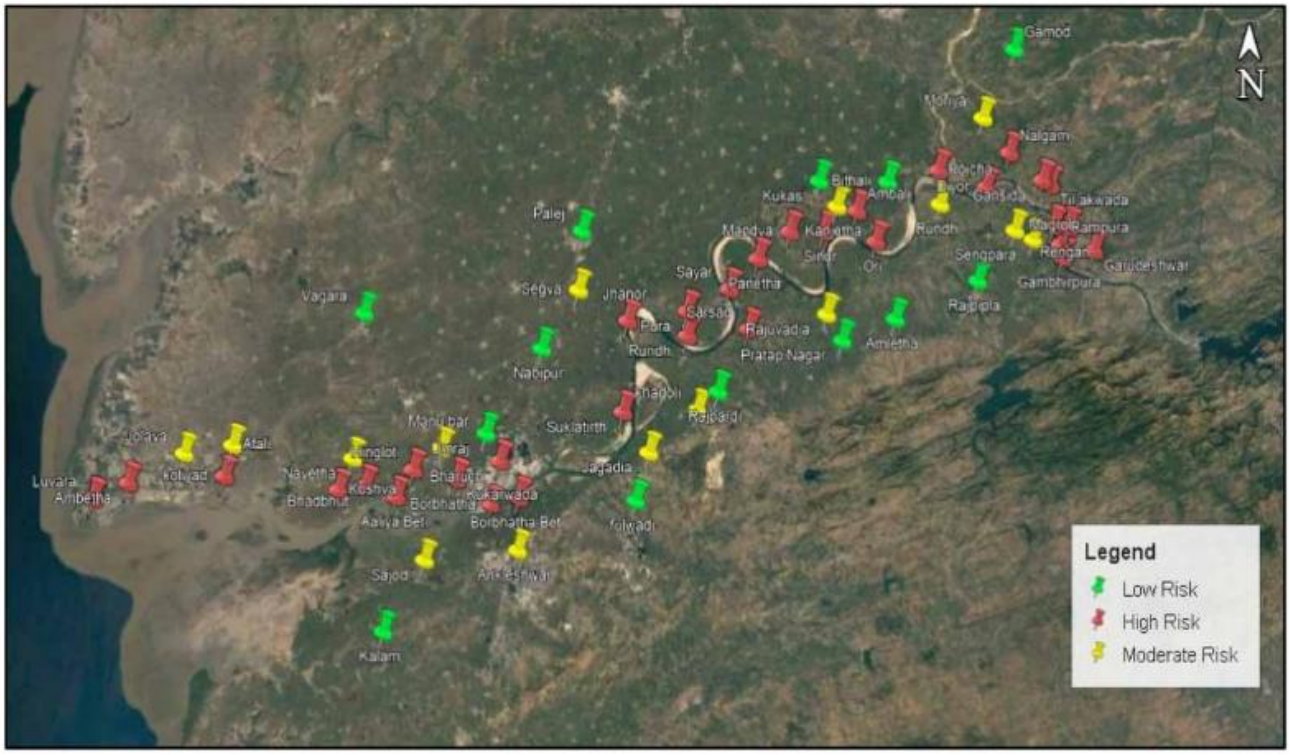

Figure 30: Map of villages indicating the level of flood risk (Source: Google Earth, earth.google.com/web/).

3.6 Flood hazard mapping in the lower Narmada Basin through hybrid machine learning and IoT-based approaches

3.6.1 Study Area and Data

This study focuses on the lower plains of the basin, extending from the Sardar Sarovar Dam to the coastal region, covering an area of about 8,730 km². This region includes parts of the Narmada, Bharuch, and Vadodara districts and is highly prone to flooding. The lower Narmada basin has experienced several major flood events, notably in 1970, 1973, 1984, 1990, 1994, and 2013. Owing to its high flood vulnerability, this coastal plain region has been selected as the study area (Fig. 31).

The upper hilly regions of the basin receive relatively high annual rainfall (1,400–1,650 mm), which contributes to downstream flooding despite the semi-arid conditions in the lower basin. The climate in the lower basin is influenced by proximity to the Arabian Sea, with temperatures typically ranging from 10°C to 40°C. The dominant land-use/land-cover (LULC) classes in the study area include agricultural cropland (61%), dense vegetation and forest (21%), and urban areas (8%).

Data Description and Processing

The data required for this study were obtained from a combination of open-source databases and government reports, as detailed in Sects. 2.2.1 and 2.2.2. A total of nine factors, comprising both flood hazard and flood vulnerability indicators, were considered for the preparation of the flood risk map. Spatial datasets corresponding to these factors were generated and integrated within a GIS environment to serve as inputs for the machine learning (ML) model.

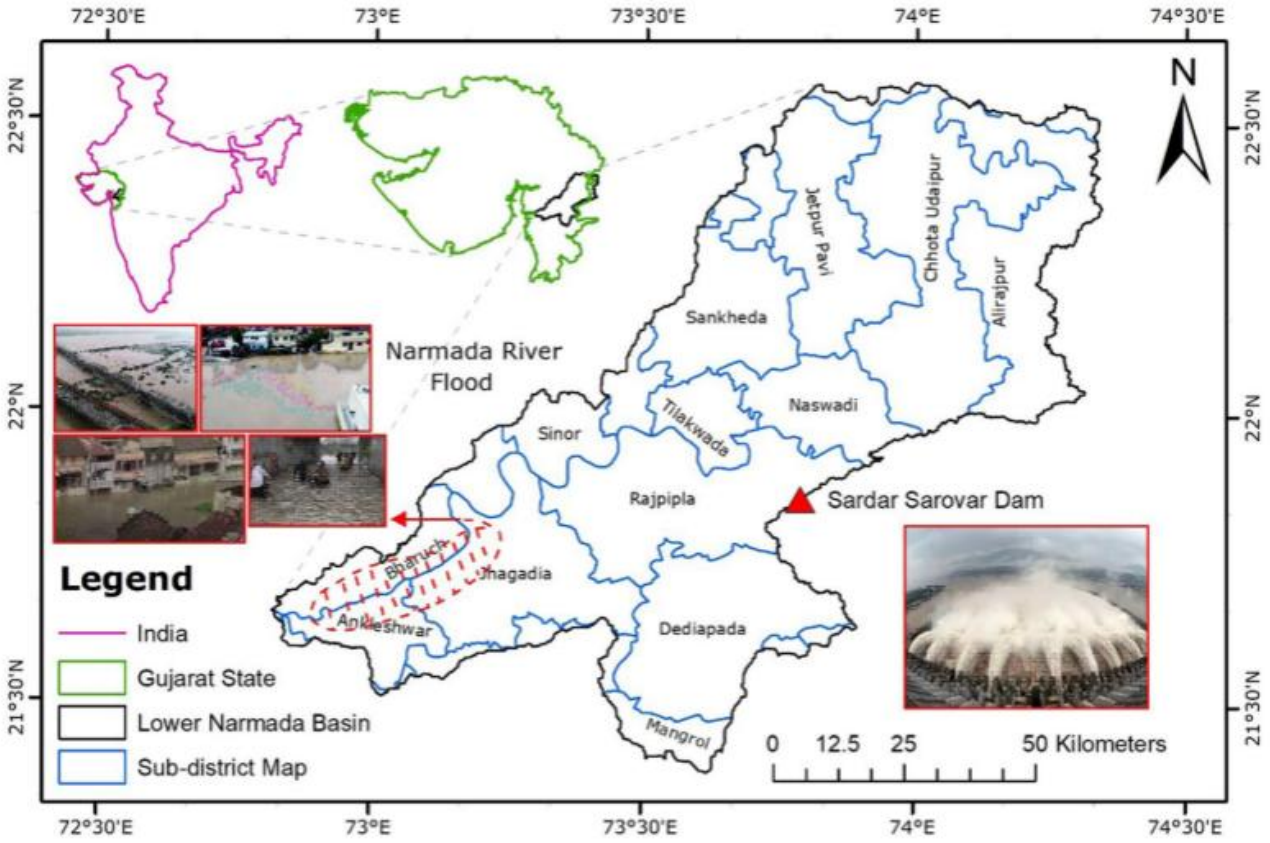

Figure 31: Location map of the study area. The highlighted lower part of the basin is frequently affected urban flood areas

3.6.2 Flood Hazard Factors

Six key variables were selected to represent flood hazard conditions in the study area: terrain elevation, slope (expressed as percentage change), distance from the main river network, drainage density, spatial distribution of average annual rainfall, and land-use/land-cover characteristics. These factors were used to characterize the physical and hydrological conditions influencing flood occurrence.

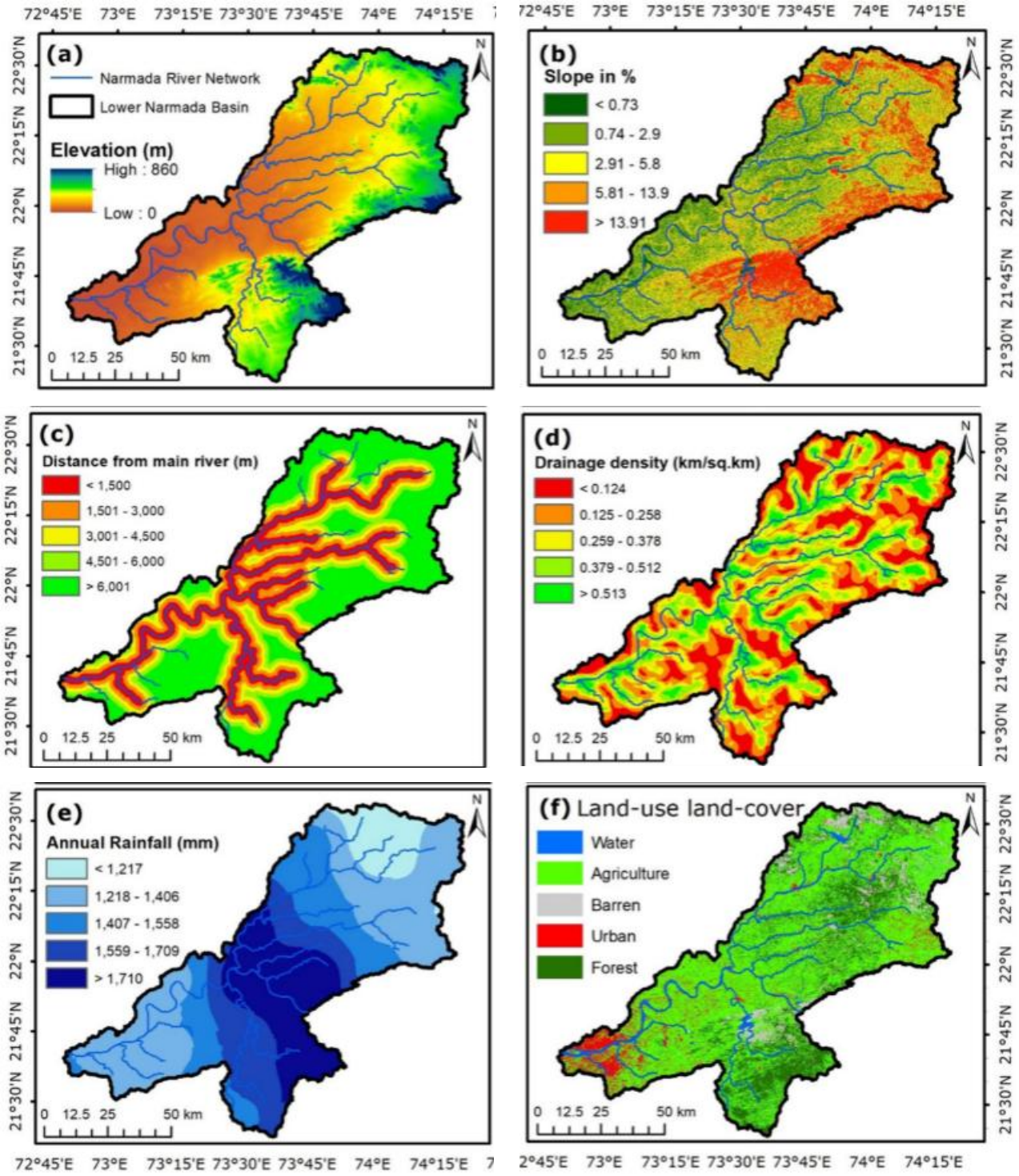

Figure 32: Flood hazard factors: a elevation, b percentage change in slope, c distance from the main river network, d drainage density, e average annual rainfall distribution, and f LULC characteristics of the study area

3.6.3 Methodology

The primary objective of this study is to develop a flood risk map for the lower Narmada basin to support effective flood prevention, mitigation planning, and associated socio-economic benefits. The region experienced a major flood event in 1994; however, detailed surveyed data on flood depth and inundation extent are not available.

To address this limitation, the first step involved developing a hydrodynamic model to generate flood inundation maps for the study area. The simulated inundation data were then integrated with nine selected flood hazard and vulnerability factors to form the input dataset for model training.

A Random Forest (RF) algorithm was employed to estimate the relative importance (weightage) of the predictor variables. The model hyperparameters were optimized using the RandomizedSearchCV technique to enhance predictive performance. Finally, the flood risk map was generated by combining the weighted contributions of all predictor variables. A schematic overview of the adopted methodology is presented in Fig. 33.

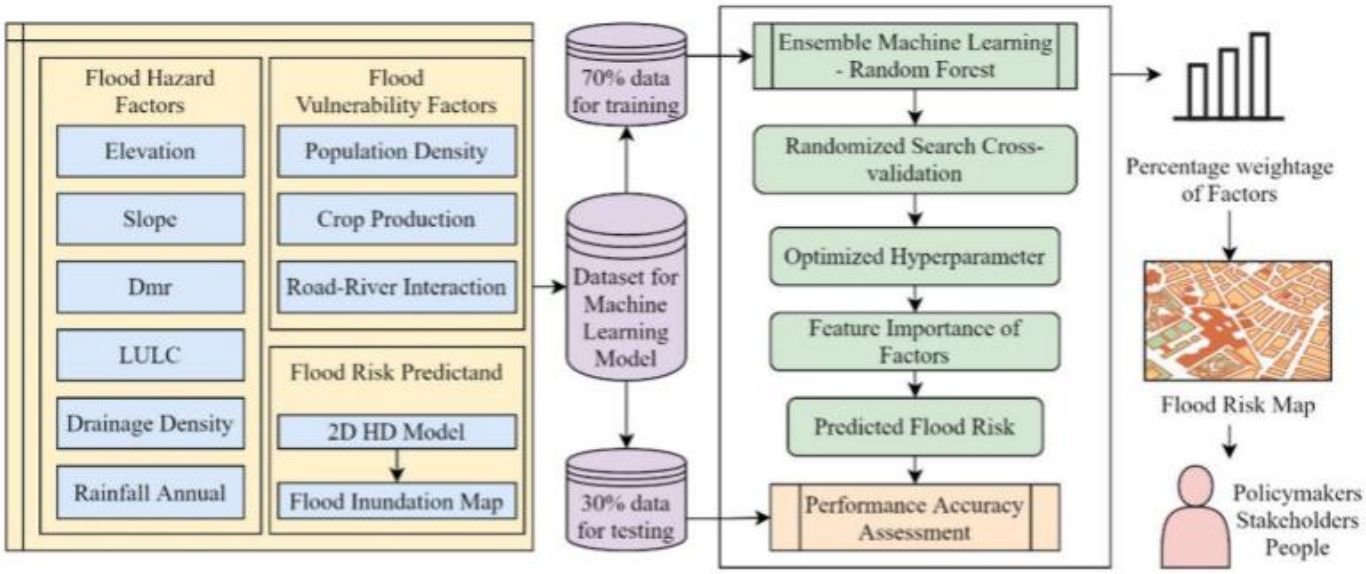

Figure 33: Schematic representation of the proposed framework for flood risk mapping. The dataset consists of flood hazard and vulnerability factors as predictors and flood inundation map as predictand was given as input to the RF model for obtaining weightage of each factor to prepare flood risk maps.

3.6.4 Results and Discussion

The present study utilizes nine predictor variables to develop the flood risk map. The calibrated and validated flood inundation map, simulated using HEC-RAS (version 6.1), was used as the target variable for training the Random Forest (RF) model. All datasets were projected onto a common coordinate reference system, namely WGS 1984 Universal Transverse Mercator (UTM). Subsequently, the data were resampled to a uniform grid resolution of 30 × 30 m using ArcGIS (version 10.8) and used as input for model training.

Results of Random Forest Model

The RF model was developed using the *scikit-learn* library in Python. Hyperparameter tuning was performed using the RandomizedSearchCV approach by evaluating combinations from a predefined

parameter grid. A total of 640 parameter combinations were explored through 300 iterations using a threefold cross-validation scheme.

While increasing the number of iterations and cross-validation folds can improve model robustness and reduce overfitting, it also increases computational time. Considering the need for timely predictions in flood forecasting applications, a balance between model accuracy and computational efficiency was maintained.

The optimal hyperparameter configuration was identified as follows: *n_estimators* = 1000, *max_depth* = 100, *max_features* = "sqrt", *min_samples_leaf* = 2, and *min_samples_split* = 10. The performance of the optimized model was evaluated using standard statistical metrics, yielding MAE = 0.34 m, MSE = 0.54 m², RMSE = 0.74 m, and R^2 = 0.98, indicating excellent predictive capability.

The predicted flood depths were compared with observed values using the test dataset . Although minor discrepancies were observed at certain grid points—primarily due to spatial homogeneity in predictor variables—the overall model performance was robust. The density distribution of predicted versus observed values shows a strong concentration along the 1:1 line ($y_{act} \approx y_{pred}$), indicating high agreement between model predictions and actual flood depths.

Flood Risk Maps

The flood risk map was developed using the feature importance weights derived from the Random Forest (RF) model. A flood hazard raster was first generated using the weighted overlay tool in ArcGIS (version 10.8), where each hazard factor was assigned its corresponding percentage weight. Similarly, a flood vulnerability raster was created by applying the respective weights to the vulnerability factors. The final flood risk map was obtained by combining the hazard and vulnerability rasters using the raster calculator tool.

The flood risk map is shown in Fig. 34. Among the hazard factors, elevation and land-use/land-cover (LULC) were identified as the most influential, with weights of 29% and 27%, respectively. Distance from the main river channel and rainfall also contributed significantly, with weights of 17% and 15%. These findings provide important insights for regional planning, particularly in regulating development activities near riverbanks to reduce flood hazard.

For vulnerability factors, population density and crop production were assigned the highest importance, with weights of 44% and 30%, respectively. This reflects the increased exposure of densely populated urban centers and agriculturally intensive areas to flood risk. Major urban settlements in the study area

are located along the riverbanks, making them highly susceptible to flooding. Additionally, agricultural activities, particularly in the deltaic regions with high soil productivity, further increase vulnerability.

The study area is also classified as highly vulnerable in the National Flood Vulnerability Assessment System developed by the Indian Space Research Organisation (ISRO) (Fig. 35), which considers factors such as probable maximum precipitation (derived from IMD gridded rainfall data), runoff potential (based on LULC and soil characteristics), drainage density, and terrain slope.

The developed flood risk map indicates that downstream urban centers, particularly Bharuch and Ankleshwar, fall within high-risk zones due to high population density and proximity to the river. Several sub-districts, including Jhagadia, Sinor, Rajpipla, and Sankheda, are categorized as moderate-risk zones, primarily due to high rainfall and low elevation. These findings highlight the need for improved stormwater drainage infrastructure and flood management strategies in these regions. In contrast, the northern and southeastern parts of the basin are classified as low-risk zones, owing to higher elevations and steeper slopes that facilitate rapid drainage.

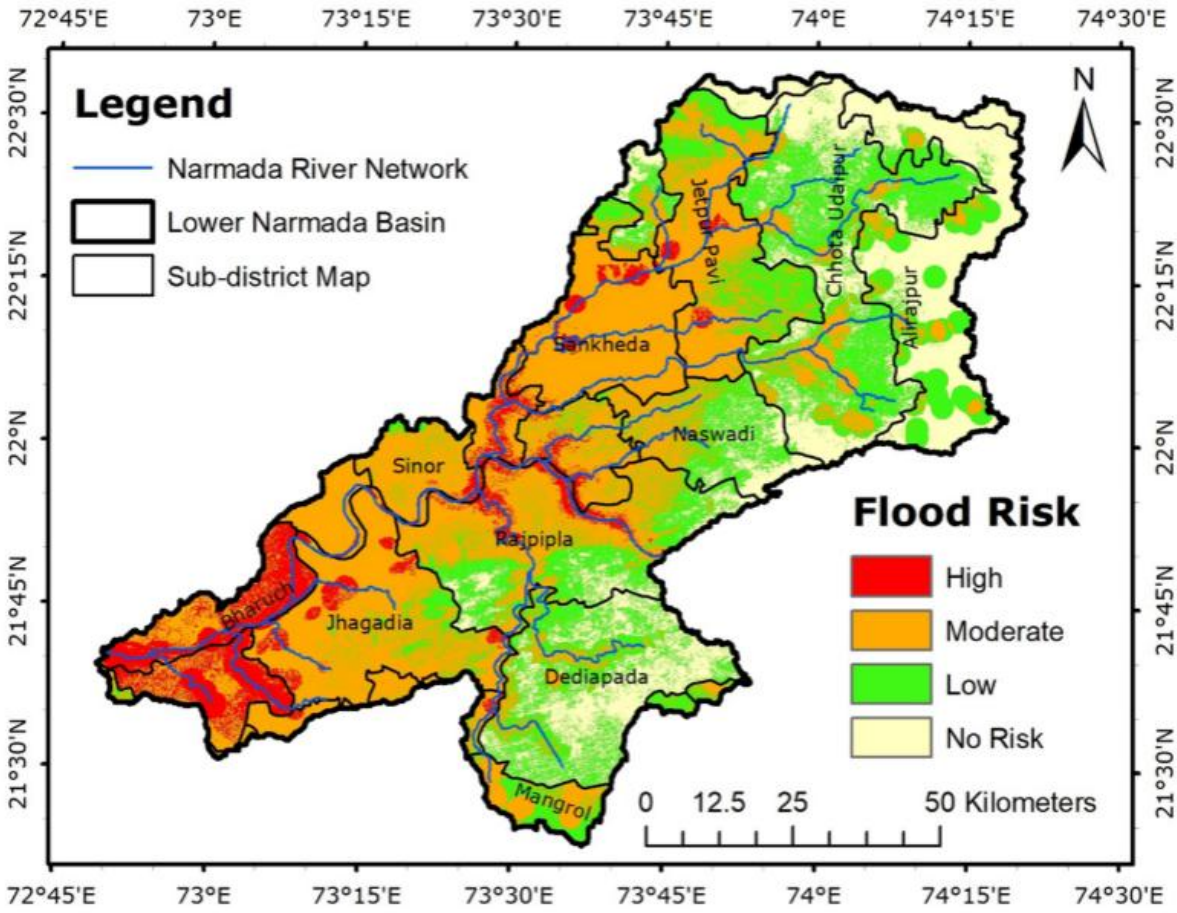

Figure 34: The developed flood risk map of the study area by multiplying the flood hazard and vulnerability map. The lower urban area of the basin is prone to high flood risk, while the upper mountainous area is prone to low or no flood risk

It is important to note that the developed flood risk map is subject to certain uncertainties arising from input data, model assumptions, and weighting schemes. The use of SRTM DEM may introduce elevation-related inaccuracies, which can propagate to derived parameters such as slope. Incorporation of high-resolution, ground-surveyed data could improve accuracy. Additionally, dynamic factors such as rainfall patterns, river morphology, and land-use changes require periodic updates to maintain model reliability. Despite these limitations, the use of categorized inputs and the ensemble nature of the RF model help reduce the impact of uncertainties and enhance the robustness of the results.

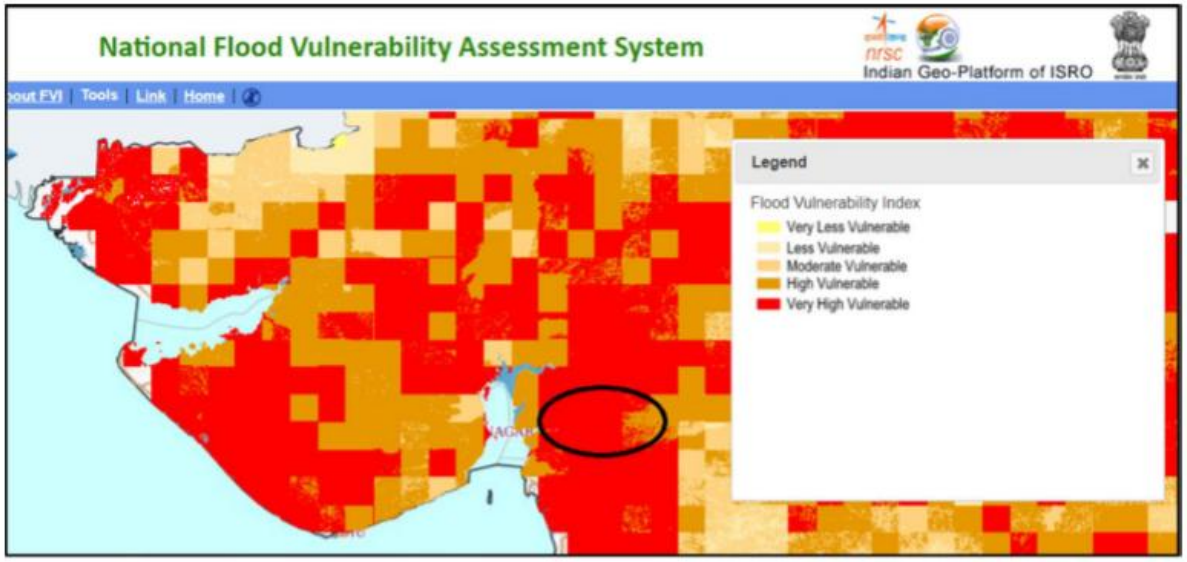

Figure 35: Flood vulnerability map developed by National Flood Vulnerability Assessment System, Indian geo-platform of ISRO using multi-criteria evaluation technique. Source https:// bhuvan- app1. nrsc. gov. in/ nfvas/#

3.7 Flood vulnerability assessment of Narmada River basin using data envelopment analysis

3.7.1 Study Area

This study area comprises 21 districts of Madhya Pradesh, including Alirajpur, Anuppur, Balaghat, Barwani, Betul, Chhindwara, Dewas, Dhar, Dindori, Harda, Hoshangabad, Indore, Jabalpur, Katni, Khandwa, Khargone, Mandla, Narsinghpur, Raisen, Sehore, and Seoni. According to the Relief and Revenue Department, Government of Madhya Pradesh (2019), the districts of Betul, Chhindwara, and Mandla experienced the highest frequency of flood events between 2005 and 2019, whereas Khandwa and Khargone were least affected.

Hydrologically, the Narmada River in Madhya Pradesh flows through a deep and well-defined channel with relatively high banks that are not frequently overtopped (NIH, 2020). However, the upper catchment receives substantial annual rainfall exceeding 1,400 mm and, in some areas, more than 1,650 mm. Intense and concentrated monsoonal rainfall during July to September often generates significant

runoff, leading to excessive flows and downstream flooding (Ray and Goel, 2019). As a result, the basin experiences recurrent flood events. Historical records indicate that major flood discharges occurred in 2013 and 2014, while the highest recorded discharge at the downstream gauging station at Garudeshwar (Gujarat) was observed in 1970, reaching approximately 0.069 million cumecs (Flood Memorandum, 2021).

The basin is also characterized by extensive hydraulic infrastructure, with approximately 3,165 water resource projects, including 29 major projects with a combined storage capacity of about 14,000 million cubic meters (NIH, 2020). Major reservoirs upstream of Hoshangabad, such as Bargi, Barna, and Tawa, influence flow regulation. However, extreme rainfall events over short durations can still result in high discharges and flooding in downstream reaches, particularly near Hoshangabad.

Land-use patterns in the basin indicate that approximately 56.9% of the area is under agriculture, 32.88% is forested, 6.13% is classified as wasteland, and about 3% is built-up area (SDMA, 2020). Flood impacts in the region are significant, particularly in districts such as Dhar, Jabalpur, Chhindwara, Balaghat, Sehore, Raisen, Hoshangabad, and Harda, which frequently experience extensive damage to infrastructure, settlements, and agricultural lands.

Recent flood events highlight the increasing vulnerability of the basin. Between 2013 and 2019, approximately 8% of the total sown area was affected by flooding. In 2019, heavy rainfall during August and September led to the submergence of around 200 villages. Similarly, the 2020 floods necessitated the evacuation of approximately 25,000 people by disaster response teams (NDRF/SDRF) and caused economic losses estimated at around USD 48 million.

These recurring flood events underscore the need for comprehensive flood risk assessment and management strategies in the Narmada basin.

3.7.2 Methodology

The overall methodology adopted for assessing flood vulnerability across the 21 districts of the Narmada River basin in Madhya Pradesh is illustrated in Fig. 36. As shown in the flowchart and formulated in Equation (1), indicators representing the adaptive capacity of the study area were selected as input variables, while indicators reflecting flood sensitivity were considered as output variables.

Data Envelopment Analysis (DEA) was employed to quantify flood vulnerability. In this approach, the efficiency score—defined as the ratio of outputs to inputs—was used to represent the Flood Vulnerability Index (FVI). Both Constant Returns to Scale (CRS) and Variable Returns to Scale (VRS) DEA models were applied to evaluate and compare the efficiency scores under different assumptions.

The efficiency values obtained from the CRS model were adopted as the FVI for the districts. These FVI values were subsequently subjected to cluster analysis to classify the districts into three categories: low, medium, and high vulnerability. Finally, the classified FVI results were used to generate a spatial map of flood vulnerability for the study area.

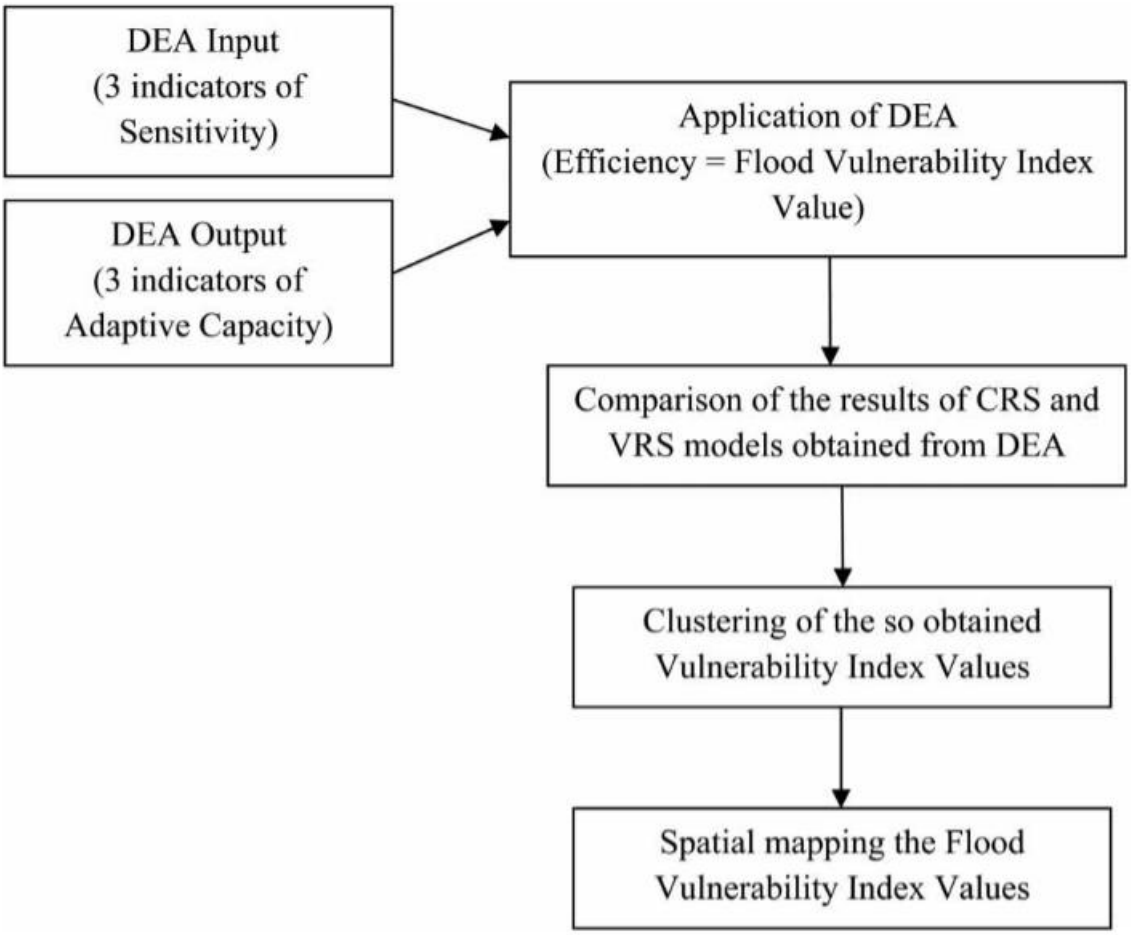

Figure 36: The methodology adopted for the development of Flood Vulnerability Index.

3.7.3 Results and Discussion

In the Data Envelopment Analysis (DEA) framework, efficiency is defined as the ratio of output to input variables. In the context of this study, higher efficiency values indicate greater flood vulnerability, as they represent higher sensitivity (e.g., population density, number of affected villages, and households below the poverty line) relative to adaptive capacity. Accordingly, the Constant Returns to Scale (CRS) efficiency values are interpreted as the Flood Vulnerability Index (FVI).

The results of the FVI values (CRS efficiencies) for all districts are illustrated in Fig. 37. Consistent with previous studies (e.g., Liu et al., 2010; Huang et al., 2019), higher efficiency values indicate more severe vulnerability in input–output-based DEA models. Out of the 21 districts analyzed, 14 districts exhibited the highest possible efficiency score (CRS efficiency = 1.00) under both CRS and Variable

Returns to Scale (VRS) models. These districts include Alirajpur, Anuppur, Balaghat, Barwani, Betul, Chhindwara, Dhar, Dindori, Harda, Indore, Jabalpur, Mandla, Raisen, and Sehore, and are therefore classified as highly flood-vulnerable. This indicates that approximately 67% of the study area falls within the high-vulnerability category.

The high vulnerability observed in these districts can be attributed to a combination of socio-economic and physical factors. Several of these regions are relatively underdeveloped in terms of infrastructure, including limited healthcare facilities and disaster management capacity. Additionally, districts with higher levels of urbanization and population density tend to exhibit greater vulnerability, as increased exposure amplifies flood impacts.

These findings highlight the need for targeted interventions in the majority of the districts, emphasizing an integrated approach that addresses both socio-economic conditions and physical flood risk factors. Improving infrastructure, enhancing adaptive capacity, and managing population pressures could significantly reduce flood vulnerability in these regions.

In contrast, only two districts—Seoni and Dewas—recorded efficiency values below 0.5, indicating relatively low flood vulnerability. Furthermore, the consistency of efficiency values between input- and output-oriented CRS models suggests that the vulnerability assessment is robust and largely independent of variations in sensitivity (output) or adaptive capacity (input) indicators.

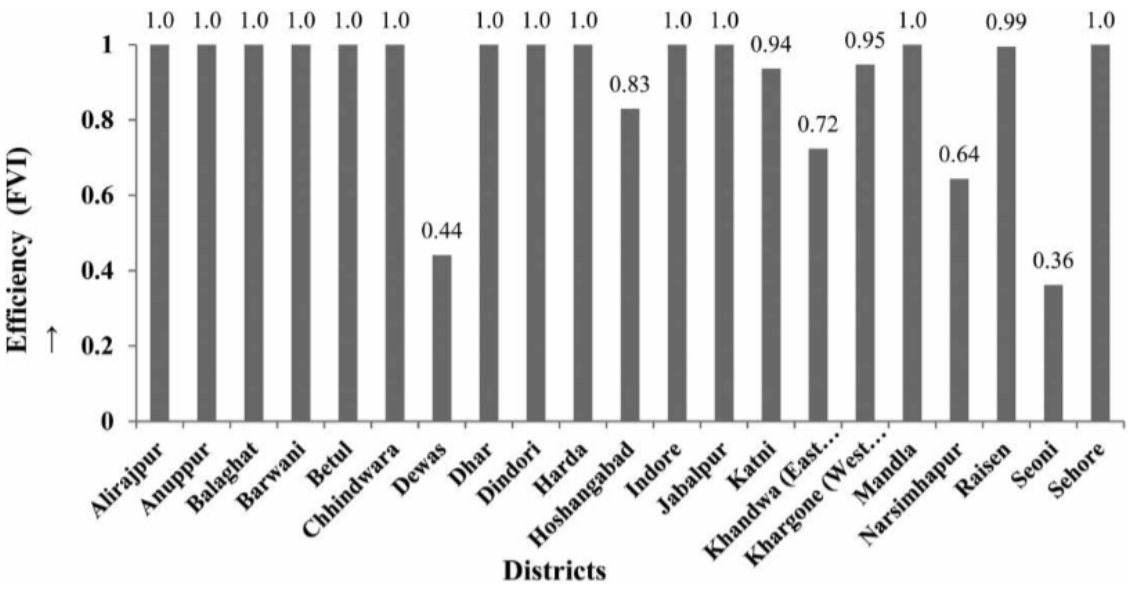

Figure 37: Flood Vulnerability Index (FVI) for various districts.

In the DEA framework, a Scale Efficiency value of unity indicates that the decision-making unit (DMU) is operating at an optimal scale. Conversely, a value less than one suggests scale inefficiency, arising from differences between CRS and VRS technical efficiencies.

In the context of this study, optimal scale is interpreted as a condition corresponding to maximum flood vulnerability. Therefore, districts with Scale Efficiency values equal to one can be considered highly vulnerable. Most districts fall into this category, indicating that their vulnerability levels are already at or near optimal scale conditions.

In contrast, three districts—Narsinghpur, Seoni, and Dewas—exhibit Increasing Returns to Scale (IRS) along with relatively low Scale Efficiency values. These districts are currently less vulnerable due to their smaller size and lower exposure. However, the presence of IRS suggests that any increase in scale, such as population growth or urban expansion, could lead to a disproportionate increase in flood vulnerability. Given the ongoing trends of urbanization in developing regions, these districts may become significantly more flood-prone in the future. This highlights the need for careful planning and controlled development in these areas, including the possibility of decentralized administrative or spatial planning strategies.

For the remaining districts, Scale Efficiency values are either equal to or close to unity, indicating that they operate near optimal scale with respect to flood vulnerability. Districts exhibiting Decreasing Returns to Scale (DRS) demonstrate a relatively lower sensitivity of outputs (vulnerability indicators) to changes in inputs (adaptive capacity factors). This implies that adverse changes in socio-economic or demographic conditions may not proportionally increase flood vulnerability, suggesting the presence of some inherent resilience.

On the other hand, districts with Increasing Returns to Scale are more sensitive to variations in input parameters, such as population density, forest cover, healthcare infrastructure, and socio-economic conditions. In these districts, even small adverse changes can significantly amplify flood vulnerability. Therefore, targeted interventions are necessary to maintain or improve adaptive capacity and prevent deterioration in socio-economic conditions.

The mean CRS efficiency value of 0.8989 indicates a generally high level of flood vulnerability across the study area. The standard deviation of the efficiency scores was 0.1929, indicating that most districts have values clustered around the mean, with relatively limited variation in flood vulnerability across the study area.

The results of the cluster analysis, classify the 21 districts into three distinct vulnerability groups using the K-means algorithm. Based on the Flood Vulnerability Index (FVI), cluster 1 (centroid = 0.99)

represents high vulnerability, cluster 2 (centroid = 0.73) corresponds to medium vulnerability, and cluster 3 (centroid = 0.40) denotes low vulnerability.

The spatial distribution of these clusters (Fig. 38) reveals that districts located at the eastern and western extremities of the state exhibit high vulnerability, as indicated by the red color. These regions are generally less developed compared to the central districts, suggesting that inadequate infrastructure and limited resources contribute significantly to increased flood vulnerability. This highlights the need for targeted policy interventions and enhanced financial allocation to improve infrastructure and resilience in these areas.

Districts located in the central part of the state, represented in yellow, exhibit moderate vulnerability, while those classified in green fall under low vulnerability. Overall, approximately 24% of the districts fall within the low to medium vulnerability categories, indicating relatively lower flood risk. Interestingly, these districts also demonstrate moderate levels of economic development, suggesting a potential relationship between balanced economic growth and reduced flood vulnerability. However, this relationship requires further investigation and validation through additional studies.

Approximately 76% of the districts in the study area fall under the high flood vulnerability category, as indicated in Figure 38. This group includes both economically advanced and densely populated districts such as Indore, Jabalpur, and Chhindwara, as well as relatively less developed districts like Alirajpur, Annupur, and Dindori. In developing regions, economically advanced districts often exhibit significant socio-economic disparities, which increase the vulnerability of marginalized populations. While these regions may possess better flood management infrastructure, high population density and urban congestion amplify their exposure to flood risks. Conversely, less developed districts, despite having lower population densities, often lack adequate mitigation measures and preparedness, making them equally or more susceptible to flood impacts.

Socio-economic conditions further influence vulnerability. Economically weaker districts tend to have limited awareness, infrastructure, and resources to cope with flood events. Evidence from recent flood events, such as those in 2019, shows that districts like Raisen, Balaghat, Harda, and Mandla required extensive relief measures, including temporary shelters, food, medical assistance, and evacuation support. Additionally, districts such as Balaghat and Chhindwara recorded high numbers of displaced individuals, while Narsinghpur, Mandla, Raisen, and Seoni experienced significant housing damage—highlighting their vulnerability.

The findings of this study are consistent with observed field data and government reports, thereby validating the effectiveness of the Data Envelopment Analysis (DEA) approach used. Based on these results, districts identified as highly vulnerable require comprehensive and efficient flood management

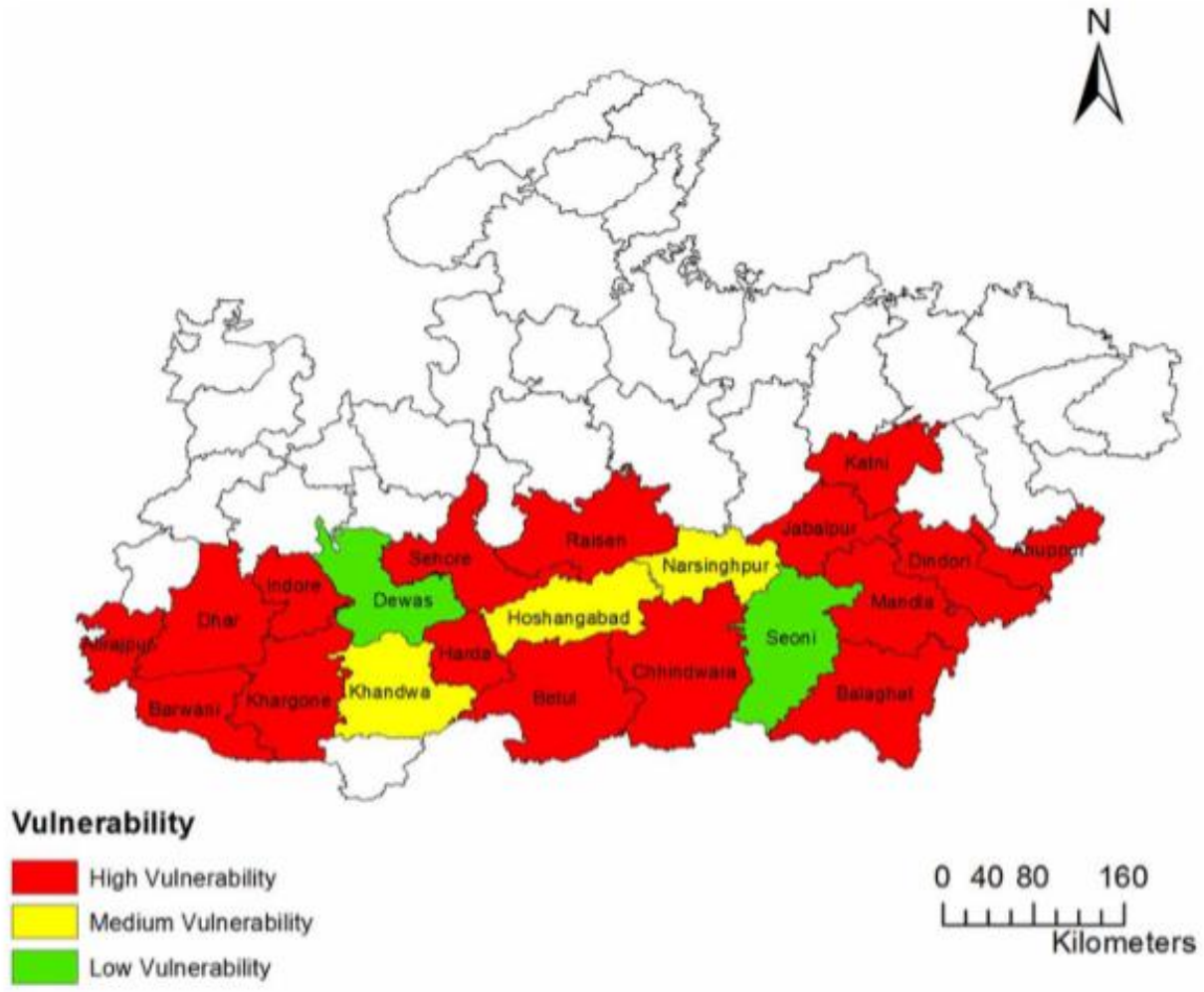

Figure 38: Spatial variation of flood vulnerability. Please refer to the online version of this paper to see this figure in colour: http://dx.doi.10.2166/wp.2021.063.

strategies. Priority should be given to strengthening healthcare infrastructure, improving communication systems, and enhancing community awareness.

From a policy perspective, District Disaster Management Authorities, established under the Disaster Management Act (2005), should consider dividing large vulnerable districts into smaller administrative or micro-management zones. Such an approach would enable more targeted planning, efficient resource allocation, and improved implementation of flood mitigation strategies. Tailored, district-specific flood management plans based on vulnerability characteristics are essential for effective risk reduction.

This study also contributes to the development of a systematic framework for assessing flood vulnerability by integrating physical, social, and economic indicators. The proposed methodology has the potential to be generalized and applied to other regions for vulnerability and resilience assessment. With appropriate adaptation, it can support the creation of comprehensive vulnerability and resilience maps, aiding decision-makers during both pre-disaster planning and post-disaster response.

Furthermore, the framework can be extended to assess vulnerability to other natural hazards such as earthquakes, landslides, droughts, and wildfires. Such integrated and data-driven approaches can support evidence-based policymaking, enhance disaster preparedness, and improve resilience across regions.

4. Conclusions

The present body of work provides a comprehensive and multi-dimensional assessment of flood dynamics, forecasting, and risk management in the Narmada River Basin by integrating hydrodynamic modelling, hydrological analysis, climate change projections, geospatial techniques, and data-driven approaches. The application of HEC-RAS (v6.0) coupled with geospatial tools demonstrated reliable simulation of flood behaviour in the Karjan River Basin, with results closely matching observed flood conditions, particularly during the 2020 event. Flood-prone areas such as Bhadam, Juna Rundh, Dhanpor, Dhamancha, and Nandod were consistently identified as highly vulnerable, largely due to backwater effects and high discharge releases from the Narmada system. Extending the analysis to climate change scenarios revealed that flood risk intensifies significantly with increasing return periods and under high-emission scenarios (RCP 8.5), leading to greater inundation extents and depths. The study further established that optimized reservoir operations using fuzzy-based approaches can substantially reduce peak flows and inundation areas across key dam-to-dam river segments, although such measures must be complemented with structural and non-structural interventions.

Advanced modelling approaches, including one-dimensional and two-dimensional hydrodynamic simulations, highlighted the importance of representing floodplain processes and hydraulic structures such as embankments, barrages, and diversion channels. The 2D modelling of the lower Narmada River demonstrated the significant influence of embankments on water levels and floodplain inundation, while also identifying potential risks to critical infrastructure such as bridges under extreme flood scenarios. Flood frequency analysis using Gumbel EV-I and Log-Pearson Type-III distributions indicated that a hybrid approach provides more reliable design flood estimates across varying return periods, which, when integrated with hydrodynamic models, enables robust flood hazard mapping and risk assessment.

Hydrological modelling combined with hierarchical clustering and Thiessen polygon methods confirmed that accurate rainfall representation is essential for reliable flood forecasting, with the existing rain gauge network proving adequate for the study region. Additionally, machine learning techniques, particularly Random Forest, demonstrated strong capability in flood risk mapping using heterogeneous datasets, identifying key controlling factors such as elevation, proximity to river channels, land use, rainfall, population density, and agricultural activity. The integration of IoT-based real-time monitoring systems was recognized as a promising advancement for improving flood prediction and early warning systems.

From a vulnerability assessment perspective, the application of Data Envelopment Analysis (DEA) revealed that a majority of districts in the Narmada Basin fall under high vulnerability categories,

emphasizing the need for improved governance, data availability, and localized planning strategies. The study aligns with Sustainable Development Goal 11, particularly in reducing disaster-related risks and enhancing resilience of vulnerable communities. Despite these advancements, limitations such as reliance on limited climate models, data scarcity, DEM inaccuracies, and the use of predominantly one-dimensional modelling approaches highlight the need for future research incorporating multi-model climate ensembles, high-resolution terrain data (e.g., UAV-based DEMs), and fully coupled two-dimensional or hybrid modelling frameworks. Overall, the integrated methodologies presented in this work provide a robust foundation for flood risk assessment, mitigation planning, and policy formulation, supporting sustainable and resilient development in the Narmada River Basin.

Combined Conclusion (Point-wise)

1. Hydrodynamic Modelling Effectiveness

(i) HEC-RAS (v6.0) integrated with geospatial techniques provides a reliable and efficient approach for flood simulation.

(ii) One-dimensional hydrodynamic modelling shows good agreement with observed flood data, such as the 2020 flood event in the Karjan Basin.

2. Flood-Prone Areas Identified

(i) Regions such as Bhadam, Juna Rundh, Dhanpor, Dhamancha, and Nandod are highly vulnerable to flooding.

(ii) Flooding in these areas is significantly influenced by backwater effects and high discharge releases from the Narmada River system.

3. Climate Change Impacts

(i) Flood extent and inundation depth increase with higher return periods ranging from 20 to 100 years.

(ii) The RCP 8.5 scenario produces more severe flooding compared to the RCP 4.5 scenario.

4. Reservoir Operation Optimization

(i) Optimized reservoir releases can reduce peak flows by approximately 50–90%.

(ii) Optimized releases can also reduce flood inundation extent by about 10–23%.

(iii) Reservoir operation strategies should be integrated with other flood mitigation measures for effective management.

5. Importance of 2D Hydrodynamic Modelling

(i) Two-dimensional hydrodynamic models better capture floodplain processes and lateral flow interactions.

(ii) Embankments significantly reduce flood inundation extent.
(iii) Embankments may increase upstream water levels by up to approximately 4 m.
(iv) Structural measures may pose risks to infrastructure such as bridges under extreme flood conditions.

6. Flood Frequency Analysis (FFA)

(i) The Log-Pearson Type-III distribution performs better for lower return periods (less than 60 years).
(ii) The Gumbel Extreme Value Type-I distribution performs better for higher return periods (greater than 60 years).
(ii) A hybrid approach improves the accuracy of design flood estimation.

7. Hydrological Modelling and Rainfall Representation

(i) The Thiessen polygon method and hierarchical clustering effectively represent areal rainfall.
(ii) The hydrological model shows strong performance with high R^2 and NSE values and low RMSE.
(iii) The existing rain gauge network is adequate for reliable flood forecasting.

8. Machine Learning in Flood Risk Mapping

(i) The Random Forest algorithm effectively handles heterogeneous datasets for flood risk assessment.
(ii) Key influencing factors include elevation, distance from the river, land use, rainfall, population, and agriculture.
(iii) Bharuch and Ankleshwar are identified as high-risk flood zones.

9. Role of Advanced Technologies

(i) IoT-based real-time monitoring systems can significantly enhance flood forecasting and early warning systems.
(ii) UAV-based high-resolution DEMs can improve modelling accuracy, especially in flat terrain regions.

10. Flood Vulnerability Assessment (DEA Approach)

(i) The majority of districts fall under high flood vulnerability categories.
(ii) The results highlight the need for improved governance, planning, and disaster management strategies.

11. Policy and Sustainability Relevance

(i) The study supports the objectives of Sustainable Development Goal 11 (SDG-11) for disaster risk

reduction.

(ii) The findings provide a scientific basis for flood mitigation planning and policy decision-making.

12. Limitations and Future Scope

(i) The study uses a limited number of climate models, and multi-model ensembles are recommended for better accuracy.

(ii) Data scarcity and DEM inaccuracies affect the precision of the modelling results.

(iii) There is a need for fully coupled or hybrid two-dimensional hydrodynamic models.

(iv) Future studies should include lower return periods (2–10 years) and detailed micro-level analysis.

.

5. Significance and Utility

The report on flood management techniques in the Narmada River Basin serves as a practical resource for understanding, analysing, and mitigating flood risks in one of India's most significant river systems. By integrating hydrological, hydrodynamic, and geospatial approaches, the study provides valuable insights that are highly relevant for researchers, engineers, planners, and policymakers involved in water resources management and disaster risk reduction.

One of the key strengths of this report lies in its integrated methodological framework, which combines traditional flood management strategies with modern technological advancements. The study effectively demonstrates the application of hydrodynamic models such as HEC-RAS, coupled with Geographic Information Systems (GIS) and remote sensing data, to simulate flood behaviour and delineate inundation zones. These modelling techniques enable accurate prediction of flood extent and depth, which is crucial for early warning systems and emergency planning. The ability to simulate real flood events, such as the 2020 flood in the Karjan River Basin, highlights the practical applicability and reliability of the adopted approach.

The report is particularly useful in identifying flood-prone areas and vulnerable regions within the basin. By analyzing spatial flood patterns and backwater effects, it pinpoints critical locations such as low-lying settlements and confluence zones that are highly susceptible to flooding. This information is essential for targeted mitigation measures, infrastructure planning, and community-level disaster preparedness.

Another significant contribution of the study is its emphasis on climate change impacts and future flood risk assessment. The report demonstrates that flood intensity and inundation extent are likely to increase under high-emission scenarios and longer return periods. This forward-looking perspective enables decision-makers to plan adaptive strategies and design resilient infrastructure capable of withstanding future uncertainties.

The inclusion of advanced techniques such as machine learning, IoT-based monitoring, and data-driven modelling further enhances the utility of the report. These approaches improve the accuracy of flood prediction, enable real-time monitoring, and support the development of efficient early warning systems. The integration of diverse datasets—including elevation, land use, rainfall, and socio-economic factors—provides a holistic understanding of flood risk dynamics.

From a management perspective, the report highlights the importance of combining structural measures (such as dams, reservoirs, and embankments) with non-structural measures (such as floodplain zoning,

early warning systems, and public awareness). This balanced approach ensures sustainable flood mitigation while minimizing environmental and socio-economic impacts.

Furthermore, the study offers valuable insights into reservoir operation and optimization, demonstrating how improved release strategies can reduce peak flows and downstream flooding. This has direct implications for dam management authorities and policy formulation in river basin planning.

Finally, the report contributes to broader developmental goals by supporting evidence-based policy making and sustainable development, particularly in alignment with disaster risk reduction objectives. It provides a scientific foundation for planning resilient communities and improving governance in flood-prone regions.

In conclusion, this report is highly beneficial as it not only enhances the understanding of flood dynamics in the Narmada Basin but also offers practical, technology-driven solutions for effective flood management. Its comprehensive and multidisciplinary approach makes it a valuable reference for both academic research and real-world implementation.

6. References

Agarwal, A., and Narain, S. (1991). *Floods, flood plains and environmental myths.* Centre for Science and Environment, New Delhi, India.

Alsabhan, W., and Dudin, B. (2023). "Real-time flood forecasting and warning: A comprehensive approach toward HCI-centric mobile app development." *Multimodal Technologies and Interaction*, 7(5), 44. https://doi.org/10.3390/mti7050044.

American Society of Civil Engineers (ASCE). 2018. *Climate-Resilient Infrastructure: Adaptive Design and Risk Management.* Reston, VA: ASCE.

Bellos, V., Papageorgaki, I., Kourtis, I., Vangelis, H., Kalogiros, I., and Tsakiris, G. (2020). "Reconstruction of a flash flood event using a 2D hydrodynamic model under spatial and temporal variability of storm." *Natural Hazards*, 101(3), 711–726.

Beven, K. (2001). *Rainfall-runoff modelling: The primer*. Wiley.

Bhargav, A., & Suresh, R. (2025). Exploring River's Flood Dynamics: Integrating HEC-RAS 1-D Modelling and Geospatial Techniques for the Karjan River in Gujarat's Narmada Basin, India. *International Journal of Environment and Climate Change*, *15*(1), 140-155.

Breiman, L. (2001). "Random forests." *Mach. Learn.* https://doi.org/10.1023/A:1010933404324.

Brunner, G. W. (2010). *HEC-RAS River Analysis System, Hydraulic Reference Manual, Version 4.1*. U.S. Army Corps of Engineers, Hydrologic Engineering Center, Davis, CA.

Brunner, G. W. (2016). *HEC-RAS River Analysis System User's Manual*. US Army Corps of Engineers.

Carrivick, J. L. (2006). "Application of 2D hydrodynamic modelling to high-magnitude outburst floods: An example from Kverkfjöll, Iceland." *Journal of Hydrology*, 321(1–4), 187–199.

Carvalho, J., Santos, J. P. V., Torres, R. T., et al. (2018). "Tree-based methods: Concepts, uses and limitations under the framework of resource selection models." *J. Environ. Inf.* https://doi.org/10.3808/jei.201600352.

Census of India, 2011. *Population enumeration data (final population)*. Office of the Registrar General and Census Commissioner, New Delhi, India.

Central Water Commission (2018). *Annual report*. Ministry of Water Resources, River Development and Ganga Rejuvenation, Government of India, New Delhi.

Central Water Commission (CWC), 2020. *Narmada Basin Organisation, Bhopal*. Ministry of Jal Shakti, Government of India.

Central Water Commission (CWC). (2014). *Narmada Basin Report.* Ministry of Water Resources, Government of India, New Delhi.

Central Water Commission (CWC). (2015). *Flood Management in India*. Ministry of Water Resources, Government of India.

Central Water Commission (CWC). (2020). *Annual Flood Report*. Government of India.

Chandole, V., Joshi, G. S., and Srivastava, V. K. 2024. "Flood Risk Mapping under Changing Climate in Lower Tapi River Basin, India." *Stochastic Environmental Research and Risk Assessment* 38 (6): 2231–2259. https://doi.org/10.1007/s00477-024-02677-4.

Choudhury, P., 2010. Reservoir flood control operation model incorporating multiple uncontrolled water flows. *Lakes Reserv. Res. Manag.* 15, 153–163.

Chowdhury, N., & Choudhary, M. (2024). Flood risk assessment of the Narmada Basin, India, under climate change scenarios. *AQUA—Water Infrastructure, Ecosystems and Society*, *73*(11), 2150-2164.

Connell, R. J., Painter, D. J., and Beffa, C. (2001). "Two-dimensional floodplain flow. II: Model validation." *Journal of Hydrologic Engineering*, 6(5), 406–415.

Cook, A., and Merwade, V. (2009). "Effect of topographic data, geometric configuration and modeling approach on flood inundation mapping." *J. Hydrol.*, 377(1–2), 131–142. https://doi.org/10.1016/j.jhydrol.2009.08.015.

Costache, R. (2019). "Flood susceptibility assessment using bivariate statistics and machine learning models: A tool for flood risk management." *Water Resour. Manage.*, 33, 3239–3256. https://doi.org/10.1007/s11269-019-02301-z.

Cunnane, C. (1988). "Methods and merits of regional flood frequency analysis." *J. Hydrol.*, 100(1–3), 269–290. https://doi.org/10.1016/0022-1694(88)90188-6.

Darabi, H., Choubin, B., Rahmati, O., et al. (2019). "Urban flood risk mapping using GARP and QUEST models: A comparative study of machine learning techniques." *J. Hydrol.*, 569, 142–154. https://doi.org/10.1016/j.jhydrol.2018.12.002.

Deb, D., and Talukdar, B. 2010. "Remote Sensing and Geographic Information System for Assessment, Monitoring, and Management of Flooded and Waterlogged Areas, North District of Tripura State, India." In *Watershed Management 2010*, 1013–1024. https://doi.org/10.1061/41143(394)92.

Deria, A., Ghannad, P., Lee, Y.C., 2020. Evaluating implications of flood vulnerability factors with respect to income levels for building long-term disaster resilience of low-income communities. *Int. J. Disaster Risk Reduct.* 48, 101608.

Eini, M., Kaboli, H. S., Rashidian, M., and Hedayat, H. (2020). "Hazard and vulnerability in urban flood risk mapping: Machine learning techniques and the role of urban districts." *Int. J. Disaster Risk Reduct.*, 50, 101687. https://doi.org/10.1016/j.ijdrr.2020.101687.

Feldman, A. D. (2000). *HEC-HMS Technical Reference Manual*. US Army Corps of Engineers.

Fernandes, D., Wu, Y., Shirodkar, P.V., Pradhan, U.K., Zhang, J., Limbu, S.M., 2020. Sources and preservation dynamics of organic matter in surface sediments of Narmada River, India illustrated by amino acids. *J. Mar. Syst.* 201, 103239.

Flood Memorandum, 2021. *Disaster management plan-2020: flood memorandum – 2020*. Sardar Sarovar Narmada Nigam Limited, Gandhinagar, Gujarat, India.

Forest Survey of India, 2017. *State of forest report 2017*. Ministry of Environment and Forests, Dehradun, India.

Ghosh, S., Mondal, A., and Mujumdar, P. P. (2016). "Detection of nonstationarity in flood series." *Journal of Hydrologic Engineering*, 21(3), 04015061.

Grigg, N. S. (2023). “Comprehensive flood risk assessment: State of the practice.” *Hydrology*, 10(2), 46. https://doi.org/10.3390/hydrology10020046.

Haq, M., Akhtar, M., Muhammad, S., Paras, S., and Rahmatullah, J. 2012. “Techniques of Remote Sensing and GIS for Flood Monitoring and Damage Assessment: A Case Study of Sindh Province, Pakistan.” *Egyptian Journal of Remote Sensing and Space Science* 15 (2): 135–141. https://doi.org/10.1016/j.ejrs.2012.07.002.

Hoshi, K., Stedinger, J. R., and Burges, S. J. (1984). “Estimation of log-normal quantiles: Monte Carlo results and first-order approximations.” *J. Hydrol.*, 71(1–2), 1–30. https://doi.org/10.1016/0022-1694(84)90069-6.

Huang, X., Huidong, J., Bai, H., 2019. Vulnerability assessment of China’s coastal cities based on DEA cross-efficiency model. *Int. J. Disaster Risk Reduct.* 36, 10109.

Hunter, N. M., Bates, P. D., Horritt, M. S., and Wilson, M. D. (2007). “Simple spatially distributed models for predicting flood inundation: A review.” *Geomorphology*, 90(3–4), 208–225.

IPCC, 2014. *Climate change 2014: impacts, adaptation, and vulnerability. Part A: global and sectoral aspects*. Cambridge University Press, Cambridge, UK and New York, USA.

Jain, S. K., Agarwal, P. K., and Singh, V. P. (2007). *Hydrology and Water Resources of India*. Springer.

Jato-Espino, D., Lobo, A., and Ascorbe-Salcedo, A. (2019). “Urban flood risk mapping using an optimized additive weighting methodology based on open data.” *J. Flood Risk Manage.* https://doi.org/10.1111/jfr3.12533.

Joshy, K. A., Chandran, S. R., and Padikkal, S. 2022. “Role of Flood Control Dams in Managing Extreme Climatic Events: A Case Study of Kerala’s Periyar Basin.” *INCOLD Journal* 11 (1): 48–52.

Karim, F., Dutta, D., Marvanek, S., Petheram, C., Ticehurst, C., Lerat, J., Kim, S., and Yang, A. (2015). “Assessing the impacts of climate change and dams on floodplain inundation and wetland connectivity in the wet–dry tropics of northern Australia.” *Journal of Hydrology*, 522, 80–94.

Kathal, P.K., 2018. Narmada: the longest westward flowing river of peninsular India. In: Singh, D. (Ed.), *The Indian rivers: scientific and socio-economic aspects*. Springer, Singapore, pp. 301–308.

Khosravi, K., Nohani, E., Maroufinia, E., and Pourghasemi, H. R. (2016). “A GIS-based flood susceptibility assessment and mapping in Iran: Comparison of frequency ratio and weights-of-evidence models with MCDM techniques.” *Nat. Hazards*, 83, 947–987. https://doi.org/10.1007/s11069-016-2357-2.

Khosravi, K., Pham, B. T., Chapi, K., et al. (2018). “Comparative assessment of decision tree algorithms for flash flood susceptibility modeling in the Haraz watershed, Iran.” *Sci. Total Environ.*, 627, 744–755. https://doi.org/10.1016/j.scitotenv.2018.01.266.

Kuiry, S., Sen, D., and Bates, P. D. (2010). “Coupled 1D–quasi-2D flood inundation model with unstructured grids.” *Journal of Hydraulic Engineering*, 136(8), 493–506.

Kumar, K.N., Rajeevan, M., Pai, D.S., et al., 2013. On the observed variability of monsoon droughts over India. *Weather Clim. Extrem.* 1, 42–50.

Li, J., Liu, X., Chen, F., 2015. Evaluation of nonstationarity in annual maximum flood series and the associations with large-scale climate patterns and human activities. *Water Resour. Manag.* 29, 1653–1668. https://doi.org/10.1007/s11269-014-0900-z.

Liu, Y., Huang, J.Y., Ma, L., 2010. Assessment of regional vulnerability to natural disasters in China based on DEA model. *Geogr. Res.* 29 (7), 1153–1162.

Liu, Y., Lu, X., Yao, Y., et al., 2021. Mapping the risk zoning of storm flood disaster based on heterogeneous data and a machine learning algorithm in Xinjiang, China. *J. Flood Risk Manag.* https://doi.org/10.1111/jfr3.12671.

Ma, M., Liu, C., Zhao, G., et al., 2019. Flash flood risk analysis based on machine learning techniques in Yunnan Province, China. *Remote Sens.* 11, 170. https://doi.org/10.3390/rs11020170.

Malik, A., and Abdalla, R. 2016. "Geospatial Modeling of the Impact of Sea Level Rise on Coastal Communities: Application to Richmond, British Columbia, Canada." *Modeling Earth Systems and Environment* 2 (3): 146. https://doi.org/10.1007/s40808-016-0199-2.

Mangukiya, N. K., & Sharma, A. (2022). Flood risk mapping for the lower Narmada basin in India: a machine learning and IoT-based framework. *Natural Hazards*, *113*(2), 1285-1304.

Mangukiya, N. K., and Andharia, B. R. 2024. "Modeling of Flood Inundation Extent in Data-Scarce Regions: A Case Study of Bhavnagar District." In *[Book/Proceedings Title]*, 13–22. https://doi.org/10.1007/978-981-99-1890-4_2.

Mangukiya, N. K., and Yadav, S. M. (2021). "Integrating 1D and 2D hydrodynamic models for semi-arid river basin flood simulation." *Int. J. Hydrol. Sci. Technol.*, 1(1), 1. https://doi.org/10.1504/IJHST.2021.10035928.

Mangukiya, N. K., Mehta, D. J., & Jariwala, R. (2022). *Flood frequency analysis and inundation mapping for lower Narmada basin, India. Water Pract Technol 17 (2): 612–622*.

Meena, R. S., and Jha, R. 2022. "Flood Inundation Modeling Using Coupled 1D–2D HEC-RAS Model in Lower Kosi River Basin, India with Limited Data." In *[Book/Proceedings Title]*, 177–188. https://doi.org/10.1007/978-981-16-9933-7_12.

Mehta, D., Dhabuwala, J., Yadav, S. M., Kumar, V., & Azamathulla, H. M. (2023). *Improving flood forecasting in Narmada river basin using hierarchical clustering and hydrological modelling, Results Eng 20 (2023) 101571*.

Mehta, D., Dhabuwala, J., Yadav, S. M., Kumar, V., and Azamathulla, H. M. 2023. "Improving Flood Forecasting in Narmada River Basin Using Hierarchical Clustering and Hydrological Modelling." *Results in Engineering* 20: 101571. https://doi.org/10.1016/j.rineng.2023.101571.

Mohapatra, P.K., Singh, R.D., 2003. Flood management in India. *Nat. Hazards* 28, 131–143. https://doi.org/10.1023/A:1021178000374.

Mondal, A., and Mujumdar, P. P. 2012. "On the Basin-Scale Detection and Attribution of Human-Induced Climate Change in Monsoon Precipitation and Streamflow." *Water Resources Research* 48 (10). https://doi.org/10.1029/2011WR011468.

Moriasi, D. N., Arnold, J. G., Van Liew, M. W., Bingner, R. L., Harmel, R. D., and Veith, T. L. (2007). "Model evaluation guidelines for systematic quantification of accuracy in watershed simulations." *Transactions of the ASABE*, 50(3), 885–900.

Mosavi, A., Ozturk, P., and Chau, K. W. (2018). "Flood prediction using machine learning models." *Water*, 10(11), 1536.

Mujumdar, P. P., and Ghosh, S. (2008). "Modeling GCM and scenario uncertainty using a possibilistic approach." *Water Resources Research*, 44(6).

Narmada Control Authority (NCA). (2018). *Annual Report*. Government of India.

National Disaster Management Authority (2008). *National disaster management guidelines: Management of floods*. Government of India, New Delhi.

National Disaster Management Authority (NDMA). (2010). *Guidelines for Flood Management*. Government of India.

National Disaster Management Authority (NDMA). 2017. *Gujarat Flood 2017: A Case Study.* New Delhi: NDMA.

Nigussie, T. A., and Altunkaynak, A. (2019). "Modeling the effect of urbanization on flood risk in Ayamama Watershed, Istanbul, Turkey, using the MIKE 21 FM model." *Natural Hazards*, 99(2), 1031–1047.

NIH, 2020. *Hydrology and water resources information system for India*. National Institute of Hydrology, Roorkee, India.

Padikkal, S., Rema, K. P., and Gopi, G. 2020. "Frequent Extreme Climatic Events in Kerala: Evolving Sustainable Management Paradigm." *Journal of the Indian Society of Coastal Agricultural Research* 38 (2): 140–146.

Pal, S. C., Chowdhuri, I., Das, B., Chakrabortty, R., Roy, P., Saha, A., and Shit, M. 2022. "Threats of Climate Change and Land Use Patterns Enhance the Susceptibility of Future Floods in India." *Journal of Environmental Management* 305: 114317. https://doi.org/10.1016/j.jenvman.2021.114317.

Papaioannou, G., Loukas, A., Vasiliades, L., Aronica, G.T., 2016. Flood inundation mapping sensitivity to riverine spatial resolution and modelling approach. *Nat. Hazards* 83, 117–132. https://doi.org/10.1007/s11069-016-2382-1.

Patel, D., and Dholakia, M. 2010. "Feasible Structural and Non-Structural Measures to Minimize Flood Effects in Lower Tapi Basin."

Pathak, S. D., Kulshrestha, M., & Kulshreshtha, M. (2021). Flood vulnerability assessment using data envelopment analysis–the case of Narmada river basin districts in central India. *Water Policy*, *23*(5), 1089-1106.

Pham, B.T., Luu, C., Van, P.T., et al., 2021. Flood risk assessment using hybrid artificial intelligence models integrated with multi-criteria decision analysis in Quang Nam Province, Vietnam. *J. Hydrol.* 592, 125815. https://doi.org/10.1016/j.jhydrol.2020.125815.

Phien, H. N., and Ajirajah, T. J. (1984). "Applications of the log Pearson type-III distribution in hydrology." *J. Hydrol.*, 73(3–4), 359–372. https://doi.org/10.1016/0022-1694(84)90008-8.

Pollard, J.A., Spencer, T., Jude, S., 2018. Big data approaches for coastal flood risk assessment and emergency response. *WIREs Clim. Change* https://doi.org/10.1002/wcc.543.

Rahman, M. M., Arya, D. S., Goel, N. K., and Dhamy, A. P. (2010). "Design flow and stage computations in the Teesta River, Bangladesh, using frequency analysis and MIKE 11 modeling." *Journal of Hydrologic Engineering*, 16(2), 176–186.

Rajaguru, S. N., Gupta, A., Kale, V. S., Mishra, S., Ganjoo, R. K., Ely, L. L., Enzel, Y., and Baker, V. R. (1995). "Channel form and processes of the flood-dominated Narmada River, India." *Earth Surface Processes and Landforms*, 20(5), 407–421.

Ramkar, P., and Yadav, S. M. 2018. "Spatiotemporal Drought Assessment of a Semi-Arid Part of Middle Tapi River Basin, India." *International Journal of Disaster Risk Reduction* 28: 414–426. https://doi.org/10.1016/j.ijdrr.2018.03.025.

Ramkar, P., Yadav, S.M., 2021. Flood risk index in data-scarce river basins using the AHP and GIS approach. *Nat. Hazards* 109, 1119–1140. https://doi.org/10.1007/s11069-021-04871-x.

Ray, L.K., Goel, N.K., 2019. Flood frequency analysis of Narmada River basin in India under non-stationary condition. *J. Hydrol. Eng.* 24 (8).

Ray, P. A., et al. (2019). "Water resources management under climate uncertainty." *Water Resources Research*, 55(5).

Relief and Revenue Department (Madhya Pradesh), 2019. *Memorandum on the situation caused by heavy rains and floods in Madhya Pradesh during June to September 2019*. Government of Madhya Pradesh, Bhopal, India.

Samarasinghe, S. M. J. S., Nandalal, H. K., Weliwitiya, D. P., Fowze, J. S. M., Hazarika, M. K., and Samarakoone, L. 2010. "Application of Remote Sensing and GIS for Flood Risk Analysis: A Case Study of Kalu-Ganga River, Sri Lanka." *International Archives of the Photogrammetry, Remote Sensing and Spatial Information Sciences* 38 (8): 110–115.

Sayers, P.B., Hall, J.W., Meadowcroft, I.C., 2002. Towards risk-based flood hazard management in the UK. *Proc. Inst. Civ. Eng. Civ. Eng.* 150, 36–42. https://doi.org/10.1680/cien.2002.150.5.36.

Sharma, A., Poonia, M., Rai, A., Biniwale, R. B., Tiwari, A., Lachure, S., Tuegel, F., Holzbecher, E., and Hinkelmann, R. 2024. "Impact of Land Use and Rainfall Change on Runoff and Flood Resilience of an Urban Environment: A Case Study of Chennai City, India." *Arabian Journal of Geosciences* 17 (7): 208. https://doi.org/10.1007/s12517-024-11985-6.

Sharma, R., Goswami, S.B., Tiwari, S., Kar, S.C., 2015. Evaluation of daily rainfall-runoff simulations in Narmada River basin. *Int. J. Earth Sci. Eng.* 8 (3), 1123–1132.

State Disaster Management Authority (Madhya Pradesh), 2018. Government of Madhya Pradesh, Bhopal, India.

State Disaster Management Authority (Madhya Pradesh), 2020. Government of Madhya Pradesh, Bhopal, India.

State Disaster Management Plan (Madhya Pradesh), 2012. *State disaster management plan*. Government of Madhya Pradesh, Bhopal, India.

Tanaka, T., Tachikawa, Y., Ichikawa, Y., and Yorozu, K. (2017). "Impact assessment of upstream flooding on extreme flood frequency analysis using a flood-inundation model." *J. Hydrol.*, 554, 370–382. https://doi.org/10.1016/j.jhydrol.2017.09.012.

Teng, J., Jakeman, A. J., Vaze, J., Croke, B. F. W., Dutta, D., and Kim, S. (2017). "Flood inundation modelling: A review of methods, recent advances, and uncertainty analysis." *Environmental Modelling & Software*, 90, 201–216.

Teng, J., Jakeman, A.J., Vaze, J., et al., 2017. Flood inundation modelling: a review of methods, recent advances and uncertainty analysis. *Environ. Model. Softw.* 90, 201–216. https://doi.org/10.1016/j.envsoft.2017.01.006.

Tewolde, M. H., and Smithers, J. C. (2006). "Flood routing in ungauged catchments using Muskingum methods." *Water SA*, 32(3), 379–388.

Ticehurst, C., Dutta, D., Karim, F., Petheram, C., and Guerschman, J. P. (2015). "Improving the accuracy of daily MODIS OWL flood inundation mapping using hydrodynamic modelling." *Natural Hazards*, 78(2), 803–820.

Timbadiya, P. V., & Krishnamraju, K. M. (2023). A 2D hydrodynamic model for river flood prediction in a coastal floodplain: PV Timbadiya and KM Krishnamraju. *Natural Hazards*, *115*(2), 1143-1165.

Timbadiya, P. V., Patel, P. L., and Porey, P. D. (2014a). "One-dimensional hydrodynamic modelling of flooding and stage hydrographs in the Lower Tapi River, India." *Current Science*, 106(5), 708–716.

Timbadiya, P. V., Patel, P. L., and Porey, P. D. (2014b). "A 1D–2D coupled hydrodynamic model for river flood prediction in a coastal urban floodplain." *J. Hydrol. Eng.*, 20(2), 05014017.

Towe, R., Dean, G., Edwards, L., et al., 2020. Rethinking data-driven decision support in flood risk management for a big data age. J. Flood Risk Manag. https://doi.org/10.1111/jfr3.12652.

Trambadia, N. K., Patel, D. P., Patel, V. M., and Gundalia, M. J. 2022. "Comparison of Two Open-Source Digital Elevation Models for One-Dimensional Hydrodynamic Flow Analysis: A Case Study of Ozat River Basin, Gujarat, India." *Modeling Earth Systems and Environment* 8 (4): 5433–5447. https://doi.org/10.1007/s40808-022-01426-2.

Trivedi, K., Patel, V., Pandya, U., and Trambadia, N. 2023. "Development of One-Dimensional Hydrodynamic Analysis in Data-Scarce Regions by Comparing Two Digital Elevation Models." *IARJSET* 10 (5). https://doi.org/10.17148/iarjset.2023.1057.

U.S. Army Corps of Engineers (2010). *HEC-RAS River Analysis System, User's Manual, Version 4.1*. Hydrologic Engineering Center, Davis, CA.

Wan, X., Yin, W., Sun, P., Tan, B., 2017. Risk division assessment of rainstorm-flood disasters based on cloud model. J. Nat. Disasters 26, 77–83. https://doi.org/10.13577/j.jnd.2017.0409.

Wang, Q., Peng, W., Dong, F., Liu, X., and Ou, N. (2020). "Simulating flow in an urban river with complex cross sections using the MIKE 21 FM model." *Water*, 12(3), 761.

Wang, Y., Colby, J. D., and Mulcahy, K. A. 2002. "An Efficient Method for Mapping Flood Extent in a Coastal Floodplain Using Landsat TM and DEM Data." *International Journal of Remote Sensing* 23 (18): 3681–3696. https://doi.org/10.1080/01431160110114484.

Winsemius, H.C., Van Beek, L.P.H., Jongman, B., et al., 2013. A framework for global river flood risk assessments. Hydrol. Earth Syst. Sci. 17, 1871–1892. https://doi.org/10.5194/hess-17-1871-2013.

Yadav, S. M., and Mangukiya, N. K. (2021). “Semi-arid river basin flood: Causes, damages, and measures.” In: *Proc., Fifth Int. Conf. on Ocean Engineering (ICOE 2019)*, Springer, 201–212. https://doi.org/10.1007/978-981-15-8506-7_16.

Yue, S., Ouarda, T. B. M., Bobée, B., Legendre, P., and Bruneau, P. (1999). “The Gumbel mixed model for flood frequency analysis.” *J. Hydrol.*, 226(1–2), 88–100. https://doi.org/10.1016/S0022-1694(99)00168-7.